Journal of Quantitative Spectroscopy & Radiative Transfer 112 (2011) 2095–2127

Contents lists available at ScienceDirect

Journal of Quantitative Spectroscopy & Radiative Transfer

journal homepage: www.elsevier.com/locate/jqsrt

Review

Scattering of electromagnetic waves by ensembles of particles and discrete random media

Victor P. Tishkovets [a], Elena V. Petrova [b], Michael I. Mishchenko [c,*]

[a] Institute of Radio Astronomy of NASU, 4 Chervonopraporna Street, Kharkiv 61002, Ukraine
[b] Space Research Institute RAS, Profsoyuznaya 84/32, Moscow 117997, Russia
[c] NASA Goddard Institute for Space Studies, 2880 Broadway, New York, NY 10025, USA

ARTICLE INFO

Available online 1 May 2011

Keywords:
Electromagnetic scattering
Multiple scattering
Coherent backscattering
Radiative transfer
Discrete random media
Near-field effects
Quasi-crystalline approximation

ABSTRACT

Current problems of the theory of multiple scattering of electromagnetic waves by discrete random media are reviewed, with an emphasis on densely packed media. All equations presented are based on the rigorous theory of electromagnetic scattering by an arbitrary system of non-spherical particles. The main relations are derived in the circular-polarization basis. By applying methods of statistical electromagnetics to a discrete random medium in the form of a plane–parallel layer, we transform these relations into equations describing the average (coherent) field and equations for the sums of ladder and cyclical diagrams in the framework of the quasi-crystalline approximation. The equation for the average field yields analytical expressions for the generalized Lorentz–Lorenz law and the generalized Ewald–Oseen extinction theorem, which are traditionally used for the calculation of the effective refractive index. By assuming that the particles are in the far-field zones of each other, we transform all equations asymptotically into the well-known equations for sparse media. Specifically, the equation for the sum of the ladder diagrams is reduced to the classical vector radiative transfer equation. We present a simple approximate solution of the equation describing the weak localization (WL) effect (i.e., the sum of cyclical diagrams) and validate it by using experimental and numerically exact theoretical data. Examples of the characteristics of WL as functions of the physical properties of a particulate medium are given. The applicability of the interference concept of WL to densely packed media is discussed using results of numerically exact computer solutions of the macroscopic Maxwell equations for large ensembles of spherical particles. These results show that theoretical predictions for spare media composed of non-absorbing or weakly absorbing particles are reasonably accurate if the particle packing density is less than ~30%. However, a further increase of the packing density and/or absorption may cause optical effects not predicted by the low-density theory and caused by near-field effects. The origin of the near-filed effects is discussed in detail.

Published by Elsevier Ltd.

Abbreviations: CB, coherent backscattering; CGC, Clebsch–Gordan coefficient; CGS, Clebsch–Gordan series; CP, circular polarization; EM, electromagnetic; LP, linear polarization; MMEs, macroscopic Maxwell equations; QED, quantum electrodynamics; RT, radiative transfer; RTE, radiative transfer equation; RTT, radiative transfer theory; VRTE, vector radiative transfer equation; WL, weak localization

* Corresponding author. Tel.: +1 212 678 5590; fax: +1 212 678 5622.
E-mail addresses: crmim2@gmail.com, mmishchenko@giss.nasa.gov (M.I. Mishchenko).

0022-4073/$ - see front matter Published by Elsevier Ltd.
doi:10.1016/j.jqsrt.2011.04.010

Contents

1. Introduction . . . 2096
2. Scattering of electromagnetic waves by a system of particles . . . 2097
2.1. Statement of problem . . . 2097
2.2. Scattering in the far-field zone . . . 2099
3. The effective refractive index . . . 2100
3.1. Calculation of the coherent field in the quasi-crystalline approximation . . . 2100
3.2. Calculation of the coherent field using the Twersky approximation for correlated scatterers . . . 2103
3.3. Random media composed of identical spherical particles . . . 2104
3.4. Far-field approximation . . . 2104
3.5. Dependence of the effective refractive index on particle concentration . . . 2104
4. Electromagnetic scattering by discrete random media . . . 2105
4.1. Ladder and cyclical diagrams . . . 2105
4.2. Equation for the incoherent part of the scattered radiation . . . 2107
4.2.1. The ladder approximation for densely packed media . . . 2107
4.2.2. The ladder approximation for sparse media . . . 2108
4.3. Equation for the coherent part of the scattered radiation . . . 2109
4.3.1. Reciprocity relations . . . 2109
4.3.2. Cyclical diagrams for densely packed media . . . 2109
4.3.3. Cyclical diagrams for sparse media . . . 2110
4.3.4. Exact backscattering direction . . . 2111
4.4. Approximate method for solving the equation for the coherent part of radiation reflected by a semi-infinite discrete random medium . . . 2111
4.4.1. Basic equations . . . 2111
4.4.2. Robustness of the approximation . . . 2113
4.4.3. CB as a function of medium characteristics: examples . . . 2114
5. Interaction of particles in the near field as revealed by scattering properties of aggregates . . . 2116
5.1. Effects of near-field interactions on scattering characteristics . . . 2117
5.1.1. Inhomogeneity of near-zone fields . . . 2117
5.1.2. Mutual shielding of particles . . . 2118
5.1.3. Examples of near-field effects in aggregates . . . 2119
5.2. Coherent backscattering and near-field effects for ensembles of particles with varying packing densities . . . 2120
5.2.1. Model description . . . 2120
5.2.2. Numerical results . . . 2121
5.2.3. Discussion . . . 2121
6. Concluding remarks . . . 2123
Acknowledgments . . . 2123
Appendix A Spherical and helical basis vectors . . . 2123
Appendix B Spherical vectors . . . 2124
Appendix C Wigner *D* functions . . . 2124
Appendix D Clebsch–Gordan coefficients . . . 2125
References . . . 2125

1. Introduction

Depending on the relation between the mean size of the scatterers, the average distance between them, and the wavelength of the incident light, scattering media can be conventionally classified into two types: (i) continuous media with fluctuations of the refractive index and (ii) media with discrete heterogeneities (particulate or powder-like media). The theoretical description of electromagnetic (EM) scattering by these two types of medium requires noticeably different approaches, although the main physical principles remain the same. The scattering theory for continuously inhomogeneous media is rather thoroughly developed (see, e.g., Refs. [1–3]), while the progress in the theory applicable to discrete media has been substantially slower, especially for particles with sizes comparable to the wavelength of the incident light λ. In this size range, the wavelength dependence of characteristics of the scattered radiation is particularly strong, which makes this case most important from the standpoint of interpretation of observational data. In the case of visible wavelengths, techniques dealing only with energetic and polarization characteristics of radiation are traditionally used [4].

The methods used in theoretical analyses of EM scattering by sparse and densely packed particulate media are substantially different. In the case of a sparse medium, the analysis is relatively straightforward due to several simplifications. If the distances between the scatterers are much greater than their sizes and the wavelength, the wave propagating from particle j to particle s can be considered spherical. Furthermore, in the vicinity of particle s this wave can be assumed to be a locally homogeneous plane wave. When describing the scattering by particle s, the simplification of a plane wave allows one to invoke such concepts of the single-scattering theory as the scattering matrix, the extinction cross section, etc. Moreover, if the scatterers are randomly

positioned throughout the medium, the scattered radiation can be represented as a sum of two parts. One of them corresponds to incoherent (diffuse) scattering and is described by the well-known radiative transfer equation (RTE) obtained by summing the so-called ladder diagrams in the diagrammatic representation of the Bethe–Salpeter equation. This part of the scattered radiation depends on the properties of the medium relatively weakly. The second part corresponds to the sum of cyclical diagrams and arises from the interference of pairs of conjugate waves scattered along the same string of particles in the medium but in opposite directions [4–10]. Constructive interference of the scattered waves manifests itself as a narrow interference peak of intensity centered at exactly the backscattering direction as well as causes a specific behavior of polarization in the backscattering domain. In the literature, this phenomenon is called weak localization (WL) of waves in a particulate medium or coherent backscattering (CB; see, e.g., Ref. [4]). One of potential manifestations of WL in the case of unpolarized incident light is a narrow branch of negative values of the degree of linear polarization near the exact backscattering direction. It is currently believed that WL causes the opposition effects in brightness and polarization observed for many atmosphereless bodies of the Solar System [11].

The interference nature of the second part of the scattered radiation implies that the coherent radiation is much stronger dependent on the properties of the medium (such as the packing density, sizes, shapes, and refractive indices of the scatterers) than the diffuse radiation. This factor allows one to interpret observational data more reliably and thoroughly, provided that an adequate theoretical model is available. Currently, however, the theoretical analysis of the interference part of the scattered radiation is still poorly developed, which hinders the full extraction of the potential information content of an optical observation.

In a densely packed medium, the sizes of the constituent scatterers and the distances between them can be comparable to the wavelength λ. In this case, effects caused by the near field can play an important role. The radiation scattered by such a medium cannot be represented as the sum of only two parts, unlike the case of a sparse medium. Moreover, on a λ scale, the fields are strongly inhomogeneous even in a statistically homogeneous and isotropic medium [12–16]. As a consequence, the description of scattering becomes substantially more involved than the approximation of a plane homogeneous wave. All these phenomena are difficult to analyze, and the existing analytical models of multiple scattering by densely packed media do not account for them at all or include them in a highly approximate way. The role of the near field in forming the brightness and polarization characteristics of the scattered radiation, especially the opposition effects, has not been properly studied. This complicates the interpretation of remote-sensing data for various objects, in particular optical observations of atmosphereless celestial bodies.

In this review, the theory of multiple scattering of EM waves by discrete random media is considered in the framework of statistical electrodynamics, the foundations of which were established by Foldy [17], Lax [18,19], and Twersky [20] (see also Ref. [4] and references therein). The scattering particulate media are assumed to be statistically homogeneous, isotropic, and non-chiral. To characterize the radiation, the Stokes parameters are used throughout.

2. Scattering of electromagnetic waves by a system of particles

2.1. Statement of problem

The theory of EM scattering by a system (cluster) of particles is most thoroughly developed for the case of spherical components. A vast list of publications devoted to the scattering of light by aggregates of spherical particles can be found in Refs. [21–28]. Although the T-matrix solution of the scattering problem is also known for systems of non-spherical particles [24,29,30] and even for aggregates of multilayer non-spherical particles [31], it is much more involved than that for spherical components and has not yet found extensive applications. There is no doubt, however, that as a basis for modeling different effects of multiple scattering and a framework for developing the theory of multiple scattering by particulate media, the exact theory of EM scattering by systems of arbitrary scatterers is utterly important.

Let us first specify the restrictions on the structure of a cluster and its components adopted thereafter. It is assumed that the constituent particles are homogeneous and that their smallest circumscribing spheres do not overlap. These assumptions allow us to calculate the scattered field by applying the so-called superposition T-matrix method ([23,24,32] and references therein).

To describe EM scattering by a cluster of N particles, we use the coordinate system shown in Fig. 1. The coordinates of the cluster components are defined by their respective position vectors $\mathbf{R}_j$ $(j=1,\ldots,N)$ in the laboratory coordinate system $\hat{\mathbf{n}}_0$ with axes (x, y, z). Throughout the paper, a bold upright letter with a caret,

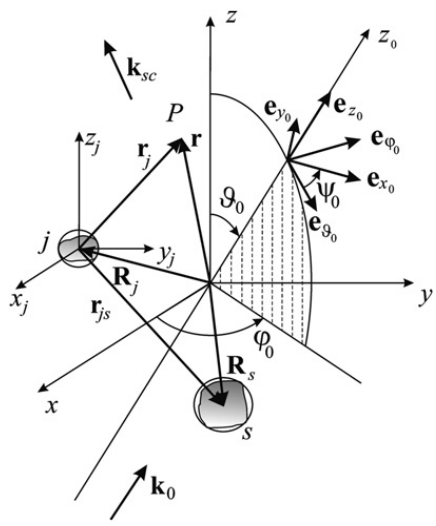

Fig. 1. Coordinate systems used to describe EM scattering by a cluster.

$\hat{\mathbf{v}}$, denotes a right-handed coordinate system (x, y, z) with the z-axis along the vector $\mathbf{v}$ while the symbol $-\hat{\mathbf{v}}$ denotes the coordinate system with axes (x, $-y$, $-z$). The origin of the laboratory coordinate system is near the center of the cluster (or in the center of the smallest circumscribing sphere of the cluster). The incident plane wave propagates along the positive z_0-axis of the coordinate system $\hat{\mathbf{k}}_0$ directed along the wave vector $\mathbf{k}_0$ ($k_0=2\pi/\lambda$). The wave scattered by the cluster propagates in the direction of the observation point along the wave vector $\mathbf{k}_{sc}$ ($k_{sc}=k_0$) of the coordinate system $\hat{\mathbf{k}}_{sc}$. The rotation from $\hat{\mathbf{n}}_0$ to $\hat{\mathbf{k}}_0$ is determined by the Euler angles φ_0, ϑ_0, and ψ_0. The Euler angles φ, ϑ, and ψ specify the rotation from $\hat{\mathbf{n}}_0$ to $\hat{\mathbf{k}}_{sc}$. Finally, the rotation from $\hat{\mathbf{k}}_0$ to $\hat{\mathbf{k}}_{sc}$ is specified by the Euler angles φ_{sc}, ϑ_{sc}, and ψ_{sc}. In addition to these reference frames, coordinate systems affixed to each scatterer are introduced. The origins of these coordinate systems are in the centers of the smallest spheres circumscribing the scatterers, while their axes are oriented parallel to those of the laboratory coordinate system (Fig. 1).

EM scattering is conveniently described by using the so-called circular-polarization (CP) basis [24]. Specifically, the electric field of a circularly polarized incident plane wave can be written as follows:

$$\mathbf{E}^{(0)}=\mathbf{e}_n(\hat{\mathbf{k}}_0)\exp(\mathrm{i}\mathbf{k}_0\mathbf{r}-\mathrm{i}\omega t), \tag{1}$$

where $\mathrm{i}=(-1)^{1/2}$, $n=\pm 1$, ω is the angular frequency, t is the time, and $\mathbf{e}_n(\hat{\mathbf{k}}_0)$ is a covariant spherical basis vector [34] in the coordinate system $\hat{\mathbf{k}}_0$ formed by the unit vectors $\mathbf{e}_{x_0}$ and $\mathbf{e}_{y_0}$ (Fig. 1). If $n=1$ then the direction of rotation of the vector (1) is clockwise when looking in the direction of the vector $\mathbf{k}_0$. If $n=-1$ then the direction of rotation is counterclockwise. The resulting polarization is called right-handed or left-handed, respectively [24]. (In optics, the reverse definition of right- and left-handed polarizations is often used; e.g., Ref. [33].) The time dependence of the scattered wave is described by the complex exponential $\exp(-\mathrm{i}\omega t)$. In what follows, this time factor will be consistently omitted.

At any point outside the particles, the field scattered by the cluster can be represented as a superposition of the fields scattered by its components [4,23,24]

$$\mathbf{E}=\sum_{j=1}^{N}\mathbf{E}^{(j)}, \tag{2}$$

where $\mathbf{E}^{(j)}$ is the field scattered by particle j. Here, the field $\mathbf{E}^{(j)}$ does not represent only the single scattering of the incident field by particle j and must be calculated with full account of the interactions between the scatterers. Each term in Eq. (2) satisfies the Helmholtz equation

$$\Delta\mathbf{E}^{(j)}+k_j^2\mathbf{E}^{(j)}=0, \tag{3}$$

where $k_j=k_0\tilde{m}_j$ and $k_j=k_0$ for the fields inside and outside the particle, respectively, and $\tilde{m}_j=\mathrm{Re}(\tilde{m}_j)+\mathrm{i}\,\mathrm{Im}(\tilde{m}_j)$ is the complex refractive index of particle j.

In the spherical coordinate system, the solution of Eq. (3) can be expressed in vector Helmholtz harmonics $\mathbf{F}^L_{JM}=z_L(k_jr_j)\mathbf{Y}^L_{JM}(\vartheta_j,\varphi_j)$ [26,34]. Here, $z_L(k_jr_j)$ is a Bessel or Hankel spherical function and $\mathbf{Y}^L_{JM}(\vartheta_j,\varphi_j)$ is the spherical vector [34]. It is further assumed that the particles carry no charge (i.e., the divergence $\Delta\cdot\mathbf{E}^{(j)}=0$). In this case, at any point P not occupied by the particles (see Fig. 1), the field $\mathbf{E}^{(j)}$ is expressed in one of the spherical vectors $\mathbf{X}_{JM}(\vartheta,\varphi)\equiv\mathbf{Y}^J_{JM}(\vartheta,\varphi)$ as follows (see, e.g., Refs. [26,34,35]):

$$\mathbf{E}^{(j)}=\sum_{LM}\left[n\bar{b}^{(j)}_{LM}h_L(k_0r_j)\mathbf{X}_{LM}(\vartheta_j,\varphi_j)+\frac{\bar{a}^{(j)}_{LM}}{k_0}\nabla\times h_L(k_0r_j)\mathbf{X}_{LM}(\vartheta_j,\varphi_j)\right]. \tag{4}$$

Eq. (4) yields the wave scattered by particle j with respect to the coordinate system affixed to this particle (Fig. 1). Here, ϑ_j and φ_j are the angular coordinates of the observation point P (i.e., of the vector $\mathbf{r}_j$) in the coordinate system of particle j. The Hankel spherical function of the first kind $h_L(x)$ is chosen as a radial function, since the scattered field must evolve into a diverging spherical wave at a large distance from the particle.

In the coordinate system of particle j, the incident external field $\mathbf{E}^{(0j)}$ of Eq. (1) can be also expanded in a series analogously to Eq. (4) [26,34,35]

$$\mathbf{E}^{(0j)}=\sum_{LM}w^{(j)}_{LM}\left[nj_L(k_0r_j)\mathbf{X}_{LM}(\vartheta_j,\varphi_j)+\frac{1}{k_0}\nabla\times j_L(k_0r_j)\mathbf{X}_{LM}(\vartheta_j,\varphi_j)\right],$$

where $w^{(j)}_{LM}=-4\pi\mathrm{i}^L\exp(\mathrm{i}\mathbf{k}_0\mathbf{R}_j)\sqrt{((2L+1)/8\pi)}D^L_{Mn}(\hat{\mathbf{n}}_0,\hat{\mathbf{k}}_0)$ and $D^L_{Mn}(\hat{\mathbf{n}}_0,\mathbf{k}_0)=D^L_{Mn}(\varphi_0,\vartheta_0,\psi_0)$ is the Wigner function [34] describing the rotation of a spherical vector from the coordinate system $\hat{\mathbf{n}}_0$ to the coordinate system $\hat{\mathbf{k}}_0$.

With respect to particle j, the external field is

$$\mathbf{E}^{(j)inc}=\mathbf{E}^{(0j)}+\sum_{s\neq j}\mathbf{E}^{(s)}. \tag{5}$$

Each term in the sum (5) is described by an equation of the type (4) in the coordinate system of particle s. To apply the T-matrix method to each particle, the field written in the coordinate system of particle s should be expanded in vector harmonics in the coordinate system of particle j. These transformations can be performed using the addition theorem for the vector Helmholtz harmonics [22,36,37]. This theorem should be applied to the field scattered by particle s in order to write this field in the coordinate system of particle j. Then, the field (5) is expressed as follows [35]:

$$\mathbf{E}^{(j)inc}=\sum_{LM}\left[b^{(j)inc}_{LM}j_L(k_0r_j)\mathbf{X}_{LM}(\vartheta_j,\varphi_j)+\frac{a^{(j)inc}_{LM}}{k_0}\nabla\times j_L(k_0r_j)\mathbf{X}_{LM}(\vartheta_j,\varphi_j)\right], \tag{6}$$

where

$$a^{(j)inc}_{LM}=w^{(j)}_{LM}+\sum_{s\neq j,lm}\left(n\bar{b}^{(s)}_{lm}\mathrm{K}_{LMlm}(\mathbf{r}_{js})+\bar{a}^{(s)}_{lm}\mathrm{H}_{LMlm}(\mathbf{r}_{js})\right), \tag{7}$$

$$b^{(j)inc}_{LM}=nw^{(j)}_{LM}+\sum_{s\neq j,lm}\left(n\bar{b}^{(s)}_{lm}\mathrm{H}_{LMlm}(\mathbf{r}_{js})+\bar{a}^{(s)}_{lm}\mathrm{K}_{LMlm}(\mathbf{r}_{js})\right). \tag{8}$$

Here $\mathrm{H}_{LMlm}(\mathbf{r}_{js})$ and $\mathrm{K}_{LMlm}(\mathbf{r}_{js})$ are the coefficients of the addition theorem for the functions $h_L(k_0r)\mathbf{X}_{LM}(\vartheta,\varphi)$ and $k_0^{-1}\nabla\times h_L(k_0r)\mathbf{X}_{LM}(\vartheta,\varphi)$ [37,38]. On the surface of the smallest circumscribing sphere of particle j, the following conditions are met: $\mathbf{r}_s=\mathbf{r}_j-\mathbf{r}_{js}$ and $r_j<r_{js}$. In this case, the radial dependence of the coefficients $\mathrm{H}_{LMlm}(\mathbf{r}_{js})$ and $\mathrm{K}_{LMlm}(\mathbf{r}_{js})$ is determined by the Hankel spherical functions.

If the cluster constituents are homogeneous isotropic spherical particles, the coefficients $\overline{a}_{LM}^{(j)}$ and $\overline{b}_{LM}^{(j)}$ can be found from the boundary conditions (see, e.g., Ref. [26]). For non-spherical particles, these coefficients are found with the T-matrix method [21,23–25,27,28,32]. Since Eq. (3) and the boundary conditions are linear, the relations between the coefficients $\overline{a}_{LM}^{(j)}$ and $\overline{b}_{LM}^{(j)}$ on one hand and those given by Eqs. (7) and (8) on the other hand must be linear and specified by the T-matrix as follows [23,24,32]:

$$n\overline{b}_{LM}^{(j)} = \sum_{lm}\left(T_{MLml}^{11(j)} b_{lm}^{(j)inc} + T_{MLml}^{12(j)} a_{lm}^{(j)inc}\right), \tag{9}$$

$$\overline{a}_{LM}^{(j)} = \sum_{lm}\left(T_{MLml}^{21(j)} b_{lm}^{(j)inc} + T_{MLml}^{22(j)} a_{lm}^{(j)inc}\right). \tag{10}$$

The individual-particle T matrices can be determined using the extended boundary condition method. Specifically, for homogeneous isotropic spherical particles

$$T_{MLml}^{11(j)} = -\delta_{Mm}\delta_{Ll} b_l^{(j)}, \quad T_{MLml}^{22(j)} = -\delta_{Mm}\delta_{Ll} a_l^{(j)}, \tag{11}$$

$$T_{MLml}^{12(j)} = 0, \quad T_{MLml}^{21(j)} = 0, \tag{12}$$

where $a_L^{(j)}$ and $b_L^{(j)}$ are the Lorenz–Mie coefficients of particle j [24]. Computer codes for the calculation of the scattering characteristics of particles of various shapes can be found on the Internet (e.g., Ref. [39]). In what follows, we assume that the T matrices of the individual particles are known.

2.2. Scattering in the far-field zone

Quite often the characteristics of the scattered radiation are considered in the far zone of the cluster. The conditions for this zone can be formulated as follows:

$$k_0(r-a_m) \gg 1, \quad 2k_0 r \gg (k_0 a_m)^2, \quad r \gg a_m,$$

where a_m is the radius of the smallest circumscribing sphere of the cluster and r is the distance to the observation point in the laboratory coordinate system [4,24]. From Eq. (4), the asymptotic formula

$$h_L(x) \approx \mathrm{i}^{-L-1}\exp(\mathrm{i}x)/x \quad (x \gg L,\ x \gg 1) \tag{13}$$

yields the following expression valid in the far-field zone (see, e.g., Ref. [35]):

$$\mathbf{E}^{(j)} = \frac{\exp(\mathrm{i}k_0 r_j)}{-\mathrm{i}k_0 r_j}\sum_{LMp}\mathrm{i}^{-L}\sqrt{\frac{2L+1}{8\pi}}\left(\overline{a}_{LM}^{(j)} + np\overline{b}_{LM}^{(j)}\right) D_{Mp}^{*L}(\hat{\mathbf{n}}_0,\hat{\mathbf{k}}_{sc})\mathbf{e}_p(\hat{\mathbf{k}}_{sc}), \tag{14}$$

where $p = \pm 1$.

Since the cluster size is much smaller than the distance to the observation point, the direction to the observation point is the same for all the particles in the cluster (Fig. 1). Eq. (14) describes an outgoing spherical wave centered at particle j. Since the projection of the field vector (14) onto the unit vector $\mathbf{e}_0(\hat{\mathbf{k}}_{sc}) \equiv \mathbf{e}_z(\hat{\mathbf{k}}_{sc})$ is zero, this wave is transverse. The wave amplitude decreases as r_j^{-1}. Unlike the field (14), the field (4) is not a transverse spherical wave and contains a radial component (along $\mathbf{r}_j$) and terms decreasing faster than r_j^{-1}. The latter statement follows from the representation of the Hankel spherical function $h_l(x)$ as a finite series containing powers x^{-n_1}, where $n_1 = 1,2,3,\ldots$ [40]. The terms decreasing faster than r^{-1} describe the near field [41] and play an important role in defining the scattering characteristics of the cluster [14–16,42].

Eq. (14) can be simplified. Let us denote

$$A_{LM}^{(j)(pn)} = \mathrm{i}^{-L}\sqrt{\frac{1}{2\pi(2L+1)}}\left(\overline{a}_{LM}^{(j)} + pn\overline{b}_{LM}^{(j)}\right), \tag{15}$$

$$\kappa_{LMlm}^{(j)(pn)} = -\mathrm{i}^{l-L}\sqrt{\frac{2l+1}{2L+1}}\left(T_{MLml}^{22(j)} + nT_{MLml}^{21(j)} + pT_{MLml}^{12(j)} + pnT_{MLml}^{11(j)}\right), \tag{16}$$

and take into account that in the far zone of the cluster $k_0 r_j \approx k_0 r - \mathbf{k}_{sc}\mathbf{R}_j$ (where r is the distance from the cluster). Simple transformations yield the following expression for the wave scattered by particle j [35]:

$$\mathbf{E}^{(j)} = \frac{\exp(\mathrm{i}k_0 r)}{-\mathrm{i}k_0 r}\exp(-\mathrm{i}\mathbf{k}_{sc}\mathbf{R}_j) \times \sum_{LMp}\frac{2L+1}{2}A_{LM}^{(j)(pn)} D_{Mp}^{*L}(\hat{\mathbf{n}}_0,\hat{\mathbf{k}}_{sc})\mathbf{e}_p^{(s)}(\hat{\mathbf{k}}_{sc}). \tag{17}$$

Here, the coefficients $A_{LM}^{(j)(pn)}$, as it follows from Eqs. (7)–(10), are determined from the system of equations

$$A_{LM}^{(j)(pn)} = \exp(\mathrm{i}\mathbf{k}_0\mathbf{R}_j)\sum_{lm}\kappa_{LMlm}^{(j)(pn)} D_{mn}^{l}(\hat{\mathbf{n}}_0,\hat{\mathbf{k}}_0) + \sum_{qlm}\kappa_{LMlm}^{(j)(pq)}\sum_{s\neq j}\sum_{l_1 m_1} A_{l_1 m_1}^{(s)(qn)} H_{lml_1 m_1}^{(q)}(\hat{\mathbf{n}}_0,\hat{\mathbf{r}}_{js}), \tag{18}$$

where $q = \pm 1$, $\hat{\mathbf{r}}_{js}$ is the coordinate system with the z-axis directed along the vector $\mathbf{r}_{js}$ (Fig. 1),

$$\begin{aligned} H_{LMlm}^{(q)}(\hat{\mathbf{n}}_0,\hat{\mathbf{r}}_{js}) &= \mathrm{i}^{l-L+2}\frac{\sqrt{2l+1}}{2\sqrt{2L+1}}\left(\mathrm{H}_{LMlm}(\mathbf{r}_{js}) + q\mathrm{K}_{LMlm}(\mathbf{r}_{js})\right) \\ &= \frac{2l+1}{2}(-1)^m\sum_{l_1}\mathrm{i}^{-l_1}h_{l_1}(k_0 r_{js})D_{m_1 0}^{l_1}(\hat{\mathbf{n}}_0,\hat{\mathbf{r}}_{js}) \\ &\quad \times C_{LMl-m}^{l_1 m_1} C_{Lql-q}^{l_1 0}, \end{aligned} \tag{19}$$

$m_1 = M - m$, and the indexed symbols C are Clebsch–Gordan coefficients (CGCs) [34].

For homogeneous isotropic spherical particles, Eqs. (11), (12), (15), (16), and (18) yield

$$A_{LM}^{(j)(pn)} = a_L^{(j)(pn)}\exp(\mathrm{i}\mathbf{k}_0\mathbf{R}_j)D_{Mn}^{L}(\hat{\mathbf{n}}_0,\hat{\mathbf{k}}_0) + \sum_{q} a_L^{(j)(pq)}\sum_{s\neq j}\sum_{lm} A_{lm}^{(s)(qn)} H_{LMlm}^{(q)}(\hat{\mathbf{n}}_0,\hat{\mathbf{r}}_{js}), \tag{20}$$

where

$$a_L^{(j)(pn)} = a_L^{(j)} + pnb_L^{(j)}. \tag{21}$$

Under the above-mentioned restrictions on the structure of the cluster and its components (i.e., the components are homogeneous and their smallest circumscribing spheres do not overlap), the above formulas define completely the field scattered by an arbitrary cluster. They yield all the scattering characteristics of the cluster, in particular, the amplitude scattering matrix relating the components of the scattered and incident fields. In the literature, these field components are determined relative to either the scattering plane (see, e.g., Refs. [43–45]) or the meridional planes of the laboratory

coordinate system (Fig. 1) formed by the z-axis and the vectors $\mathbf{k}_0$ and $\mathbf{k}_{sc}$ (see, e.g., Refs. [4,24,46]). In what follows, we consider the field components with respect to the meridional planes $(z,\mathbf{k}_0)$ and $(z,\mathbf{k}_{sc})$ of the laboratory coordinate system. Then the amplitude scattering matrix $\mathbf{S}(\mathbf{k}_0,\mathbf{k}_{sc})$ is defined by the relation

$$E_p = \frac{1}{k_0 r}\sum_n S_{pn}(\mathbf{k}_0,\mathbf{k}_{sc})E_n^{(0)}, \tag{22}$$

where $n,p=\pm 1$. Note that the matrix $\mathbf{S}(\mathbf{k}_0,\mathbf{k}_{sc})$ in Eq. (22) is dimensionless, unlike the amplitude scattering matrix defined in Refs. [4,24].

In the CP-representation, the basis unit vectors in the meridional planes $(z,\mathbf{k}_0)$ and $(z,\mathbf{k}_{sc})$ are the covariant helicity basis vectors $\mathbf{e}_n^{(h)}(\hat{\mathbf{k}}_0)$ and $\mathbf{e}_p^{(h)}(\hat{\mathbf{k}}_{sc})$, respectively. The helicity orts $\mathbf{e}_n^{(h)}(\hat{\mathbf{k}}_0)$ and $\mathbf{e}_n^{(h)}(\hat{\mathbf{k}}_{sc})$ are formed by the unit vectors $\mathbf{e}_\vartheta$ and $\mathbf{e}_\varphi$ of the spherical coordinate system [34] in the given meridional planes. The rotation from the vector $\mathbf{e}_n^{(h)}(\hat{\mathbf{k}}_0)$ to the vector $\mathbf{e}_n(\hat{\mathbf{k}}_0)$ and from the vector $\mathbf{e}_p^{(h)}(\hat{\mathbf{k}}_{sc})$ to the vector $\mathbf{e}_p(\hat{\mathbf{k}}_{sc})$ is described by the rotation matrices depending on the Euler angles ψ_0 and ψ, respectively (Fig. 1). After accounting for Eqs. (2), (17), and (22), we have

$$S_{pn}(\mathbf{k}_0,\mathbf{k}_{sc}) = \sum_{j=1}^{N} t_{pn}^{(j)}(\mathbf{k}_0,\mathbf{k}_{sc}), \tag{23}$$

where the amplitude matrix of a component particle is given by [35,47]

$$t_{pn}^{(j)}(\mathbf{k}_0,\mathbf{k}_{sc}) = \exp(-\mathrm{i}\mathbf{k}_{sc}\mathbf{R}_j + \mathrm{i}n\psi_0 - \mathrm{i}p\psi) \times \sum_{LM}\frac{2L+1}{2}A_{LM}^{(j)(pn)}D_{Mp}^{*L}(\hat{\mathbf{n}}_0,\hat{\mathbf{k}}_{sc}). \tag{24}$$

These formulas will be used below both for the calculation of the scattering characteristics of ensembles of particles and for the derivation of equations describing the radiation scattered by a discrete random medium.

3. The effective refractive index

3.1. Calculation of the coherent field in the quasi-crystalline approximation

One of the main quantities used to describe the propagation of radiation in a discrete random medium is the so-called complex effective refractive index m_{eff} (or the effective propagation constant $k_0 m_{eff}$). Its imaginary part is directly related to the extinction coefficient of the medium. For a sparse medium, m_{eff} is determined from the optical theorem [3,23,24,43,45,48,49], while for a densely packed medium it is found from the generalized Lorentz–Lorenz law [3,50–55]. To derive analytical expressions for the generalized Lorentz–Lorenz law and the generalized Ewald–Oseen extinction theorem, the point of departure is given by Eqs. (6), (7), and (8). After substituting Eqs. (9) and (10) in Eqs. (7) and (8), the latter transform into a system of linear algebraic equations determining the expansion coefficients of the field exciting particle j. This system of equations, which is one of the forms of the Foldy–Lax multiple-scattering equations (see, e.g., Refs. [4,23,24], is used to calculate the so-called average or coherent field. The latter calculation is reduced to ensemble averaging of the coefficients $a_{LM}^{(j)inc}$ and $b_{LM}^{(j)inc}$, which is done in the framework of the quasi-crystalline approximation [3,19]. Hereinafter, we assume that the ergodic hypothesis [4] is valid. These transformations result in two independent systems of equations [3,19,50–55]; one of them is the analytical expression of the generalized Lorentz–Lorenz law, and the other, represents the generalized Ewald–Oseen extinction theorem.

Unlike the above-described scheme, the derivation of the equation for the effective refractive index given below is based on ensemble averaging of the field (4). Since Eqs. (6)–(10) are linear, the averaging of this field yields the field resulting from the scattering of the *average* field by particle j. In the framework of this approach, the transformations required for the analytical representations of the generalized Lorentz–Lorenz law and the generalized Ewald–Oseen extinction theorem are less cumbersome, since the system of equations (18) determining the coefficients $\overline{a}_{LM}^{(j)}$ and $\overline{b}_{LM}^{(j)}$ via Eq. (15) is more compact than the system of equations for the coefficients $a_{LM}^{(j)inc}$ and $b_{LM}^{(j)inc}$. Moreover, for a medium composed of identical spherical particles, the analytical expression for the generalized Ewald–Oseen extinction theorem is simpler than that derived in Ref. [3].

The field (4) depends on the coordinates and states of all N particles. The distribution of the N particles and their states can be described by the N-particle probability density function $P(\mathbf{R}_1,...,\mathbf{R}_N,\zeta_1,...,\zeta_N)$, where $\mathbf{R}_j$ is the radius-vector of the origin of particle j in the laboratory coordinate system (Fig. 1) and ζ_i denotes its state. (The state of a particle means a complete set of parameters defining its size, shape, refractive index, orientation, etc.) The function

$$P(\mathbf{R}_1,\ldots\mathbf{R}_N,\zeta_1,\ldots\zeta_N)\prod_i^N d\mathbf{R}_i\, d\zeta_i \tag{25}$$

gives the probability of finding particle 1 within the volume $d\mathbf{R}_1$ centered at $\mathbf{R}_1$ and with its state in the region $d\zeta_1$ centered at ζ_1, particle 2 within the volume $d\mathbf{R}_2$ centered at $\mathbf{R}_2$ and with its state in the region $d\zeta_2$ centered at ζ_2, and so on, and particle N within the volume $d\mathbf{R}_N$ centered at $\mathbf{R}_N$ and with its state in the region $d\zeta_N$ centered at ζ_N. The probability density function (25) is normalized to unity:

$$\int P(\mathbf{R}_1,\ldots\mathbf{R}_N,\zeta_1,\ldots\zeta_N)\prod_{i=1}^N d\mathbf{R}_i\, d\zeta_i = 1,$$

where the integration is performed over the entire range of particle positions and states.

Recall that the field equations (4) were derived by assuming that the smallest spheres circumscribing the particles do not overlap. In addition, in order to simplify the calculation, we will assume that the radii of these circumscribing spheres are the same, which means that some of the spheres are not the smallest circumscribing spheres of the respective particles. However, each particle is located at the center of its circumscribing sphere. These assumptions allow us to express $P(\mathbf{R}_1,\ldots\mathbf{R}_N,\zeta_1,\ldots\zeta_N)$ as follows:

$$P(\mathbf{R}_1,\ldots\mathbf{R}_N,\zeta_1,\ldots\zeta_N) = P(\mathbf{R}_1,\ldots\mathbf{R}_N)\prod_{j=1}^N P_j(\zeta_j), \tag{26}$$

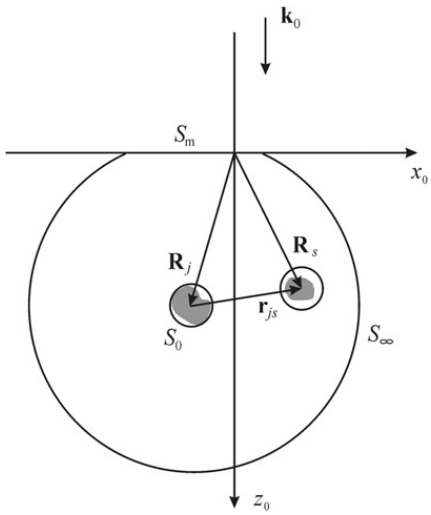

Fig. 2. Geometry of scattering by a semi-infinite medium. The contours S_0 and S_∞ and the segment S_m depict, respectively, the sphere circumscribing particle j, the sphere of a larger radius also circumscribing particle j, and the part of the boundary of the medium bounded by the intersection of the contour S_∞ and the plane x_0y_0 (see text).

where $P(\mathbf{R}_1,\ldots,\mathbf{R}_N)$ is the probability density function depending on the particle coordinates and normalized to unity, $P_j(\zeta_j)$ is the probability density function depending on the state of particle j and also normalized to unity. The representation (26) makes the averaging over particle positions independent of the averaging over their states.

Let us restrict the discussion to the simplest case of a semi-infinite medium and assume that the incident radiation propagates normally to the boundary of the medium. The geometry of the problem is shown in Fig. 2. In the coordinate system considered, the plane x_0y_0 coincides with the boundary of the medium, while the incident wave propagates along the axis z_0 directed into the medium.

Assume that the number of particles $N\to\infty$ and that all of the particles are randomly positioned in the half-space $z_0\geq 0$ as well as randomly oriented. The first step is to average the field (4) over particle states. As seen from Eqs. (4) and (15), this averaging can be reduced to the averaging of the coefficients $A_{LM}^{(j)(pn)}$. Let us denote

$$A_{LM}^{(pn)}(\mathbf{R}_j)=\left\langle A_{LM}^{(j)(pn)}\right\rangle_\zeta=\int A_{LM}^{(j)(pn)}P_j(\zeta_j)\,d\zeta_j,$$

$$\kappa_{LMlm}^{(pn)}=\left\langle \kappa_{LMlm}^{(j)(pn)}\right\rangle_\zeta=\int \kappa_{LMlm}^{(j)(pn)}P_j(\zeta_j)\,d\zeta_j,$$

where the angular brackets indicate the averaging over the state of particle j. Then the system of equations (18) is reduced to

$$A_{LM}^{(pn)}(\mathbf{R}_j)=\exp(\mathrm{i}\mathbf{k}_0\mathbf{R}_j)\sum_{lm}\kappa_{LMlm}^{(pn)}\delta_{mn}+\sum_{qlm}\kappa_{LMlm}^{(pq)}\sum_{s\neq j}\sum_{l_1m_1}A_{l_1m_1}^{(qn)}(\mathbf{R}_s)H_{lml_1m_1}^{(q)}(\hat{\mathbf{n}}_0,\hat{\mathbf{r}}_{js}). \tag{27}$$

Here, we took into account that the incident radiation propagates normally to the boundary of the medium ($\vartheta_0=0$). In this case, one can assume that $\varphi_0=\psi_0=0$, which yields $D_{mn}^l(\hat{\mathbf{n}}_0,\hat{\mathbf{k}}_0)=\delta_{mn}$. Further transformations consist of the averaging of the coefficients $A_{LM}^{(pn)}(\mathbf{R}_j)$ over the particle coordinates. To this end, let us represent the function $P(\mathbf{R}_1,\ldots,\mathbf{R}_N)$ as

$$\begin{aligned}P(\mathbf{R}_1,\ldots\mathbf{R}_N)&=P(\mathbf{R}_j)P(\mathbf{R}_1,\ldots,\mathbf{R}_j',\ldots,\mathbf{R}_N|\mathbf{R}_j)\\&=P(\mathbf{R}_j)P(\mathbf{R}_i|\mathbf{R}_j)P(\mathbf{R}_1,\ldots,\mathbf{R}_j',\ldots,\mathbf{R}_i',\ldots,\mathbf{R}_N|\mathbf{R}_j,\mathbf{R}_i)\end{aligned} \tag{28}$$

[3,19,53], where $P(\mathbf{R}_j)$ is the probability of finding a particle at the point $\mathbf{R}_j$, $P(\mathbf{R}_1,\ldots,\mathbf{R}_j',\ldots,\mathbf{R}_N|\mathbf{R}_j)$ is the conditional probability of finding the remaining particles at the corresponding points (the primed $\mathbf{R}_j'$ means that the variable $\mathbf{R}_j$ is absent), $P(\mathbf{R}_i|\mathbf{R}_j)$ is the conditional probability of finding a particle at the point $\mathbf{R}_i$ if it is known that there is a particle at the point $\mathbf{R}_j$, and $P(\mathbf{R}_1,\ldots,\mathbf{R}_j',\ldots,\mathbf{R}_i',\ldots,\mathbf{R}_N|\mathbf{R}_j,\mathbf{R}_i)$ is the conditional probability of finding the remaining particles at the corresponding points. If N is large and the system of particles is statistically homogeneous and isotropic, the function $P(\mathbf{R}_i|\mathbf{R}_j)$ depends only on the distance between the particles

$$P(\mathbf{R}_i|\mathbf{R}_j)=\eta g(|\mathbf{R}_j-\mathbf{R}_i|)/(N-1)=\eta g(r_{ij})/(N-1), \tag{29}$$

where $g(r)$ is the pair correlation function for the system of identical solid spheres (see, e.g., Refs. [3,52]) and η is the particle concentration (to be more specific, the concentration of spheres circumscribing the particles). Note that $g(r)=0$ if $r<2\tilde{a}$, where $\tilde{a}$ is the radius of the spheres circumscribing the particles, while the integral of $\eta g(r)$ over the volume occupied by the scattering medium is equal to $N-1$. For identical spherical particles, $g(r)$ can be calculated using the Percus–Yevick approximation [56].

Note that the above assumption of equal radii of the spheres circumscribing the particles is of secondary importance. It only allows one to write the function $P(\mathbf{R}_i|\mathbf{R}_j)$ in the simple form (29). For a polydisperse ensemble of spherical particles, this function is more complicated, which leads to more convoluted final formulas (see, e.g., Ref. [3]).

Since the particles are randomly positioned and randomly oriented (i.e., the medium is statistically homogeneous and isotropic), the averaging of the coefficients (27) over particle coordinates while accounting for Eq. (28) yields the following equation:

$$\left\langle A_{LM}^{(pn)}(\mathbf{R}_j)\right\rangle_j=\exp(\mathrm{i}\mathbf{k}_0\mathbf{R}_j)\sum_{lm}\kappa_{LMlm}^{(pn)}\delta_{mn}+\eta\sum_{qlm}\kappa_{LMlm}^{(pq)}\times\sum_{l_1m_1}\int\left\langle A_{l_1m_1}^{(qn)}(\mathbf{R}_s)\right\rangle_{js}g(r_{js})H_{lml_1m_1}^{(q)}(\hat{\mathbf{n}}_0,\hat{\mathbf{r}}_{js})\,d\mathbf{R}_s, \tag{30}$$

where $\langle A_{LM}^{(pn)}(\mathbf{R}_j)\rangle_j$ is the configurational average corresponding to a fixed particle j, $\langle A_{l_1m_1}^{(qn)}(\mathbf{R}_s)\rangle_{js}$ is the average corresponding to fixed particles j and s, and the integral in Eq. (30) is taken over the medium volume excluding the volume of the sphere with the radius $2\tilde{a}$ and centered at the point $\mathbf{R}_j$.

The extension of expansion (28) to an arbitrary number of fixed particles supplements Eq. (30) with a hierarchy of equations wherein the configurational average for one fixed particle is determined by the configurational average for two fixed particles. The latter, in turn, is determined by the average for three fixed particles, etc. In the quasi-crystalline approximation, the average for two fixed particles is assumed to be equal to the average for one fixed particle [3,19,50–55]. This assumption

allows one to truncate the hierarchy of equations, which transforms Eq. (30) into the system of equations

$$\left\langle A_{LM}^{(pn)}(\mathbf{R}_j)\right\rangle = \exp(\mathrm{i}\mathbf{k}_0\mathbf{R}_j)\sum_{lm}\kappa_{LMlm}^{(pn)}\delta_{mn} + \eta\sum_{qlm}\kappa_{LMlm}^{(pq)}\sum_{l_1m_1}\int\left\langle A_{l_1m_1}^{(qn)}(\mathbf{R}_s)\right\rangle g(r_{js})H_{lml_1m_1}^{(q)}(\hat{\mathbf{n}}_0,\hat{\mathbf{r}}_{js})d\mathbf{R}_s, \tag{31}$$

where $\langle A_{LM}^{(pn)}(\mathbf{R}_i)\rangle$ is the average for one fixed particle at a point $\mathbf{R}_i$.

To solve system (31), let $\langle A_{LM}^{(pn)}(\mathbf{R}_i)\rangle$ be represented as

$$\left\langle A_{LM}^{(pn)}(\mathbf{R}_i)\right\rangle = B_{LM}^{(pn)}\exp(\mathrm{i}m_{eff}\mathbf{k}_0\mathbf{R}_i), \tag{32}$$

where m_{eff} is the complex effective refractive index of the medium, and the coefficients $B_{LM}^{(pn)}$ are already independent of the position (coordinates) of the scatterer. The approximation (32) is assumed to be valid for all $z_0 \geq 0$, including those in the near-surface layer of the medium with a thickness of approximately several radii $\tilde{a}$, where the depth dependence of $\langle A_{LM}^{(pn)}(\mathbf{R}_i)\rangle$ is expectedly more complex. Moreover, this approximation completely ignores the details of the boundary of the medium, including potential surface roughness. In spite of these drawbacks, this approximation allows one to derive an equation for obtaining m_{eff} with accuracy acceptable in many applications.

When the equality $\mathbf{R}_s = \mathbf{R}_j + \mathbf{r}_{js}$ and relations (32) are taken into account, the system of equations (31) is transformed into

$$B_{LM}^{(pn)}\exp(\mathrm{i}m_{eff}\mathbf{k}_0\mathbf{R}_j) = \exp(\mathrm{i}\mathbf{k}_0\mathbf{R}_j)\sum_{lm}\kappa_{LMlm}^{(pn)}\delta_{mn} + \eta\exp(\mathrm{i}m_{eff}\mathbf{k}_0\mathbf{R}_j)\sum_{qlm}\kappa_{LMlm}^{(pq)}\sum_{l_1m_1}B_{l_1m_1}^{(qn)} \times\int g(r_{js})\exp(\mathrm{i}m_{eff}\mathbf{k}_0\mathbf{r}_{js})H_{lml_1m_1}^{(q)}(\hat{\mathbf{n}}_0,\hat{\mathbf{r}}_{js})d\mathbf{r}_{js}. \tag{33}$$

The substitution of the coefficients (19) in the integral on the right-hand side of Eq. (33) yields

$$\int g(r_{js})\exp(\mathrm{i}m_{eff}\mathbf{k}_0\mathbf{r}_{js})H_{LMlm}^{(q)}(\hat{\mathbf{k}}_0\hat{\mathbf{r}}_{js})d\mathbf{r}_{js} = \frac{2l+1}{2}(-1)^m\sum_{l_1}\mathrm{i}^{-l_1}C_{LMl-m}^{l_1m_1}C_{Lql-q}^{l_10}(J_1+J_2), \tag{34}$$

where $m_1 = M-m$,

$$J_1 = \int(g(r_{js})-1)h_{l_1}(k_0r_{js})D_{m_10}^{l_1}(\hat{\mathbf{n}}_0,\hat{\mathbf{r}}_{js})\exp(\mathrm{i}m_{eff}\mathbf{k}_0\mathbf{r}_{js})d\mathbf{r}_{js}, \tag{35}$$

$$J_2 = \int h_{l_1}(k_0r_{js})D_{m_10}^{l_1}(\hat{\mathbf{n}}_0,\hat{\mathbf{r}}_{js})\exp(\mathrm{i}m_{eff}\mathbf{k}_0\mathbf{r}_{js})d\mathbf{r}_{js}. \tag{36}$$

The integral (35) can be calculated easily by assuming that the point j is at least several radii $\tilde{a}$ deep, so that $g(r) = 1$. Then, after accounting for the representation

$$\exp(\mathrm{i}m_{eff}\mathbf{k}_0\mathbf{r}) = \sum_l \mathrm{i}^l(2l+1)j_l(m_{eff}k_0r)d_{00}^l(\hat{\mathbf{k}}_0\hat{\mathbf{r}}),$$

where $j_l(m_{eff}k_0r)$ is the Bessel spherical function and $d_{00}^l(\hat{\mathbf{k}}_0\hat{\mathbf{r}})$ is the Wigner d function [34], simple calculations yield the following form of the integral (35):

$$J_1 = \frac{4\pi}{k_0^3}\mathrm{i}^{l_1}\delta_{m_10}\int_\rho^\infty(g(x)-1)h_{l_1}(x)j_{l_1}(m_{eff}x)x^2\,dx, \tag{37}$$

where $\rho = 2k_0\tilde{a}$.

Since the coefficients $H_{LMlm}^{(q)}(\hat{\mathbf{k}}_0\hat{\mathbf{r}}_{js})$ and the function $\exp(\mathrm{i}m_{eff}\mathbf{k}_0\mathbf{r}_{js})$ are solutions of the scalar Helmholtz equation, the volume integral (36) can be transformed into the surface integral with the help of Green's theorem (see, e.g., Refs. [3,50–52]). To this end, we write the integral J_2 in the form

$$J_2 = \frac{1}{k_0^2(1-m_{eff}^2)}\int\Big[h_{l_1}(k_0r_{js})D_{m_10}^{l_1}(\hat{\mathbf{n}}_0,\hat{\mathbf{r}}_{js})\Delta\big(\exp(\mathrm{i}m_{eff}\mathbf{k}_0\mathbf{r}_{js})\big) - \exp(\mathrm{i}m_{eff}\mathbf{k}_0\mathbf{r}_{js})\Delta\Big(h_{l_1}(k_0r_{js})D_{m_10}^{l_1}(\hat{\mathbf{n}}_0,\hat{\mathbf{r}}_{js})\Big)\Big]d\mathbf{r}_{js},$$

where Δ is the Laplace operator. With the help of Green's theorem, this integral is transformed into the integral over the surface of the medium minus the integral over the surface of the sphere having a radius $2\tilde{a}$. The former integral can be represented as the integral over a part of the sphere S_∞ of a large radius centered at the point $\mathbf{R}_j$ and the integral over a part of the surface S_m (Fig. 2). The contribution of the integral over S_∞ is zero if the radius of the sphere approaches infinity. Then

$$J_2 = \frac{1}{k_0^2(1-m_{eff}^2)}\int_{S_\infty+S_m-2S_0}\mathbf{n}\cdot\Big[h_{l_1}(k_0r_{js})D_{m_10}^{l_1}(\hat{\mathbf{n}}_0,\hat{\mathbf{r}}_{js}) \times\nabla(\exp(\mathrm{i}m_{eff}\mathbf{k}_0\mathbf{r}_{js})) - \exp(\mathrm{i}m_{eff}\mathbf{k}_0\mathbf{r}_{js})\nabla(h_{l_1}(k_0r_{js})D_{m_10}^{l_1}(\hat{\mathbf{n}}_0,\hat{\mathbf{r}}_{js}))\Big]ds = \frac{1}{k_0^2(1-m_{eff}^2)}(J_{S_m}-J_{2S_0}), \tag{38}$$

where $\mathbf{n}$ is the upward normal along the integration surface.

The integral J_{2S_0} over the surface of the sphere with a radius $2\tilde{a}$ is easily calculated and reduced to the expression

$$J_{2S_0} = 4\pi\mathrm{i}^{l_1}\delta_{m_10}\frac{\rho^2}{k_0}\Big[m_{eff}h_{l_1}(\rho)j_{l_1}'(m_{eff}\rho)-h_{l_1}'(\rho)j_{l_1}(m_{eff}\rho)\Big], \tag{39}$$

where the prime denotes the first derivative. To calculate the integral J_{S_m} over the surface S_m, we use the following representation [57]:

$$y_l(\mathbf{r}) = h_l(kr)P_l(\cos\vartheta) = (-\mathrm{i})^lP_l\left(\frac{1}{\mathrm{i}k}\frac{\partial}{\partial z}\right)h_0(kr),$$

where $P_l(x)$ is the lth degree Legendre polynomial. Then we have [3]

$$J_{S_m} = -\delta_{m_10}\int_S ds\left[y_{l_1}(\mathbf{r})\frac{\partial\exp(\mathrm{i}m_{eff}\mathbf{k}_0\mathbf{r})}{\partial z}-\exp(\mathrm{i}m_{eff}\mathbf{k}_0\mathbf{r})\frac{\partial y_{l_1}(\mathbf{r})}{\partial z}\right]_{z=-z_j} = -2\pi\mathrm{i}^{l_1+1}\delta_{m_10}\frac{1+m_{eff}}{k_0}\exp(-\mathrm{i}m_{eff}\mathbf{k}_0\mathbf{R}_j)\exp(\mathrm{i}\mathbf{k}_0\mathbf{R}_j). \tag{40}$$

Upon taking into account relations (34)–(40) and the unitary property of the CGCs [34], the system of equations (33) takes the form

$$B_{LM}^{(pn)}\exp(\mathrm{i}m_{eff}\mathbf{k}_0\mathbf{R}_j) = \exp(\mathrm{i}\mathbf{k}_0\mathbf{R}_j)\sum_{lm}\kappa_{LMlm}^{(pn)}\delta_{mn} + \frac{3\xi}{2\tilde{x}^3}\exp(\mathrm{i}m_{eff}\mathbf{k}_0\mathbf{R}_j)\sum_{qlm}\kappa_{LMlm}^{(pq)}\sum_{l_1m_1}\delta_{mm_1}(-1)^{m_1}(2l_1+1)$$

$$\times B^{(qn)}_{l_1m_1}F^{(q)}_{ll_1m_1}-\frac{3\mathrm{i}\xi}{4\tilde{x}^3(1-m_{eff})}\exp(\mathrm{i}\mathbf{k}_0\mathbf{R}_j)\sum_{qlm}\kappa^{(pq)}_{LMlm}\delta_{mq}$$
$$\times\sum_{l_1m_1}\delta_{mm_1}\delta_{m_1q}(-1)^{m_1}(2l_1+1)B^{(qn)}_{l_1m_1}. \quad (41)$$

Here $\xi=4\pi\eta\tilde{a}^3/3$ is the filling factor of the circumscribing spheres, $\tilde{x}=k_0\tilde{a}$,

$$F^{(q)}_{LlM}=\sum_{l_1}C^{l_10}_{LMl-M}C^{l_10}_{Lql-q}f_{l_1},$$

$$f_l=\int_\rho^\infty(g(x)-1)h_l(x)j_l(m_{eff}x)x^2\,dx$$
$$-\frac{\rho^2}{1-m^2_{eff}}\left[m_{eff}h_l(\rho)j'_l(m_{eff}\rho)-h'_l(\rho)j_l(m_{eff}\rho)\right].$$

Equality (41) should be obeyed for any $\mathbf{R}_j$ and m_{eff}. Hence, it can be represented by two independent equations, as follows:

$$B^{(pn)}_{LM}-\frac{3\xi}{2\tilde{x}^3}\sum_{qlm}\kappa^{(pq)}_{LMlm}\sum_{l_1m_1}\delta_{mm_1}(-1)^{m_1}(2l_1+1)B^{(qn)}_{l_1m_1}F^{(q)}_{ll_1m_1}=0, \quad (42)$$

$$(1-m_{eff})\sum_{lm}\kappa^{(pn)}_{LMlm}\delta_{mn}$$
$$=\mathrm{i}\frac{3\xi}{4\tilde{x}^3}\sum_{qlm}\kappa^{(pq)}_{LMlm}\delta_{mq}\sum_{l_1m_1}\delta_{mm_1}\delta_{m_1q}(-1)^{m_1}(2l_1+1)B^{(qn)}_{l_1m_1}. \quad (43)$$

The former represents one of the versions of the generalized Lorentz–Lorenz law [3,50–55]. The linear homogeneous system of equations (42) has a non-trivial solution if its determinant is equal to zero. This condition allows us to determine the effective refractive index m_{eff}, which depends on the properties of the medium: the shape, sizes, refractive index, and packing density of the particles.

The second equation, (43), represents one of the versions of the generalized Ewald–Oseen extinction theorem [3]. The first term in Eq. (43) describes the effect of the incident external wave (1) on the particle centered at $\mathbf{R}_j$. The second term describes the fields induced by the particles located at the surface of the medium. Equality (43) is obeyed for arbitrary particles (in the framework of the above assumptions). This means that the sum of the field of the incident wave and the fields induced by all the particles at the surface of the medium is equal to zero. In other words, the particles at the surface of the medium produce the field that cancels the original incident wave. As in the case of point-like Rayleigh particles [33], this cancellation occurs at all points of the medium, including those in the immediate vicinity of its boundary, since the approximation (32) is rather rough.

3.2. Calculation of the coherent field using the Twersky approximation for correlated scatterers

Analytical expressions for the generalized Lorentz–Lorenz law and the generalized Ewald–Oseen extinction theorem can be obtained using another method of ensemble averaging which provides simpler and more instructive representations than that resulting from the quasi-crystalline approximation. This method is based on the formulation of the solution of the system of equations (27) as an expansion in a series by iterations. This series is conveniently interpreted as an order-of-scattering expansion. It is worth noting, however, that such an interpretation is purely mathematical [58] and does not imply that multiple scattering is a real physical phenomenon. The expressions for the scattered field (2) and the systems of equations (18) and (20) are time-independent. These relations describe the radiation scattered by a cluster of particles as if it is a unified, single object. Therefore, the order-of-scattering interpretation does not correspond to a real multiple-scattering process requiring the lag of waves to be accounted for, when considering their propagation between the particles. However, this interpretation facilitates the use of diagrams in order to analyze the resulting iteration series in a simple and ostensive way [1–4,48,59]. In terms of multiple scattering, this series describes all possible scattering schemes, to which "Feynman diagrams" can be assigned. Some of these schemes are shown in Fig. 3. The first diagram corresponds to the first term on the right-hand side of system (27) and, consequently, to single scattering by particle j. After the substitution of this term in the second one in place of $A^{(qn)}_{l_1m_1}(\mathbf{R}_s)$, the latter corresponds to double scattering, first by particle s and then by particle j (the second diagram), etc. The last diagram in Fig. 3 illustrates a scattering sequence that goes through a particle more than once. Such diagrams can also occur for all higher orders of scattering.

The transformations required for ensemble averaging are analogous to those used in the calculation of the coherent field in a sparse medium [4,59]. Specifically, each term of the series can be averaged using the Twersky approximation [4,20,59], whereby all scattering schemes corresponding to the scattering by the same particle more than once (e.g., the last scheme in Fig. 3) are ignored. Unlike the case of a sparse media, for closely packed media it is necessary to consider the correlation in the particle distribution described by Eq. (29) accounting for pair correlations. Finally, the transformations yield a series that is convolved with the system of linear equations congruous with system (31). In other words, the quasi-crystalline approximation is equivalent to

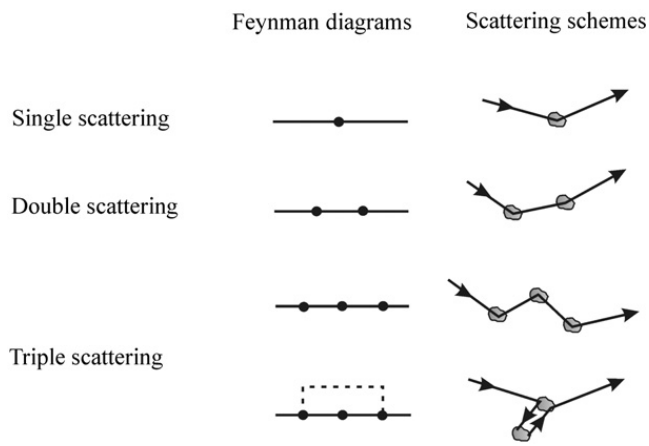

Fig. 3. Scattering schemes and the corresponding diagrams for the first three orders of scattering.

the Twersky approximation if the pair correlations are accounted for [53].

3.3. Random media composed of identical spherical particles

For a medium composed of identical spherical particles, the analytical representations of the generalized Lorentz–Lorenz law and the generalized Ewald–Oseen extinction theorem become much simpler than Eqs. (42) and (43). As follows from Eqs. (11), (12), (15), and (16), the indices in Eq. (41) take the following values: $M=m=m_1=n$, and in the last term, $M=m=m_1=q=n$. This results in the following form of Eqs. (42) and (43):

$$B_{Ln}^{(pn)}+\frac{3\xi}{2\tilde{x}^3}\sum_q a_L^{(pq)}\sum_l(2l+1)B_{ln}^{(qn)}F_{Lln}^{(q)}=0, \tag{44}$$

$$m_{eff}=1+\mathrm{i}\frac{3\xi}{4\tilde{x}^3}\sum_l(2l+1)B_{ln}^{(nn)}, \tag{45}$$

where $a_L^{(pq)}$ is the linear combination of the Lorenz–Mie coefficients (21). Eq. (44) (derived by Mackowski [60] and Tishkovets and Jockers [61]) is essentially identical to the effective propagation constant relations derived by Varadan et al. [52] and Tsang and Kong [3] for a system of identical spherical particles. With regard to the analytical expression for the generalized Ewald–Oseen extinction theorem (45), it is significantly simpler than that given by Tsang and Kong [3]. For sparse media, it yields directly the effective refractive index of the medium.

3.4. Far-field approximation

Let the particles in the medium be in the far zones of each other. Then, accounting for the asymptotic representation (13) and the Clebsch–Gordan series (CGS; [34]), we obtain

$$H_{LMlm}^{(q)}(\hat{\mathbf{n}}_0,\hat{\mathbf{r}}_{js})=\frac{2l+1}{2}\frac{\exp(\mathrm{i}k_0r_{js})}{-\mathrm{i}k_0r_{js}}D_{Mq}^{L}(\hat{\mathbf{n}}_0,\hat{\mathbf{r}}_{sj})D_{mq}^{*l}(\hat{\mathbf{n}}_0,\hat{\mathbf{r}}_{sj}). \tag{46}$$

Note that the Wigner D functions in Eq. (19) depend on the Euler angles determining the rotation of the coordinate systems $\hat{\mathbf{n}}_0\to\hat{\mathbf{r}}_{js}$, while in Eq. (46) they depend on the angles determining the rotation $\hat{\mathbf{n}}_0\to-\hat{\mathbf{r}}_{js}$ (or $\hat{\mathbf{n}}_0\to\hat{\mathbf{r}}_{sj}$).

If the incident radiation propagates normally to the boundary of the medium, the iteration expansion of Eq. (20) yields the following expression:

$$A_{LM}^{(j)(pn)}=a_L^{(j)(pn)}\exp(\mathrm{i}\mathbf{k}_0\mathbf{R}_j)\delta_{Mn}+\sum_q a_L^{(j)(pq)}\sum_{slm}a_l^{(s)(qn)}H_{LMlm}^{(q)}(\hat{\mathbf{n}}_0\hat{\mathbf{r}}_{js})\exp(\mathrm{i}\mathbf{k}_0\mathbf{R}_s)\delta_{mn}+\cdots \tag{47}$$

The first term on the right-hand side corresponds to single scattering by a particle centered at $\mathbf{R}_j$, while the second one corresponds to double scattering. This expansion can be continued to an arbitrary iteration. For sparse media, one may assume that the probability of finding a particle inside a volume element dV is independent of the positions of all the other particles and is given by $P(\mathbf{R}_j)=dV/V_0$, where V_0 is the volume of the scattering medium (see, e.g., Ref. [4]). Then, in the framework of the Twersky approximation, the ensemble averaging of the series (47) is reduced to the calculation of integrals of the same type. One of such integrals results from the averaging of the second term on the right-hand side of Eq. (47). After substituting Eq. (46), the averaging of this term is reduced to the calculation of the following integral:

$$\int d\mathbf{R}_s\frac{\exp(\mathrm{i}k_0r_{js}+\mathrm{i}\mathbf{k}_0\mathbf{R}_s)}{-\mathrm{i}k_0r_{js}}D_{Mq}^{L}(\hat{\mathbf{n}}_0,\hat{\mathbf{r}}_{sj})D_{mq}^{*l}(\hat{\mathbf{n}}_0,\hat{\mathbf{r}}_{sj})=-\delta_{Mq}\delta_{mq}\frac{2\pi}{k_0^3}\mathbf{k}_0\mathbf{R}_j\exp(\mathrm{i}\mathbf{k}_0\mathbf{R}_j). \tag{48}$$

The averaging of the other terms of the series (47) results in a series representing the degree-of-argument expansion of the exponential. Finally, for a medium consisting of identical spherical particles, we obtain

$$\left\langle A_{LM}^{(j)(pn)}(\mathbf{R}_j)\right\rangle=a_L^{(pn)}\exp\left[\mathrm{i}\mathbf{k}_0\mathbf{R}_j\left(1+\mathrm{i}\frac{3\xi}{4\tilde{x}^3}\sum_l(2l+1)a_l^{(nn)}\right)\right]. \tag{49}$$

Comparison with Eq. (32) yields

$$B_{Ln}^{(nn)}=a_L^{(nn)}, \tag{50}$$

$$m_{eff}=1+\mathrm{i}\frac{3\xi}{4\tilde{x}^3}\sum_l(2l+1)a_l^{(nn)}. \tag{51}$$

The substitution of Eq. (50) into Eq. (45) also yields an expression for m_{eff} identical to Eq. (51).

3.5. Dependence of the effective refractive index on particle concentration

According to Eq. (51), the imaginary part of the effective refractive index for a sparse medium depends on the particle concentration linearly. For densely packed media, this dependence is essentially nonlinear. Fig. 4 illustrates

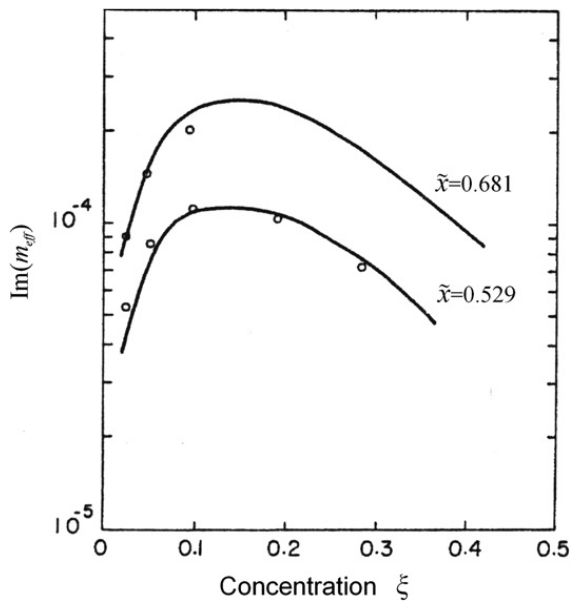

Fig. 4. Dependence of Im(m_{eff}) on the parameter ξ for two media composed of spherical latex particles suspended in water (after Ref. [52]). The curves are labeled by the corresponding particle size parameters $\tilde{x}=0.681$ and 0.529; the refractive index of the particles relative to a vacuum is 1.588. The theoretical data are shown by curves, while the points depict measurement data. The radiation source is a laser beam with a wavelength of $\lambda=632.8$ nm.

the dependence of $\mathrm{Im}(m_{eff})$ on the concentration and sizes of non-absorbing spherical latex particles suspended in water [52]. It can be seen that with increasing particle concentration, the extinction of radiation in the medium first becomes stronger, reaches a maximum, and then weakens. Such a non-monotonic dependence of the extinction on concentration is typical of particles with sizes comparable to or smaller than the wavelength [54,55]. This phenomenon is explained by the fact that the particulate medium becomes essentially continuous in terms of its optical properties when the packing density is sufficiently high. As a consequence, the extinction is mostly determined by the absorption of radiation by the particles and, for non-absorbing particles, $\mathrm{Im}(m_{eff})$ can even tend to zero.

It is worth noting that the effective refractive index m_{eff}, strictly speaking, is not completely analogous to the refractive index of a continuous medium determining the propagation of a time-harmonic electromagnetic wave in the medium [58]. However, the effective refractive index introduced as the bulk characteristic of a particulate medium substantially simplifies the derivation of equations describing multiple scattering. In the following section, we will use this property to derive the RT and WL equations.

Another important aspect should also be noted. The above relations were derived under the assumption that the approximation (32) is valid for all $z_0 \geq 0$. However, in a strongly absorbing medium, this approximation can be violated because the effect of mutual shielding of particles plays an important role and, consequently, the scattering characteristics of the medium are primarily determined by the upper layer of particles [16]. Therefore, the structure of the surface of the medium should be taken into account. This subject, however, is beyond the scope of this review. In the following sections, we assume that the absorption in the medium is not very strong, so that the effects of the surface structure can be ignored.

4. Electromagnetic scattering by discrete random media

4.1. Ladder and cyclical diagrams

For many applications related to remote-sensing studies of different object, especially in planetary astrophysics, the scattering into the backward hemisphere ($\vartheta > \pi/2$) is mostly important and interesting; it will, thus, be our main focus. As a rule, in studies of this kind, the detector receives a collimated beam of radiation. We will, therefore, assume that the receiver is in the far-field zone of the entire system of particles (or the medium), i.e., the scattering angles for all the scatterers in the system (or the medium) are the same.

In the backscattering domain, the coherency (density) matrix $\boldsymbol{\rho}$ (or the Stokes parameters) [3,4,24,46] are determined only by the scattered radiation [4]:

$$\rho_{\mu\nu} \propto \langle E_\mu E_\nu^* \rangle, \tag{52}$$

where $\mu,\nu = \pm 1$, E_μ, E_ν are the components of the field (2) in the CP-representation, the asterisk denotes the complex-conjugate value, and the averaging over the ensemble is denoted by angular brackets. The dimension of the proportionality constant in Eq. (52) depends on the system of physical units used [3,4,24,46]. The 2×2 coherency matrix and four Stokes parameters can be grouped into a 4×1 coherency column vector and a 4×1 Stokes column vector, respectively [4,24].

One of the main characteristics of the scattering object is the 4×4 coherency phase matrix $\mathbf{Z}^{\mathbf{J}}(\mathbf{k}_0,\mathbf{k}_{sc})$ [3,4,24], which transforms the coherency column vector of the incident radiation, $\mathbf{J}^{inc}$, into the coherency column vector of the scattered radiation, $\mathbf{J}^{sc}$ [4]

$$\mathbf{J}^{sc} = \frac{1}{(k_0 r)^2} \mathbf{Z}^{\mathbf{J}}(\mathbf{k}_0,\mathbf{k}_{sc}) \mathbf{J}^{inc}. \tag{53}$$

The explicit form of the matrix $\mathbf{Z}^{\mathbf{J}}(\mathbf{k}_0,\mathbf{k}_{sc})$ follows from the representation (22). Substituting Eq. (22) into Eq. (52) and accounting for Eqs. (23) and (24), we can see that the elements of the matrix $\mathbf{Z}^{\mathbf{J}}(\mathbf{k}_0,\mathbf{k}_{sc})$ are determined by the relations

$$\begin{aligned} &\left\langle S_{pn}(\mathbf{k}_0,\mathbf{k}_{sc}) S_{\mu\nu}^*(\mathbf{k}_0,\mathbf{k}_{sc}) \right\rangle \\ &\quad = \left\langle \sum_j t_{pn}^{(j)}(\mathbf{k}_0,\mathbf{k}_{sc}) t_{\mu\nu}^{*(j)}(\mathbf{k}_0,\mathbf{k}_{sc}) \right\rangle + \left\langle \sum_{j,s\neq j} t_{pn}^{(j)}(\mathbf{k}_0,\mathbf{k}_{sc}) t_{\mu\nu}^{*(s)}(\mathbf{k}_0,\mathbf{k}_{sc}) \right\rangle, \end{aligned} \tag{54}$$

where $p,n,\mu,\nu = \pm 1$.

A relation similar to Eq. (53) can be also written for the Stokes column vector. The matrix $\mathbf{Z}(\mathbf{k}_0,\mathbf{k}_{sc})$ transforming the Stokes column vector of the incident radiation into that of the scattered radiation is called the Stokes phase matrix [4]. The formulas relating the coherency matrix and the Stokes parameters as well as the formulas describing the requisite transformations for representing the phase matrices in the linear-polarization (LP) basis can be found, for example, in the books by Dolginov et al. [46] and Mishchenko et al. [4].

For the random non-chiral (i.e., macroscopically mirror-symmetric) media considered here, the matrix $\mathbf{Z}(\mathbf{k}_0,\mathbf{k}_{sc})$ written in the LP basis contains only eight non-zero elements [4,24]. Specifically, if the Stokes parameters are defined in the same way as by Mishchenko et al. [4], these elements can be written in the following form [4,24,42,61]:

$$\begin{aligned} &Z_{11} = \sum_{pn} \left\langle |S_{pn}|^2 \right\rangle, \; Z_{21} = Z_{12} = -\sum_{pn} \left\langle S_{pn} S_{-pn}^* \right\rangle, \\ &Z_{22} = \sum_{pn} \left\langle S_{pn} S_{-p-n}^* \right\rangle, \; Z_{33} = \sum_{pn} \left\langle S_{pn} S_{-p-n}^* \right\rangle \mathrm{i}^{p-n}, \\ &Z_{44} = \sum_{pn} \left\langle |S_{pn}|^2 \right\rangle \mathrm{i}^{p-n}, \; Z_{43} = -Z_{34} = \mathrm{i} \sum_{pn} \left\langle S_{pn} S_{p-n}^* \right\rangle \mathrm{i}^{p-n}. \end{aligned} \tag{55}$$

Here, for brevity, we omitted the dependence of the matrix (54) on the vectors $\mathbf{k}_0$ and $\mathbf{k}_{sc}$.

Our main objective now is to derive equations for the elements of the matrix (54). The most developed and efficient technique is based on the expansion of the matrix (24) in an order-of-scattering series (recall that the term "order of scattering" is a purely mathematical concept). The substitution of this series in Eq. (54) yields a series containing all possible schemes of scattering to

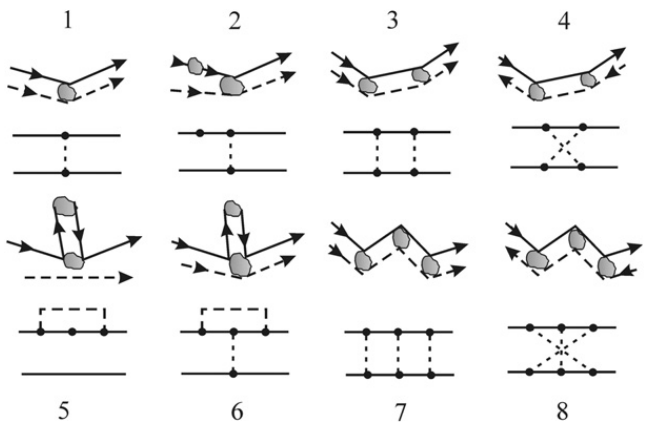

Fig. 5. Scattering schemes and the corresponding diagrams.

which the corresponding Feynman diagrams can be assigned, in analogy to the calculation procedure for the average field. Examples of such scattering schemes and the corresponding diagrams are depicted in Fig. 5. For the sake of definiteness, we will assume that the upper (solid) and lower (dashed) lines in the scattering schemes correspond to the direct (i.e., involving the matrix $\mathbf{S}(\mathbf{k}_0,\mathbf{k}_{sc})$) and complex-conjugate (i.e., involving the matrix $\mathbf{S}^*(\mathbf{k}_0,\mathbf{k}_{sc})$) wave paths, respectively. Diagrams 1, 3, and 7 correspond to single, double, and triple scattering; the direct and complex-conjugate waves propagate in the same direction and along the same string of particles. Diagrams 4 and 8 correspond to double and triple scattering of the direct and complex-conjugate waves propagating along the same string of particles but in opposite directions.

Using the diagram representation, the set of scattering schemes in the order-of-scattering series can be efficiently summed up while avoiding complicated and cumbersome analytical calculations. Let us exemplify this process by calculating the sum of diagrams of types 1 and 2, i.e., all diagrams containing one vertical line. First, we calculate the sum of all similar diagrams containing an arbitrary number of points, for example, in the upper horizontal line on the left of the vertical line. In the summation and averaging over the ensemble of such diagrams, we can use the method described in the preceding section, when summing the diagrams shown in Fig. 3. In analogy with the calculations of the average field, the Twersky approximation is used [4,20]. The result of the summation and averaging can be shown by a diagram of type 1 in Fig. 5, in which the upper horizontal line on the left of the vertical line corresponds to the average field. According to the preceding section, this means that the field exciting a given particle, which is the ensemble-averaged sum of the external incident wave and the waves coming from the other particles, is analytically expressed by the wave corresponding to the propagation constant $m_{eff}k_0$.

An analogous procedure applied to the same diagrams, but with an arbitrary number of points in the lower horizontal line on the left of the vertical line, yields a diagram of type 1, in which the lower left horizontal line corresponds to the complex-conjugate average field. This procedure can be applied to the waves propagating from a given particle to the observation point (or to other particle), i.e., to diagrams containing points lying on the right of the vertical line. This results in a diagram of type 1 in which all horizontal lines correspond to the average field. A similar procedure is applicable to diagrams with two vertical lines, three vertical lines, etc. Its result is a set of diagrams of types 1, 3, 7, etc., where the horizontal lines show the average field. Because of their specific appearance, these diagrams are called ladder diagrams [2–4]. They correspond to the incoherent (diffuse) scattering of radiation by the medium. For a sparse medium, the analytical summation and ensemble averaging of the ladder diagrams leads to the classical vector RTE (VRTE) [4].

The above-described procedure of summing and averaging over the ensemble can also be applied to all diagrams of types 4 and 8. Such diagrams are called cyclical diagrams. They correspond to the interference of a pair of waves propagating along the same string of particles but in opposite directions. In the angular range close to the exact backscattering direction, the interference of such waves is constructive and results in CB[4–10,62–65].

For sparse discrete random media, the methods of summing the ladder and cyclical diagrams are currently rather well developed [2–4,47]. It is assumed that in such media the particles are in the far-field zones of each other, which allows one to ignore other classes of diagrams. However, the approximation of ladder and cyclical diagrams can misrepresent optical effects typical of closely packed media, for example, those related to the near field [12–16,42]. These effects will be considered in the following sections.

Although the diagrammatic method described above is applicable to media of rather complex shapes, we will limit ourselves to a homogeneous isotropic plane–parallel layer. Then the resulting equations are rather simple in appearance, which allows one to solve them numerically and to analyze the dependence of the matrix $\mathbf{Z}^{\mathbf{J}}(\mathbf{k}_0,\mathbf{k}_{sc})$ or $\mathbf{Z}(\mathbf{k}_0,\mathbf{k}_{sc})$ on the properties of the medium. The corresponding scattering geometry is depicted in Fig. 6. The z-axis of the laboratory coordinate system is directed inside the medium, while the xy plane represents its upper boundary. The incident radiation propagates in the meridional plane ($\mathbf{k}_0 z$) determined by the azimuth angle φ_0, while the scattered radiation propagates in the meridional plane ($\mathbf{k}_{sc} z$) determined by

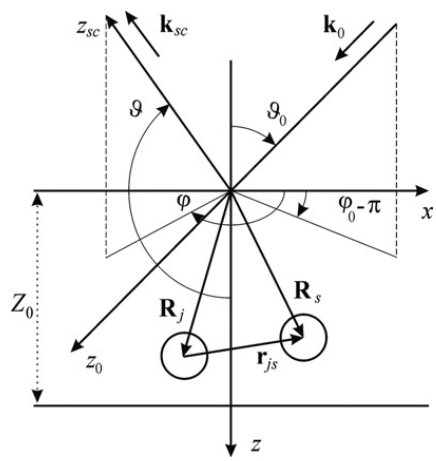

Fig. 6. Scattering by a layer of discrete random medium.

the azimuth angle φ. The layer thickness is Z_0, and the coordinates of the centers of identical spheres circumscribing the particles are defined by the radius-vectors $\mathbf{R}_i$.

The ladder–cyclical approximation allows us to write the elements of the matrix (54) as

$$\left\langle S_{pn}(\mathbf{k}_0,\mathbf{k}_{sc})S^*_{\mu\nu}(\mathbf{k}_0,\mathbf{k}_{sc})\right\rangle = S_{pn\mu\nu} = S^{(L)}_{pn\mu\nu} + S^{(C)}_{pn\mu\nu}, \tag{56}$$

where the matrices $\mathbf{S}^{(L)}$ and $\mathbf{S}^{(C)}$ correspond to incoherent (the sum of the ladder diagrams) and coherent (the sum of the cyclical diagrams) contributions, respectively. Let us first consider the equation for the sum of the ladder diagrams.

4.2. Equation for the incoherent part of the scattered radiation

4.2.1. The ladder approximation for densely packed media

The starting point in the derivation is the matrix (24) and the system of equations (18). To proceed from these relations directly to the calculation of the sums of the ladder and the cyclical diagrams, it is necessary to replace the propagation constant k_0 by $m_{eff}k_0$, i.e., to characterize the medium by the effective refractive index m_{eff}. From simple geometrical considerations, it follows that the changes in the amplitude and phase of the incident wave as it propagates from the entrance point to particle j will be taken into account if the following substitution is made in Eq. (18) [35,47,61]:

$$\mathbf{k}_0\mathbf{R}_j \Rightarrow \mathbf{K}_0\mathbf{R}_j, \tag{57}$$

where

$$\mathbf{K}_0 = \mathbf{k}_0 + k_0\mathbf{n}_0\frac{m_{eff}-1}{\cos\vartheta_0}. \tag{58}$$

Here $\mathbf{n}_0$ is the unit vector along the z-axis. A similar consideration of the wave propagating from particle j to an exit point shows that the changes in the amplitude and phase will be accounted for if the following substitution is made in Eq. (24):

$$\mathbf{k}_{sc}\mathbf{R}_j \Rightarrow \mathbf{K}\mathbf{R}_j, \tag{59}$$

where

$$\mathbf{K} = \mathbf{k}_{sc} + k_0\mathbf{n}_0\frac{m_{eff}-1}{\cos\vartheta}. \tag{60}$$

Then the product of two elements of the amplitude matrix is

$$\begin{aligned} &t^{(j)}_{pn}(\mathbf{k}_0,\mathbf{k}_{sc})t^{*(j)}_{\mu\nu}(\mathbf{k}_0,\mathbf{k}_{sc}) \\ &\quad = \exp(\mathrm{i}\mathbf{R}_j(\mathbf{K}^*-\mathbf{K}))\exp\left[-\mathrm{i}\psi_0(\nu-n)+\mathrm{i}\psi(\mu-p)\right] \\ &\qquad \times\sum_{LMlm}\frac{(2L+1)(2l+1)}{4}A^{(j)(pn)}_{LM}A^{*(j)(\mu\nu)}_{lm}D^{*L}_{Mp}(\hat{\mathbf{n}}_0,\hat{\mathbf{k}}_{sc})D^{l}_{m\mu}(\hat{\mathbf{n}}_0,\hat{\mathbf{k}}_{sc}). \end{aligned} \tag{61}$$

To obtain the equation for the coefficients $A^{(j)(pn)}_{LM}A^{*(j)(\mu\nu)}_{lm}$, let us expand the solution of system (18) into the following order-of-scattering series:

$$\begin{aligned} A^{(j)(pn)}_{LM} &= \exp(\mathrm{i}\mathbf{K}_0\mathbf{R}_j)\sum_{lm}\kappa^{(j)(pn)}_{LMlm}D^{l}_{mn}(\hat{\mathbf{n}}_0,\hat{\mathbf{k}}_0) \\ &\quad + \sum_{qlm}\kappa^{(j)(pq)}_{LMlm}\sum_{sl_1m_1}H^{(q)}_{lml_1m_1}(\hat{\mathbf{n}}_0,\hat{\mathbf{r}}_{js}) \\ &\quad \times\sum_{l_2m_2}\kappa^{(s)(qn)}_{l_1m_1l_2m_2}D^{l_2}_{m_2n}(\hat{\mathbf{n}}_0,\hat{\mathbf{k}}_0)\exp(\mathrm{i}\mathbf{K}_0\mathbf{R}_s)+\cdots \end{aligned} \tag{62}$$

where the coefficients $H^{(q)}_{lml_1m_1}(\hat{\mathbf{n}}_0,\hat{\mathbf{r}}_{js})$ describe the propagation of waves between the particles. In these coefficients, the propagation constant k_0 should also be replaced by $m_{eff}k_0$. The Hankel functions in the coefficients $H^{(q)}_{lml_1m_1}(\hat{\mathbf{n}}_0,\hat{\mathbf{r}}_{js})$ (Eq. (19)) are represented as follows [40]:

$$h_l(k_0x) = \frac{\exp(\mathrm{i}k_0x)}{k_0x}\varsigma_l(k_0x). \tag{63}$$

The function $\varsigma_l(k_0x)$ describes the near field between the particles. It is a finite series that can be calculated using a recurrent relation analogous to that for the Hankel function, with initial values

$$\varsigma_0(x) = -\mathrm{i} \quad \text{and} \quad \varsigma_1(x) = -\left(1+\frac{\mathrm{i}}{x}\right).$$

The changes in the amplitude and phase of the wave propagating between particles can be taken into account if k_0 is replaced by $m_{eff}k_0$ in the exponential of Eq. (63) and the latter is substituted in the coefficients $H^{(q)}_{lml_1m_1}(\hat{\mathbf{n}}_0,\hat{\mathbf{r}}_{js})$ (Eq. (19)).

A series similar to Eq. (62) can be written for a wave with initial and final polarizations ν and μ, respectively. We then multiply the first series by the complex conjugate of the second one. In the resulting series, we keep only the scattering schemes that represent the propagation of both waves along the same path, i.e., those corresponding to ladder diagrams (see Fig. 5). This series can be transformed into the following system of equations [35]:

$$\begin{aligned} A^{(j)(pn)}_{LM}A^{*(j)(\mu\nu)}_{L_1M_1} &= \exp\left[\mathrm{i}\mathbf{R}_j(\mathbf{K}_0-\mathbf{K}^*_0)\right] \\ &\quad + \sum_{lml_1m_1}\kappa^{(j)(pn)}_{LMlm}\kappa^{*(j)(\mu\nu)}_{L_1M_1l_1m_1}D^{l}_{mn}(\hat{\mathbf{n}}_0,\hat{\mathbf{k}}_0)D^{*l_1}_{m_1\nu}(\hat{\mathbf{n}}_0,\hat{\mathbf{k}}_0) \\ &\quad + \sum_{qq_1lml_1m_1}\kappa^{(j)(pq)}_{LMlm}\kappa^{*(j)(\mu q_1)}_{L_1M_1l_1m_1}\sum_{sl_2m_2l_3m_3}A^{(s)(qn)}_{l_2m_2} \\ &\quad \times A^{*(s)(q_1\nu)}_{l_3m_3}H^{(q)}_{lml_2m_2}(\hat{\mathbf{n}}_0,\hat{\mathbf{r}}_{js})H^{*(q_1)}_{l_1m_1l_3m_3}(\hat{\mathbf{n}}_0,\hat{\mathbf{r}}_{js}). \end{aligned} \tag{64}$$

To average relations (61) and (64) over configurations, the quasi-crystalline approximation can be used. The system of equations (64) also contains, of course, the propagation schemes corresponding to the scattering of both waves, direct and complex-conjugate, by the same particle two and more times. As mentioned above, these schemes are ignored in the quasi-crystalline approximation. Thus, only the scattering schemes corresponding to ladder diagrams are kept.

Let us introduce the notation

$$B^{(z)(pn)(\mu\nu)}_{LMlm} = \exp\left[\mathrm{i}(n-\nu)\psi_0\right]\left\langle A^{(j)(pn)}_{LM}A^{*(j)(\mu\nu)}_{lm}\right\rangle,$$

$$\kappa^{(pn)}_{LMlm}\kappa^{*(\mu\nu)}_{L_1M_1l_1m_1} = \left\langle \kappa^{(j)(pn)}_{LMlm}\kappa^{*(j)(\mu\nu)}_{L_1M_1l_1m_1}\right\rangle_{\zeta}.$$

Then, after averaging over configurations, the following relation for the matrix $\mathbf{S}^{(L)}$ per unit area of the upper boundary can be obtained [35]

$$\begin{aligned} S^{(L)}_{pn\mu\nu} &= \frac{\eta}{k_0}\sum_{LMlm}\frac{(2L+1)(2l+1)}{4}D^{*L}_{Mp}(\varphi,\vartheta,0)D^{l}_{m\mu}(\varphi,\vartheta,0) \\ &\quad \times\int_0^{k_0Z_0}B^{(z)(pn)(\mu\nu)}_{LMlm}\exp\left(\frac{\tau z}{\cos\vartheta}\right)dz, \end{aligned} \tag{65}$$

where $\tau = 2\mathrm{Im}(m_{eff})$.

The coefficients $B_{LMlm}^{(z)(pn)(\mu\nu)}$ can be found from the following system of equations:

$$B_{LML_1M_1}^{(z)(pn)(\mu\nu)} = \exp\left(-\frac{\tau z}{\cos\vartheta_0}\right) \times \sum_{lml_1m_1} \kappa_{LMlm}^{(pn)} \kappa_{L_1M_1l_1m_1}^{*(\mu\nu)} D_{mn}^{l}(\varphi_0,\vartheta_0,0) D_{m_1\nu}^{*l_1}(\varphi_0,\vartheta_0,0) + \eta \sum_{qq_1lml_1m_1} \kappa_{LMlm}^{(pq)} \kappa_{L_1M_1l_1m_1}^{*(\mu q_1)} \sum_{l_2m_2l_3m_3} \int g(r_{js}) \times B_{l_2m_2l_3m_3}^{(y)(qn)(q_1\nu)} H_{lml_2m_2}^{(q)}(\hat{\mathbf{n}}_0,\hat{\mathbf{r}}_{js}) H_{l_1m_1l_3m_3}^{*(q_1)}(\hat{\mathbf{n}}_0,\hat{\mathbf{r}}_{js})\, d\mathbf{r}_{js}, \tag{66}$$

where $y = z + k_0 r_{js}\cos\vartheta_{js}$.

Eqs. (65) and (66) describe the incoherent (diffuse) part of the radiation scattered by a densely packed random medium composed of arbitrary particles provided that the spheres circumscribing the particles have the same radius and do not overlap. Under these conditions, it is still problematic to simplify these equations substantially. Even for a medium composed of identical spherical particles they are still too complex, although it is possible to reduce them to a form suitable for numerical analysis [61]. The equations become much simpler under the assumption that the waves propagating between the particles are spherical (implying that the particles are in the far-field zones of each other). This approximation is valid, strictly speaking, only for very sparse media. However, it can be applied, at least for the sake of qualitative analysis, to rather closely packed media provided that the particles are non-absorbing or weakly absorbing. As is evident from Eqs. (19), (63), (64), and (66), the influence of particle s on particle j decreases with increasing the distance between these particles as r_{js}^{-2}. However, the number of such particles s increases as r_{js}^{3}. The influence of particle s on particle j also decreases due to extinction; however, extinction can even decrease with increasing concentration of particles (see Fig. 4) if the medium is not strongly absorbing. As a result, close neighbors may contribute to the radiation exciting a given particle less than the remote particles do. If this is the case then the far-field approximation is justified. In particular, for such media, the approximation based on the classical VRTE, wherein the extinction coefficient and the phase function are calculated by accounting for the correlation between the particles, can be used [3,66].

4.2.2. The ladder approximation for sparse media

We will now derive the equation for the incoherent part of the reflected radiation under the assumption that the particles are in the far-field zones of each other. To avoid cumbersome calculations, we will first obtain the equation for the model of spherical particles and then generalize it to the case of arbitrary particles. In the far-field approximation, the coefficients $H_{LMlm}^{(q)}(\hat{\mathbf{n}}_0,\hat{\mathbf{r}}_{js})$ are determined from Eq. (46). The product of two such coefficients can be represented with the use of Clebsch–Gordan series (CGS; [34]) in the following way:

$$H_{LMlm}^{(q)}(\hat{\mathbf{n}}_0,\hat{\mathbf{r}}_{js}) H_{L_1M_1l_1m_1}^{*(q_1)}(\hat{\mathbf{n}}_0,\hat{\mathbf{r}}_{js}) = \frac{(2l+1)(2l_1+1)}{4} \frac{\exp(-\tau k_0 r_{js})}{(k_0 r_{js})^2} \times \sum_{L_2M_2L_3M_3} (-1)^{M+m} C_{L-ML_1M_1}^{L_2M_2} C_{L-qL_1q_1}^{L_2q_0} C_{l-ml_1m_1}^{L_3M_3} C_{l-ql_1q_1}^{L_3q_0} \times D_{M_2q_0}^{*L_2}(\hat{\mathbf{n}}_0,\hat{\mathbf{r}}_{sj}) D_{M_3q_0}^{L_3}(\hat{\mathbf{n}}_0,\hat{\mathbf{r}}_{sj}), \tag{67}$$

where $q_0 = q_1 - q$.

We now take into account Eqs. (11), (12) and (16), substitute Eq. (67) in Eq. (66), and expand the products of two Wigner D functions into a CGS. Denote

$$\chi_L^{(pn)(\mu\nu)} = \left\langle \chi_L^{(j)(pn)(\mu\nu)} \right\rangle_\zeta, \tag{68}$$

where the angular brackets indicate the averaging over the particle sizes and refractive indices,

$$\chi_{L_1}^{(j)(pn)(\mu\nu)} = \sum_{Ll} \frac{(2L+1)(2l+1)}{4} a_L^{(j)(pn)} a_l^{*(j)(\mu\nu)} C_{L-nl\nu}^{L_1M_0} C_{L-pl\mu}^{L_1N_0},$$

$M_0 = \nu - n$, $N_0 = \mu - p$, and the coefficients $a_L^{(j)(pn)}$ are determined from Eq. (21). Since we assume that the influence of the close neighbors on a given particle is weak relative to that of the distant particles, $g(x) = 1$ can be assumed. Note that the latter assumption is not necessary, and all the transformations can also be made with $g(x) \neq 1$. Accounting for the unitary property of the CGCs yields [47]

$$S_{pn\mu\nu}^{(L)} = \frac{\eta}{k_0} \sum_{LM} D_{MN_0}^{L}(\varphi-\varphi_0,\vartheta,0) \int_0^{k_0 Z_0} \alpha_{LM}^{(z)(pn)(\mu\nu)} \exp\left(\frac{\tau z}{\cos\vartheta}\right) dz, \tag{69}$$

where the coefficients $\alpha_{LM}^{(z)(pn)(\mu\nu)}$ can be determined from the system of equations

$$\alpha_{LM}^{(z)(pn)(\mu\nu)} = \chi_L^{(pn)(\mu\nu)} d_{MM_0}^{L}(\vartheta_0) \exp\left(-\frac{\tau z}{\cos\vartheta_0}\right) + \frac{2\pi\eta}{k_0^3} \sum_{qq_1} \chi_L^{(pq)(\mu q_1)} \sum_l \int \alpha_{lM}^{(y)(qn)(q_1\nu)} \times \exp(-\tau\rho) d_{Mq_0}^{L}(\omega) d_{Mq_0}^{l}(\omega) \sin\omega\, d\omega\, d\rho. \tag{70}$$

Here, ρ,ω are the polar coordinates of the integration point relative to the point z, the angle ω ($0 \le \omega \le \pi$) is measured from the direction of $-\mathbf{n}_0$ (Fig. 7), $y = z - \rho\cos\omega$, and $d_{Mm}^{L}(\vartheta)$ is the Wigner d function [34]. The upper limit of integration over ρ is $z/\cos\omega$ if $\omega < \pi/2$ and $(z - k_0 Z_0)/\cos\omega$ if $\omega > \pi/2$,

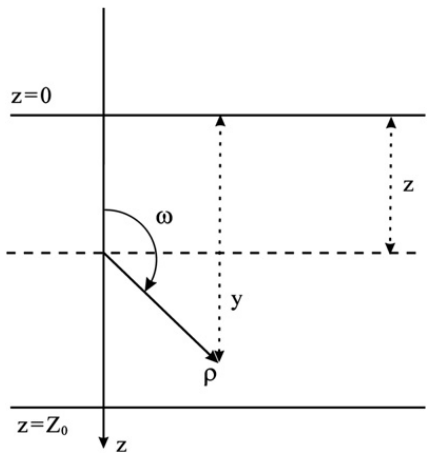

Fig. 7. Explanation of the coefficients appearing in Eq. (70).

i.e., the integral in Eq. (70) stands for

$$\int = \int_0^{\pi/2} \sin\omega d\omega \int_0^{z/\cos\omega} d\rho + \int_{\pi/2}^{\pi} \sin\omega d\omega \int_0^{(z-k_0Z_0)/\cos\omega} d\rho. \tag{71}$$

Relations (69) and (70) represent one of the forms of the classical VRTE for a plane–parallel medium in the CP basis. The coefficients (68) are those in the expansion of the scattering matrix $\tilde{t}^{(j)}_{pn}\tilde{t}^{*(j)}_{\mu\nu}$ (not the phase matrix [24]) of an isolated particle j in Wigner d functions:

$$\tilde{t}^{(j)}_{pn}\tilde{t}^{*(j)}_{\mu\nu} = \sum_L \chi_L^{(j)(pn)(\mu\nu)} d^L_{M_0N_0}(\vartheta).$$

They play an important role in the radiative transfer theory (RTT) [3,4,67]. (More specifically, in the RTT the matrix $\tilde{t}^{(j)}_{pn}\tilde{t}^{*(j)}_{\mu\nu}$ is expanded in generalized spherical functions, which are closely related to the Wigner d functions [34].) To generalize Eqs. (69) and (70) for the case of an arbitrary statistically isotropic medium, one should simply replace the coefficients (68) by the corresponding coefficients for randomly oriented arbitrarily shaped particles. A more general approach to the derivation of the VRTE in the case of arbitrarily shaped and arbitrarily oriented particles is given in Refs [4,68]. Methods for finding the numerical solution of the classical RTE are well developed [4,67].

4.3. Equation for the coherent part of the scattered radiation

4.3.1. Reciprocity relations

The equation for the coherent (interference) part of the reflected radiation is also derived by using the expansion of the system of equations (18) in the corresponding order-of-scattering series. However, the derivation procedure differs significantly. Each cyclical diagram corresponds to the interference of two waves propagating along the same path, but in opposite directions. In the series (62), the wave is first scattered by particle s and finally by particle j. It is easy to write the series corresponding to the wave that is scattered first by particle j, propagates along the same string of particles, but in the opposite direction, and finally is scattered by particle s. However, the direct multiplication of these series yields a series to which the existing methods of ensemble averaging cannot be applied. This problem could be solved if one of the original series were transformed in such a way that the wave propagation direction is reversed, i.e., if the reciprocity principle were applied to one of the series. Let us exemplify this problem by considering double scattering (the second term in Eq. (62)).

From the symmetry relation for the T-matrix (see, e.g., Refs. [3,24])

$$T^{w\nu(j)}_{MLml} = (-1)^{M+m} T^{\nu w(j)}_{-ml-ML} \quad (w,\nu = 1,2),$$

it follows that

$$\kappa^{(j)(pn)}_{LMlm} = (-1)^{l-L+M+m} \frac{2l+1}{2L+1} \kappa^{(j)(np)}_{l-mL-M}. \tag{72}$$

Symmetry relations for the CGCs and Wigner functions [34] result in the following symmetry relation for the coefficients $H^{(q)}_{LMlm}(\hat{\mathbf{n}}_0,\hat{\mathbf{r}}_{js})$:

$$H^{(q)}_{LMlm}(\hat{\mathbf{n}}_0,\hat{\mathbf{r}}_{js}) = (-1)^{L+M+l+m} \frac{2l+1}{2L+1} H^{(q)}_{l-mL-M}(\hat{\mathbf{n}}_0,-\hat{\mathbf{r}}_{js}). \tag{73}$$

Substituting the second term of Eq. (62) in Eq. (24) and accounting for Eqs. (72) and (73) yields

$$\begin{aligned}
&\exp(-\mathrm{i}\mathbf{k}_{sc}\mathbf{R}_j + \mathrm{i}n\psi_0 - \mathrm{i}p\psi) \sum_{LMqlm} \frac{2L+1}{2} \kappa^{(j)(pq)}_{LMlm} D^{*L}_{Mp}(\hat{\mathbf{n}}_0,\hat{\mathbf{k}}_{sc}) \\
&\quad \times \sum_{l_1m_1} H^{(q)}_{lml_1m_1}(\hat{\mathbf{n}}_0,\hat{\mathbf{r}}_{js}) \sum_{l_2m_2} \kappa^{(s)(qn)}_{l_1m_1l_2m_2} D^{l_2}_{m_2n}(\hat{\mathbf{n}}_0,\hat{\mathbf{k}}_0) \exp(\mathrm{i}\mathbf{k}_0\mathbf{R}_s) \\
&= \exp\left[\mathrm{i}\mathbf{k}_0\mathbf{R}_s - \mathrm{i}n(\pi-\psi_0) + \mathrm{i}p(\pi-\psi)\right] \\
&\quad \times \sum_{ql_2m_2l_1m_1} \frac{2l_2+1}{2} \kappa^{(s)(nq)}_{l_2m_2l_1m_1} D^{*l_2}_{m_2n}(\hat{\mathbf{n}}_0,-\hat{\mathbf{k}}_0) \\
&\quad \times \sum_{lm} H^{(q)}_{l_1m_1lm}(\hat{\mathbf{n}}_0,-\hat{\mathbf{r}}_{js}) \sum_{l_2m_2} \kappa^{(j)(qp)}_{lmLM} D^L_{Mp}(\hat{\mathbf{n}}_0,-\hat{\mathbf{k}}_{sc}) \exp(-\mathrm{i}\mathbf{k}_{sc}\mathbf{R}_j).
\end{aligned} \tag{74}$$

Any higher scattering order can be handled analogously. Let $t^{(js)}_{pn}(\mathbf{k}_0,\mathbf{k}_{sc})$ be the amplitude scattering matrix for the radiation with the initial polarization n propagating along the vector $\mathbf{k}_0$, scattered first by particle s, then scattered by particle j in the direction $\mathbf{k}_{sc}$, and having the final polarization p. Then, for any scattering order, Eq. (74) can be written in a compact form as

$$t^{(js)}_{pn}(\mathbf{k}_0,\mathbf{k}_{sc}) = t^{(sj)}_{np}(-\mathbf{k}_{sc},-\mathbf{k}_0). \tag{75}$$

4.3.2. Cyclical diagrams for densely packed media

When the reciprocity relations (74) and (75) are taken into account, the equation for the interference part can be derived in the same way as that for the incoherent part. Let us write the series analogous to that of Eq. (62) for the polarization of the incident and scattered waves μ and ν, respectively. After Eqs. (74) and (75) are applied to each terms of this series, we form the complex-conjugate series and multiply it by the series (62). In each term of the resulting series, we keep only the schemes that correspond to cyclical diagrams (see Fig. 5). The resulting series can be transformed into the following equation [35]:

$$\begin{aligned}
&\sum_{\sigma\neq j} t^{(j)}_{pn}(\mathbf{k}_0,\mathbf{k}_{sc}) t^{*(\sigma)}_{\nu\mu}(\mathbf{k}_0,\mathbf{k}_{sc}) + t^{(0j)}_{pn}(\mathbf{k}_0,\mathbf{k}_{sc}) t^{*(0j)}_{\nu\mu}(\mathbf{k}_0,\mathbf{k}_{sc}) \\
&\quad = \exp\left[-\mathrm{i}\mathbf{R}_j(\mathbf{K}+\mathbf{K}_0^*)\right] \exp\left[\mathrm{i}\psi(\nu-p) - \mathrm{i}\psi_0(\mu-n) + \mathrm{i}\pi(\mu-\nu)\right] \\
&\quad \times \sum_{LMlm} \frac{(2L+1)(2l+1)}{4} A^{(j)(pn)}_{LM} A^{*(j)(\mu\nu)}_{lm} D^{*L}_{Mp}(\hat{\mathbf{n}}_0,\hat{\mathbf{k}}_{sc}) D^l_{m\mu}(\hat{\mathbf{n}}_0,-\hat{\mathbf{k}}_0),
\end{aligned} \tag{76}$$

where the matrix $t^{(0j)}_{pn}(\mathbf{k}_0,\mathbf{k}_{sc}) = \exp[\mathrm{i}\mathbf{R}_j(\mathbf{K}_0-\mathbf{K})]\tilde{t}^{(j)}_{pn}(\mathbf{k}_0,\mathbf{k}_{sc})$ corresponds to single scattering and the product $A^{(j)(pn)}_{LM} A^{*(j)(\mu\nu)}_{lm}$ is determined from the following system of equations:

$$\begin{aligned}
A^{(j)(pn)}_{LM} A^{*(j)(\mu\nu)}_{L_1M_1} &= \exp[\mathrm{i}\mathbf{R}_j(\mathbf{K}_0+\mathbf{K}^*)] \sum_{lml_1m_1} \kappa^{(j)(pn)}_{LMlm} \kappa^{*(j)(\mu\nu)}_{L_1M_1l_1m_1} \\
&\quad \times D^l_{mn}(\hat{\mathbf{n}}_0,\hat{\mathbf{k}}_0) D^{*l_1}_{m_1\nu}(\hat{\mathbf{n}}_0,-\hat{\mathbf{k}}_{sc}) \\
&\quad + \sum_{qq_1lml_1m_1} \kappa^{(j)(pq)}_{LMlm} \kappa^{*(j)(\mu q_1)}_{L_1M_1l_1m_1} \sum_{sl_2m_2l_3m_3} A^{(s)(qn)}_{l_2m_2} A^{*(s)(q_1\nu)}_{l_3m_3} \\
&\quad \times H^{(q)}_{lml_2m_2}(\hat{\mathbf{n}}_0,\hat{\mathbf{r}}_{js}) H^{*(q_1)}_{l_1m_1l_3m_3}(\hat{\mathbf{n}}_0,\hat{\mathbf{r}}_{js}).
\end{aligned} \tag{77}$$

The propagation and extinction of the waves between the scatterers is described here by the coefficients $H^{(q)}_{LMlm}(\hat{\mathbf{n}}_0,\hat{\mathbf{r}}_{js})$, analogously to the system of equations (64). Like Eq. (64), the system (77) contains scattering schemes corresponding to direct and complex-conjugate sequences involving the same scatterer more than once. After omitting these schemes, the system (77) corresponds to the sum of cyclical diagrams only.

Let us now average the expressions (76) and (77) over the ensemble. Denote

$$F^{(z)(pn)(\mu\nu)}_{LMlm} = \exp(\mathrm{i}\nu\psi - \mathrm{i}\nu\pi + \mathrm{i}n\psi_0) \times \exp[-\mathrm{i}\mathbf{R}_j(\mathbf{k}_0+\mathbf{k}_{sc})]\left\langle A^{(j)(pn)}_{LM} A^{*(j)(\mu\nu)}_{lm}\right\rangle_\zeta,$$

where the angular brackets indicate the averaging over the orientations and microphysical properties of the particles. Applying the quasi-crystalline approximation yields

$$S^{(C)}_{pn\nu\mu} + S^1_{pn\nu\mu} = \frac{\eta}{k_0}\sum_{LMlm}\frac{(2L+1)(2l+1)}{4} \times D^{*L}_{Mp}(\varphi,\vartheta,0)D^{l}_{m\mu}(\pi+\varphi_0,\pi-\vartheta_0,0) \times \int_0^{k_0Z_0} F^{(z)(pn)(\mu\nu)}_{LMlm}\exp(-\mathrm{i}\tilde{\varepsilon}z)\,dz, \tag{78}$$

where the matrix $\mathbf{S}^1$ corresponds to single scattering, the matrices $\mathbf{S}^{(C)}$ and $\mathbf{S}^1$ are per unit area of the upper boundary of the medium,

$$\tilde{\varepsilon} = \left(\frac{m_{eff}-1}{\cos\vartheta} + \frac{m^*_{eff}-1}{\cos\vartheta_0}\right),$$

and the coefficients $F^{(z)(pn)(\mu\nu)}_{LMlm}$ are determined from the following system of equations:

$$\begin{aligned}\mathsf{F}^{(z)(pn)(\mu\nu)}_{LML_1M_1} &= \exp(\mathrm{i}\tilde{\varepsilon}^*z) \times \sum_{lml_1m_1}\kappa^{(pn)}_{LMlm}\kappa^{*(\mu\nu)}_{L_1M_1l_1m_1}D^{l}_{mn}(\varphi_0,\vartheta_0,0)D^{*l_1}_{m_1\nu}(\pi+\varphi,\pi-\vartheta,0)\\ &+\eta\sum_{qq_1lml_1m_1}\kappa^{(pq)}_{LMlm}\kappa^{*(\mu q_1)}_{L_1M_1l_1m_1}\sum_{l_2m_2l_3m_3}\int g(r_{js})F^{(y)(qn)(q_1\nu)}_{l_2m_2l_3m_3}\\ &\times H^{(q)}_{lml_2m_2}(\hat{\mathbf{n}}_0,\hat{\mathbf{r}}_{js})H^{*(q_1)}_{l_1m_1l_3m_3}(\hat{\mathbf{n}}_0,\hat{\mathbf{r}}_{js})\exp[\mathrm{i}\mathbf{r}_{js}(\mathbf{k}_0+\mathbf{k}_{sc})]\,d\mathbf{r}_{js},\end{aligned} \tag{79}$$

where $y = z + k_0 r_{js}\cos\vartheta_{js}$.

Eqs. (78) and (79) describe the sum of the cyclical diagrams for a plane–parallel layer of densely packed discrete random medium. Like the equation for the sum of the ladder diagrams, they become substantially simpler only under the assumption that the waves propagating between the particles are spherical. As follows from the preceding section, the far-field approximation can be applied to moderately and weakly absorbing media, at least for a qualitative analysis of the multiple-scattering effects. In the next subsection, we will use this approximation and the model of spherical particles to derive an equation describing the WL effect. As was the case with incoherent scattering, the final equations will be generalized to the case of arbitrary particles.

4.3.3. Cyclical diagrams for sparse media

As a first step, we exclude from the consideration the single-scattering contribution, i.e., the first term on the right-hand sides of Eqs. (77) and (79). To this end, we substitute Eq. (79) in Eq. (78) and use the following representation:

$$\begin{aligned}&D^{*L}_{Mp}(\varphi,\vartheta,0)D^{L_1}_{M_1\mu}(\pi+\varphi_0,\pi-\vartheta_0,0)\\ &\quad= (-1)^{L_1}\exp(-\mathrm{i}p\psi-\mathrm{i}\mu\psi_0)D^{*L}_{Mp}(\hat{\mathbf{n}}_0,\hat{\mathbf{k}}_{sc})D^{L_1}_{M_1-\mu}(\hat{\mathbf{n}}_0,\hat{\mathbf{k}}_0)\\ &\quad= (-1)^{L_1}\exp(-\mathrm{i}p\psi-\mathrm{i}\mu\psi_0)\sum_m D^{*L}_{Mm}(\hat{\mathbf{n}}_0,\hat{\mathbf{k}}_0)\\ &\quad\times D^{*L}_{mp}(\hat{\mathbf{k}}_0,\hat{\mathbf{k}}_{sc})D^{L_1}_{M_1-\mu}(\hat{\mathbf{n}}_0,\hat{\mathbf{k}}_0).\end{aligned} \tag{80}$$

In Eq. (80), we expand the product of two Wigner D functions of the same argument in the CGS and substitute it in Eq. (78). Accounting for relations (11), (12), (16), and (46) and the expansion analogous to Eq. (67),

$$\begin{aligned}&H^{(q)}_{LMlm}(\hat{\mathbf{n}}_0,\hat{\mathbf{r}}_{js})H^{*(q_1)}_{L_1M_1l_1m_1}(\hat{\mathbf{n}}_0,\hat{\mathbf{r}}_{js})\\ &\quad= \frac{(2l+1)(2l_1+1)}{4}\frac{\exp(-\tau k_0 r_{js})}{(k_0r_{js})^2}\sum_{L_2M_2}(-1)^{M+q}C^{L_2M_2}_{L-ML_1M_1}\\ &\quad\times C^{L_2q_0}_{L-qL_1q_1}D^{*L_2}_{M_2q_0}(\hat{\mathbf{n}}_0,\hat{\mathbf{r}}_{sj})D^{*l}_{mq}(\hat{\mathbf{n}}_0,\hat{\mathbf{r}}_{sj})D^{l_1}_{m_1q_1}(\hat{\mathbf{n}}_0,\hat{\mathbf{r}}_{sj}),\end{aligned}$$

yields

$$S^{(C)}_{pn\nu\mu} = \frac{2\pi\eta^2}{k_0^4}\sum_{qq_1LM}(-1)^L\exp(\mathrm{i}M\varphi_1)\theta^{*(q_1\mu)(qp)}_{LM} \times \int_0^{k_0Z_0}\beta^{(z)(qn)(q_1\nu)}_{LM}\exp(-\varepsilon_1 z)\,dz. \tag{81}$$

Here,

$$\theta^{*(q_1\mu)(qp)}_{LM} = \exp(-\mathrm{i}p\psi-\mathrm{i}\mu\psi_0)\sum_{M_1}\Theta^{*(q_1\mu)(qp)}_{LM_1}D^{L}_{MM_1}(\hat{\mathbf{n}}_0,\hat{\mathbf{k}}_0), \tag{82}$$

$$\Theta^{(pn)(\mu\nu)}_{L_1M} = \sum_{Ll}\frac{(2L+1)(2l+1)}{4}\left\langle a^{(j)(pn)}_L a^{*(j)(\mu\nu)}_l\right\rangle_\zeta \times(-1)^{l+m}C^{L_1M}_{L-nl-m}C^{L_1\mu-p}_{L-pl\mu}D^{l}_{m\nu}(\hat{\mathbf{k}}_0,\hat{\mathbf{k}}_{sc}),$$

$m=-M-n$, the coefficients $a^{(j)(pn)}_L$ and $a^{(j)(\mu\nu)}_l$ are defined by Eq. (21),

$$\varepsilon_1 = \mathrm{i}\left(\frac{m_{eff}-1}{\cos\vartheta} + \frac{m^*_{eff}-1}{\cos\vartheta_0} + 2\cos\frac{\vartheta_{sc}}{2}\cos\vartheta_1\right),$$

$$\begin{aligned}\beta^{(z)(qn)(q_1\nu)}_{LM} &= \frac{k_0^3}{2\pi}(-1)^q\exp\left(\mathrm{i}2z\cos\frac{\vartheta_{sc}}{2}\cos\vartheta_1 - \mathrm{i}M\varphi_1\right)\\ &\times\sum_{lml_1m_1}\int F^{(y)((qn)(q_1\nu)}_{lml_1m_1}\frac{(2l+1)(2l_1+1)}{4}\\ &\times\frac{\exp\left[\mathrm{i}\mathbf{r}_{js}(\mathbf{k}_0+\mathbf{k}_{sc})-\tau k_0 r_{js}\right]}{(k_0r_{js})^2}\\ &\times D^{*L}_{Mq_0}(\hat{\mathbf{n}}_0,\hat{\mathbf{r}}_{sj})D^{*l}_{mq}(\hat{\mathbf{n}}_0,\hat{\mathbf{r}}_{sj})D^{l_1}_{m_1q_1}(\hat{\mathbf{n}}_0,\hat{\mathbf{r}}_{sj})\,d\mathbf{r}_{js},\end{aligned} \tag{83}$$

and ϑ_1,φ_1 are the spherical angles of the vector $\mathbf{k}_1 = \mathbf{k}_0 + \mathbf{k}_{sc}$ in the coordinate system $\hat{\mathbf{n}}_0$.

The system of equations for the coefficients (83) follows from system (79). After simple, though cumbersome transformations, it is reduced to the system of equations [47]

$$\beta^{(z)(pn)(\mu\nu)}_{LM} = \exp(-\varepsilon^*_1 z)\overline{B}^{(z)(pn)(\mu\nu)}_{LM} + \frac{2\pi\eta}{k_0^3}\sum_{qq_1lm}\chi^{(pq)(\mu q_1)}_L \mathrm{i}^{M-m}\int\beta^{(y)(qn)(q_1\nu)}_{lm}\exp(-\tau\rho)$$

$$\times d^{L}_{MN_0}(\omega)d^{l}_{mN_0}(\omega)J_{m-M}\left(2\rho\sin\vartheta_1\cos\frac{\vartheta_{sc}}{2}\sin\omega\right)$$
$$\times\sin\omega\, d\omega\, d\rho. \tag{84}$$

Here $N_0=\mu-p$, $J_m(x)$ is the Bessel function, the angle ω is the same as in system (70), and the integral in Eq. (84) is defined according to Eq. (71) (see Fig. 7).

The coefficients $\overline{B}^{(z)(pn)(\mu\nu)}_{LM}$ correspond to double scattering and take the form

$$\overline{B}^{(z)(pn)(\mu\nu)}_{LM}=\sum_{lm}\exp(-im\varphi_1)\theta^{(pn)(\mu\nu)}_{lm}i^{M-m}\int\exp(-\tilde{\tau}\rho)$$
$$\times d^{L}_{MN_0}(\omega)d^{l}_{mN_0}(\omega)J_{m-M}\left(2\rho\sin\vartheta_1\cos\frac{\vartheta_{sc}}{2}\sin\omega\right)$$
$$\times\sin\omega\, d\omega\, d\rho, \tag{85}$$

where $\tilde{\tau}=2\mathrm{Im}(m_{eff})-\varepsilon_1^*\cos\omega$.

The coefficients $\theta^{(pn)(\mu\nu)}_{LM}$ given by Eq. (82) are independent of the angles ψ_0 and ψ. With the use of the addition theorem for the Wigner D functions and the CGS, they can be expressed as [47]

$$\theta^{(pn)(\mu\nu)}_{LM}=(-1)^{M-n}\sum_{L_1M_1lm}\frac{(2L_1+1)(2l+1)}{4}\left\langle a^{(j)(pn)}_{L_1}a^{*(j)(\mu\nu)}_{l}\right\rangle_{\zeta}$$
$$\times(-1)^{l}C^{LM}_{L_1-M_1l-m}C^{L\mu-p}_{L_1-pl\mu}D^{L_1}_{M_1n}(\varphi_0,\vartheta_0,0)D^{l}_{m\nu}(\varphi,\vartheta,0).$$

WL manifests itself in a narrow range of angles close to the exact backscattering direction. If in this range the elements of the scattering matrix of an individual particle (averaged over the particle characteristics) depend weakly on the scattering angle then the coefficients $\theta^{(pn)(\mu\nu)}_{LM}$ can be simplified. In the limit $\mathbf{k}_{sc}\to-\mathbf{k}_0$ the approximate equality $D^{l}_{m\nu}(\varphi,\vartheta,0)\approx(-1)^{l}D^{l}_{m-\nu}(\varphi_0,\vartheta_0,0)$ holds. Then the coefficients $\theta^{(pn)(\mu\nu)}_{LM}$ take the form

$$\theta^{(pn)(\mu\nu)}_{LM}\approx(-1)^{M-n}D^{L}_{-M,\nu-n}(\varphi_0,\vartheta_0,0)\chi^{(pn)(\mu\nu)}_{L}$$
$$=(-1)^{\nu}D^{*L}_{M,n-\nu}(\varphi_0,\vartheta_0,0)\chi^{(pn)(\mu\nu)}_{L}. \tag{86}$$

Eqs. (81)–(85) describe the interference part of the scattered radiation. They can be generalized for the media composed of non-spherical randomly oriented particles in the same way as the equations for the incoherent part. Specifically, the coefficients $\chi^{(pn)(\mu\nu)}_{L}$ and $\theta^{(pn)(\mu\nu)}_{lm}$ should be replaced by the corresponding coefficients for non-spherical particles. Relation (86) can be used in this generalization.

Eqs. (81)–(85) are valid under the same conditions as the RTE. However, the equations for the interference part are much more complex than the RTE. Unlike Eqs. (69) and (70), the system of Fredholm equations (84) has an oscillating kernel and an oscillating external term. Equations of this kind are very difficult to solve numerically. Below, we will consider one of the approximate methods for solving the equation for the coherent part of the reflected radiation. It is based on certain relations between the elements of the matrices for the coherent and incoherent components in the exact backscattering direction.

4.3.4. Exact backscattering direction

The direction of exact backscattering ($\mathbf{k}_{sc}=-\mathbf{k}_0$) is of particular interest for the interpretation of radar and lidar observations of different objects. In this direction, the coherent intensity is maximal and can be comparable to the diffuse (incoherent) intensity [3,4,8,62,65,69,70].

For $\mathbf{k}_{sc}=-\mathbf{k}_0$, comparison of Eqs. (78) and (79) with Eqs. (65) and (66) yields

$$S^{(L)}_{pn\mu\nu}=S^{(C)}_{pn\nu\mu}+S^{1}_{pn\nu\mu}. \tag{87}$$

In the LP basis, these relations become more complicated. Recalling Eqs. (54) and (56), we obtain from the matrices (55) and (87):

$$2Z^{(C)}_{11}+2Z^{(1)}_{11}=Z^{(L)}_{11}+Z^{(L)}_{22}-Z^{(L)}_{33}+Z^{(L)}_{44}, \tag{88}$$

$$2Z^{(C)}_{22}+2Z^{(1)}_{22}=Z^{(L)}_{11}+Z^{(L)}_{22}+Z^{(L)}_{33}-Z^{(L)}_{44}, \tag{89}$$

$$2Z^{(C)}_{33}+2Z^{(1)}_{33}=-Z^{(L)}_{11}+Z^{(L)}_{22}+Z^{(L)}_{33}+Z^{(L)}_{44}, \tag{90}$$

$$2Z^{(C)}_{44}+2Z^{(1)}_{44}=Z^{(L)}_{11}-Z^{(L)}_{22}+Z^{(L)}_{33}+Z^{(L)}_{44}, \tag{91}$$

where the matrices $\mathbf{Z}^{(C)}$ and $\mathbf{Z}^{(L)}$ correspond to the coherent and incoherent parts of the reflected radiations, respectively, and the matrix $\mathbf{Z}^{(1)}$ represents single scattering.

Equalities (88)–(91) were initially derived for sparse media by Mishchenko [70] with the use of the Saxon's reciprocity relation [71]. However, as one can see, they are also valid for densely packed media. Relations (87) and (88)–(91) are important, since they allow one to calculate all the observable characteristics of WL for the direction $\mathbf{k}_{sc}=-\mathbf{k}_0$ directly from the solution of the RTE.

It is worth noting that equalities analogous to Eqs. (87) and (88)–(91) are valid for any system of particles, as is seen from Eqs. (61), (64), (76), and (77). They follow from the reciprocity relation (75).

4.4. Approximate method for solving the equation for the coherent part of radiation reflected by a semi-infinite discrete random medium

4.4.1. Basic equations

The equations describing WL are very difficult to analyze. In Refs. [72–75], they were solved using the double-scattering approximation, which allows one to analyze WL as a function of medium properties. The quantitative description of the angular dependences of WL characteristics is a real challenge even in the framework of the far-field approximation (i.e., for sparse media). This problem has been fully solved only for a semi-infinite medium composed of non-absorbing Rayleigh scatterers provided that the incident radiation propagates normally to the boundary of the medium [76,77]. Therefore, numerical modeling of CB is sometimes based on Monte-Carlo methods [78]. Unfortunately, this requires considerable expenses of computer time and becomes impracticable in the case of a medium composed of polydisperse and/or non-spherical particles. Below we consider a simple approximate method for the numerical solution of the equation for the coherent part of the reflected radiation in the case of a semi-infinite medium illuminated by external radiation propagating perpendicularly to the boundary of the medium.

If the radiation propagates perpendicularly to the boundary of the medium, the angles defining Eqs. (81)–(85) are as follows:

$$\vartheta_0=0,\quad \vartheta_1=\tfrac{\vartheta}{2},\quad \vartheta_{sc}=\vartheta,\quad \phi_1=\phi,$$

while the coefficients $\theta_{lm}^{(pn)(\mu\nu)}$ take the form

$$\theta_{LM}^{(pn)(\mu\nu)}=\exp(\mathrm{i}n(\varphi-\varphi_0)+\mathrm{i}M\phi)\tilde{\Theta}_{LM}^{(pn)(\mu\nu)},$$

where

$$\tilde{\Theta}_{L_1M_1}^{(pn)(\mu\nu)}=\sum_{Llm}\frac{(2L+1)(2l+1)}{4}\times\left\langle a_L^{(j)(pn)}a_l^{*(j)(\mu\nu)}\right\rangle_\zeta(-1)^{l+m}C_{L-nl-m}^{L_1M_1}C_{L-pl\mu}^{L_1\mu-p}d_{m\nu}^l(\vartheta)$$

and $m=-M_1-n$.

Then Eq. (81) can be reduced to read [47,79]

$$S_{pn\nu\mu}^{(C)}=\frac{2\pi\eta^2}{k_0^4}\exp[\mathrm{i}(n-\mu)(\varphi-\varphi_0)]\sum_{qq_1LM}(-1)^L\tilde{\Theta}_{LM}^{*(q_1\mu)(qp)}\times\int_0^{k_0Z_0}\beta_{LM}^{(z)(qn)(q_1\nu)}\exp(-\tilde{\varepsilon}_1z)\,dz,\tag{92}$$

where

$$\tilde{\varepsilon}_1=\mathrm{Im}(m_{eff})\left(1-\frac{1}{\cos\vartheta}\right)+\mathrm{i}(1+\cos\vartheta)\left(\frac{\mathrm{Re}(m_{eff})-1}{\cos\vartheta}+1\right),$$

and the coefficients $\beta_{LM}^{(z)(qn)(q_1\nu)}$ are determined from the following system of equations:

$$\beta_{LM}^{(z)(pn)(\mu\nu)}=\exp(-\tilde{\varepsilon}_1^*z)\tilde{B}_{LM}^{(z)(pn)(\mu\nu)}+\frac{2\pi\eta}{k_0^3}\sum_{qq_1lm}\chi_l^{(pq)(\mu q_1)}\mathrm{i}^{M-m}\int\beta_{lm}^{(y)(qn)(q_1\nu)}\exp(-\tau\rho)\times d_{MN_0}^L(\omega)d_{mN_0}^l(\omega)J_{m-M}(\rho\sin\vartheta\sin\omega)\sin\omega\,d\omega\,d\rho.\tag{93}$$

The coefficients $\tilde{B}_{LM}^{(z)(pn)(\mu\nu)}$ corresponding to double scattering take the form

$$\tilde{B}_{LM}^{(z)(pn)(\mu\nu)}=\sum_{lm}\tilde{\Theta}_{lm}^{(pn)(\mu\nu)}\mathrm{i}^{M-m}\int\exp(-\rho\tilde{\tau}_1)\times d_{MN_0}^L(\omega)d_{mN_0}^l(\omega)J_{m-M}(\rho\sin\vartheta\sin\omega)\sin\omega\,d\omega\,d\rho,\tag{94}$$

where $\tilde{\tau}_1=2\mathrm{Im}(m_{ef})-\tilde{\varepsilon}_1^*\cos\omega$. Recall now that the integrals in Eqs. (93) and (94) are defined according to Eq. (71). In Eqs. (93) and (94), the upper limit of integration over ρ is $z/\cos\omega$ if $\omega<\pi/2$ (for downwelling radiation) and approaches infinity if $\omega>\pi/2$ (for upwelling radiation) (see Fig. 7).

The azimuthal dependence in Eq. (92) is caused by the definition of the Stokes parameters of the incident and scattered radiation with respect to different meridional planes. If the radiation propagates perpendicularly to the boundary of the medium then the Stokes parameters can be defined with respect to the planes going through the vectors $\mathbf{k}_0$ and $\mathbf{k}_{sc}$. Then $\exp[\mathrm{i}(n-\mu)(\varphi-\varphi_0)]=1$, and the azimuthal dependence disappears.

Let us denote

$$\gamma_{LM}^{(pn)(\mu\nu)}=2\mathrm{Re}(\tilde{\varepsilon}_1)\int_0^\infty\beta_{LM}^{(z)(pn)(\mu\nu)}\exp(-\tilde{\varepsilon}_1z)\,dz.\tag{95}$$

Then the matrix Eq. (92) becomes

$$S_{pn\nu\mu}^{(C)}=\frac{\pi\eta^2}{k_0^4\mathrm{Re}(\tilde{\varepsilon}_1)}\sum_{qq_1LM}(-1)^L\tilde{\Theta}_{LM}^{*(q_1\mu)(qp)}\gamma_{LM}^{(qn)(q_1\nu)}.\tag{96}$$

To derive an equation for the coefficients $\gamma_{LM}^{(qn)(q_1\nu)}$ appearing in Eq. (96), we multiply the coefficients of Eq. (93) by $2\mathrm{Re}(\tilde{\varepsilon}_1)\exp(-\tilde{\varepsilon}_1z)$ and integrate over z. The integration of the first term on the right-hand side of Eq. (93) yields the following result [72–74]:

$$Q_{LM}^{(pn)(\mu\nu)}=2\mathrm{Re}(\tilde{\varepsilon}_1)\int_0^\infty\tilde{B}_{LM}^{(z)(pn)(\mu\nu)}\exp(-\tilde{\varepsilon}_1z)\,dz=\sum_{lm}\tilde{\Theta}_{lm}^{(pn)(\mu\nu)}\int_0^\pi d_{MN_0}^L(\omega)d_{mN_0}^l(\omega)I_{|m-M|}(c,f)\sin\omega\,d\omega.$$

Here,

$$I_m(c,f)=\mathrm{i}^{-m}\frac{c^m}{\sqrt{c^2+f^2}(f+\sqrt{c^2+f^2})^m},\tag{97}$$

$$c=\sin\theta\sin\omega,$$

and

$$f=2\mathrm{Im}(m_{eff})+|\cos\omega|\mathrm{Im}(m_{eff})\left(1-\frac{1}{\cos\vartheta}\right)+\mathrm{i}\cos\omega(1+\cos\vartheta)\left(\frac{\mathrm{Re}(m_{eff})-1}{\cos\vartheta}+1\right).$$

The integration of the second term on the right-hand side of Eq. (93) corresponding to the radiation coming to the point z "from above" (see Eq. (71) and Fig. 7), is not very complicated and yields [80]

$$2\mathrm{Re}(\tilde{\varepsilon}_1)\mathrm{i}^{M-m}\int_0^\infty\exp(-\tilde{\varepsilon}_1z)\,dz\times\int_0^{z/\cos\omega}\beta_{lm}^{(y)(qn)(q_1\nu)}\exp(-\tau\rho)J_{m-M}(c\rho)\,d\rho=\gamma_{lm}^{(qn)(q_1\nu)}I_{|m-M|}(c,f).$$

The main complexity lies in the integration of the term corresponding to the radiation coming "from below" (Fig. 7). We will calculate it approximately, assuming that

$$\beta_{lm}^{(y)(qn)(q_1\nu)}\approx\beta_{lm}^{(z)(qn)(q_1\nu)}\exp(-w\tau\rho|\cos\omega|).\tag{98}$$

In other words, we assume that the coefficient $\beta_{lm}^{(y)(qn)(q_1\nu)}$ at a point y can be approximately represented as the value of this coefficient at the point z multiplied by $\exp(-w\tau\rho|\cos\omega|)$, where w is a parameter whose value can be determined from a certain condition. In the RT theory for a semi-infinite atmosphere, a representation similar to Eq. (98) is applied in order to describe the radiation field at large optical depths [81]. However, the corresponding equation is valid only for very large optical depths and cannot be used directly to determine w in our case since the characteristics of the reflected radiation are controlled primarily by the upper layers of the medium. Therefore, to determine w we will invoke the condition considered below (see Eq. (101)).

The integration of the last term, upon taking full account of Eq. (98), yields the following expression:

$$2\mathrm{Re}(\tilde{\varepsilon}_1)\mathrm{i}^{M-m}\int_0^\infty\exp(-\tilde{\varepsilon}_1z)\,dz\int_0^\infty\beta_{lm}^{(y)(qn)(q_1\nu)}\times\exp(-\tau\rho)J_{m-M}(c\rho)\,d\rho$$

$$= \gamma_{lm}^{(qn)(q_1\nu)} I_{|m-M|}(c,e),$$

where

$$e = 2\mathrm{Im}(m_{eff})(1+w|\cos\omega|). \tag{99}$$

Thus, the approach considered results in the following system of linear algebraic equations for the coefficients of Eq. (95):

$$\gamma_{LM}^{(pn)(\mu\nu)} = Q_{LM}^{(pn)(\mu\nu)} + \frac{2\pi\eta}{k_0^3}\sum_{qq_1lm}\chi_l^{(pq)(\mu q_1)}\gamma_{lm}^{(qn)(q_1\nu)}G_{LMlm}, \tag{100}$$

where

$$\begin{aligned} G_{LMlm} = &\int_0^{\pi/2}\Big(I_{|M_2|}(c,f)d_{MN_0}^L(\omega)d_{mN_0}^l(\omega) \\ &+ I_{|M_2|}(c,e)(-1)^{L+l+M+m}d_{M-N_0}^L(\omega)d_{m-N_0}^l(\omega)\Big)\sin\omega\, d\omega \\ = &\sum_{L_2=|L-l|}^{L+l} C_{LMl-m}^{L_2M_2}C_{LN_0l-N_0}^{L_20}(-1)^m \\ &\times\int_0^{\pi/2}\Big(I_{|M_2|}(c,f)+(-1)^{L_2+M_2}I_{|M_2|}(c,e)\Big) \\ &\times d_{M_20}^{L_2}(\omega)\sin\omega\, d\omega, \end{aligned}$$

and $M_2 = M-m$.

The solution of the system of equations (100) can be obtained, for example, by the method of iterations. Then the LP reflection matrix $\mathbf{R}$ can be calculated using Eqs. (55) and (56):

$$\mathbf{R} = \mathbf{R}^{(L)} + \mathbf{R}^{(C)} = -\frac{\pi}{2k_0^2\cos\vartheta}(\mathbf{Z}^{(L)}+\mathbf{Z}^{(C)}),$$

where $\mathbf{R}^{(L)}$ is the diffuse reflection matrix and $\mathbf{R}^{(C)}$ is the reflection matrix for the interference component. It is assumed that the incident flux per unit area perpendicular to the incident beam is proportional to π.

In the case of the exact backscattering ($\vartheta = 180^\circ$), the matrix $\mathbf{R}^{(C)}$ is related to the matrix $\mathbf{R}^{(L)}$ via the simple formulas (88)–(91). In particular,

$$2R_{11}^{(L)} = R_{11}^{(C)} + R_{22}^{(C)} - R_{33}^{(C)} + R_{44}^{(C)} + R_{11}^{(1)} + R_{22}^{(1)} - R_{33}^{(1)} + R_{44}^{(1)}, \tag{101}$$

where $\mathbf{R}^{(1)}$ is the single-scattering reflection matrix.

We use the latter formula to determine the parameter w in Eq. (99). Specifically, having solved the RTE for given parameters of the medium, we determine the element $R_{11}^{(L)}$. Then, when solving system (100), we select the value of the parameter w such that equality (101) is satisfied.

Thus, in the framework of the above approach, the contribution of the double-scattering component is calculated exactly, while the contribution of the higher orders of scattering is calculated approximately. Below we will evaluate the accuracy of this approximation by using exact numerical results computed for a medium composed of non-absorbing Rayleigh scatterers [4,82] as well as experimental data by Wolf and Maret [8].

4.4.2. Robustness of the approximation

We compare first the results of calculations for a semi-infinite medium composed of non-absorbing Rayleigh scatterers. Figs. 8a and b show the dependence of the enhancement factor

$$\tilde{\zeta}_I(\tilde{q}) = \frac{R_{11}^{(L)}(0)+R_{11}^{(C)}(\tilde{q})}{R_{11}^{(L)}(0)}$$

and the degree of linear polarization

$$P(\tilde{q}) = -\frac{R_{21}^{(C)}(\tilde{q})}{R_{11}^{(L)}(0)+R_{11}^{(C)}(\tilde{q})}$$

on the parameter $\tilde{q} = k_0 l_{ext}\alpha$, where $\alpha = \pi - \vartheta$ is the phase angle and

$$l_{ext} = \frac{1}{2k_0\,\mathrm{Im}(m_{eff})}.$$

The expression for the effective refractive index is given by Eq. (51). The microphysical parameters of the particles

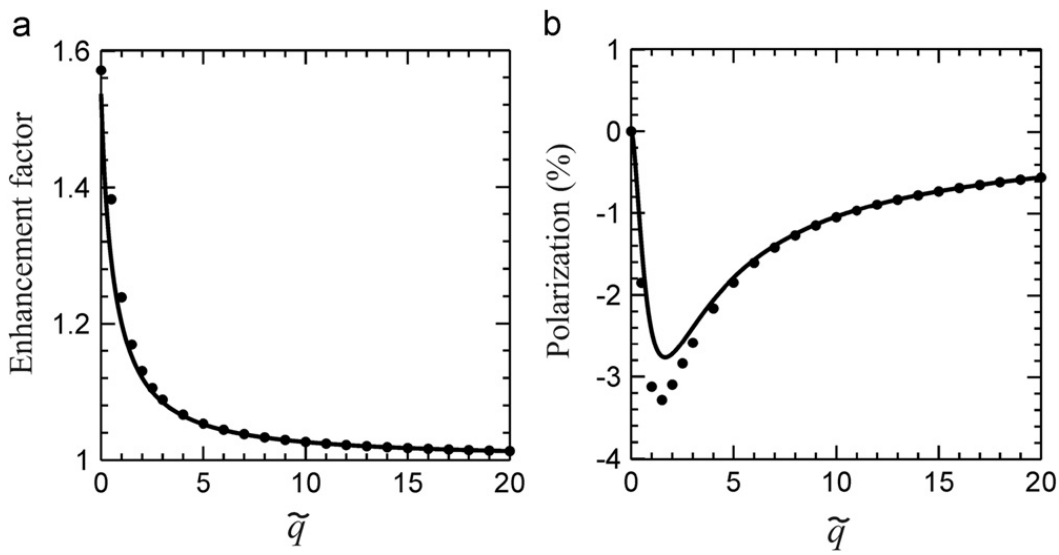

Fig. 8. Enhancement factor $\tilde{\zeta}_I(\tilde{q})$ and degree of linear polarization $P(\tilde{q})$ as functions of the parameter $\tilde{q}$ for a semi-infinite medium composed of non-absorbing Rayleigh particles with $\tilde{x} = 0.01$ and $\tilde{m} = 1.5$. The solid curves depict the exact results [82] while the dots show the result of using approximate formulas.

are as follows: $\tilde{x}=0.01$ and $\tilde{m}=1.5+i0$, where $\tilde{x}$ is the size parameter and $\tilde{m}$ is the refractive index. In Fig. 8, the solid curves depict the numerically exact results [4,82], while the dots show the result of using the approximate equations derived above, with the value $w=-0.21$ calculated from equality (101). This particular value implies that

$$(R_{11}^{(C)}+R_{22}^{(C)}-R_{33}^{(C)}+R_{44}^{(C)}+R_{11}^{1}+R_{22}^{1}-R_{33}^{1}+R_{44}^{1})/2=1.149,$$

whereas the solution of the RTE yields $R_{11}^{(L)}=1.147$.

It should be noted that a negative value of w results in an increase in the coefficients of Eq. (98) with increasing depth z. This behavior can be explained by the increasing radiation density in a non-absorbing (or weakly absorbing) medium with increasing optical depth [67].

Fig. 8 demonstrates a high accuracy of the approximation as applied to the medium composed of non-absorbing Rayleigh scatterers. We will now analyze the robustness of the approximation as applied to a medium composed of wavelength-sized particles. In Fig. 9 the dots show the results of laboratory measurements of co- and cross-polarized components of light reflected by monodisperse spherical polystyrene particles suspended in water [8], i.e., $R_{VV}=(R_{11}+R_{22}+2R_{12})/2$ and $R_{VH}=(R_{11}-R_{22})/2$, respectively. The diameter of the particles is 460 nm, the wavelength of the incident light is 515 nm, and the particle volume concentration is $\xi=0.1$. The solid curves depict the results of theoretical computations. The refractive index of the polystyrene particles is taken to be $\tilde{m}=1.59$, and the value of the parameter w calculated from Eq. (101) is -0.0796. This value corresponds to

$$(R_{11}^{(C)}+R_{22}^{(C)}-R_{33}^{(C)}+R_{44}^{(C)}+R_{11}^{1}+R_{22}^{1}-R_{33}^{1}+R_{44}^{1})/2=1.173,$$

whereas the respective solution of the RTE gives $R_{11}^{(L)}=1.176$. The calculated co- and cross-polarized components are normalized to the experimental data at $\alpha=0.6^{\circ}$. The effective refractive index of the medium is calculated using Eq. (51).

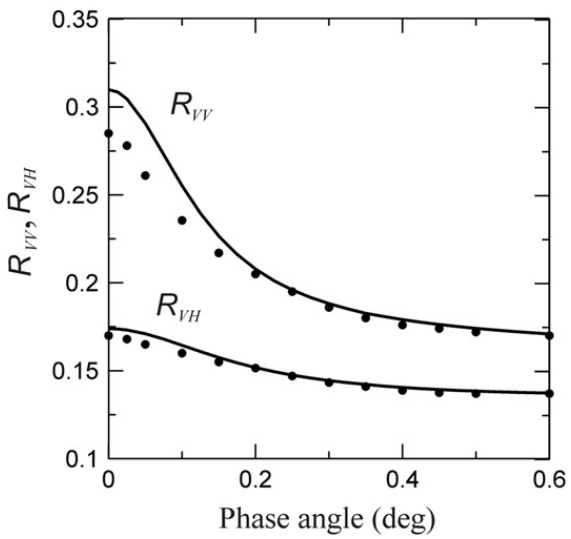

Fig. 9. Comparison of experimental (dots; adapted from Ref. [8]) and theoretical (solid curves) results for a semi-infinite medium composed of monodisperse spherical polystyrene particles suspended in water.

As seen from Fig. 9, the approximation provides a good accuracy also for the case of a medium composed of wavelength-sized particles. The relative accuracy of the calculations is better than 10%, which should be acceptable in many applications. Unfortunately, we have no reliable experimental or theoretical results which would allow us to test the proposed technique for larger particles and other values of the parameters characterizing the scattering medium. Note, however, that the comparison of the experimental and theoretical results was made without invoking any free model parameters: only the actual, independently measured physical parameters (particle size, refractive index, and concentration as well as the wavelength of light) were used in the calculation. The approximation can easily be extended to the case of oblique illumination and to media consisting of non-spherical particles (see Section 4.3.3).

It should be noted that such a simple theoretical technique can be developed only for a semi-infinite medium. In the case of a medium of finite optical thickness, the analytical integration in Eqs. (92) and (93) results in very complex formulas and does not yield a system of algebraic equations similar to that in Eq. (100).

4.4.3. CB as a function of medium characteristics: examples

Theoretical examples of the interference peak $R_{11}(\alpha)/R_{11}(0)$ and the degree of linear polarization $P(\alpha)=-R_{12}(\alpha)/R_{11}(\alpha)$ as functions of the parameters of the semi-infinite scattering medium are presented in Figs. 10–12a. The effective refractive index was calculated according to Eq. (51) for all the models; the constituent particles are assumed to be identical spheres a size parameter of $\tilde{x}=2$ and a refractive index of $\tilde{m}=1.5$. Fig. 10 shows how the intensity and polarization change with particle packing density (concentration) ξ. It is evident that the half-width of the interference intensity peak grows linearly with increasing concentration, which has been discussed extensively in theoretical (e.g., Refs. [9,10,63,73,74]) and experimental (e.g., Refs. [8,65]) studies. The same linear dependence is also typical of the phase angle of minimal polarization (Fig. 10b) provided that the polarization of the incoherent component is small [74]. The inversion angle (the phase angle at which polarization switches sign from negative to positive) also increases with increasing ξ; in other words, the range of phase angles affected by WL broadens. This behavior of polarization is caused by the increase of the imaginary part of the effective refractive index (i.e., extinction) with increasing concentration.

In Fig. 11, the interference peak and the degree of linear polarization of the reflected radiation are depicted for three values of the imaginary part of the particle refractive index $\mathrm{Im}(\tilde{m})$. As before, $\tilde{x}=2$ and $\mathrm{Re}(\tilde{m})=1.5$. It is seen that increasing $\mathrm{Im}(\tilde{m})$ leads to an increase of the half-width of the intensity peak and the angle of minimal polarization. These traits are also explained by the increase of $\mathrm{Im}(m_{eff})$ with $\mathrm{Im}(\tilde{m})$. The deepening of the polarization minimum with $\mathrm{Im}(\tilde{m})$ is caused by the strengthening of the positive polarization branch for the radiation singly scattered by the particles.

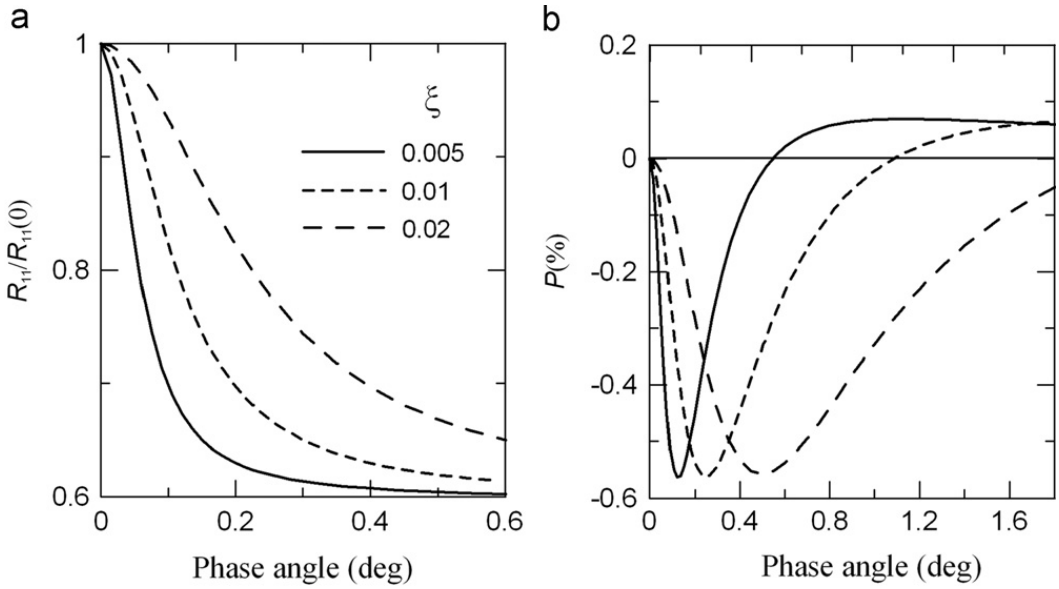

Fig. 10. (a) The interference peak $R_{11}(\alpha)/R_{11}(0)$ and (b) the degree of linear polarization for unpolarized incident light $P(\alpha) = -R_{12}(\alpha)/R_{11}(\alpha)$ for $\tilde{x} = 2$, $\tilde{m} = 1.5$, and three values of the packing density ξ.

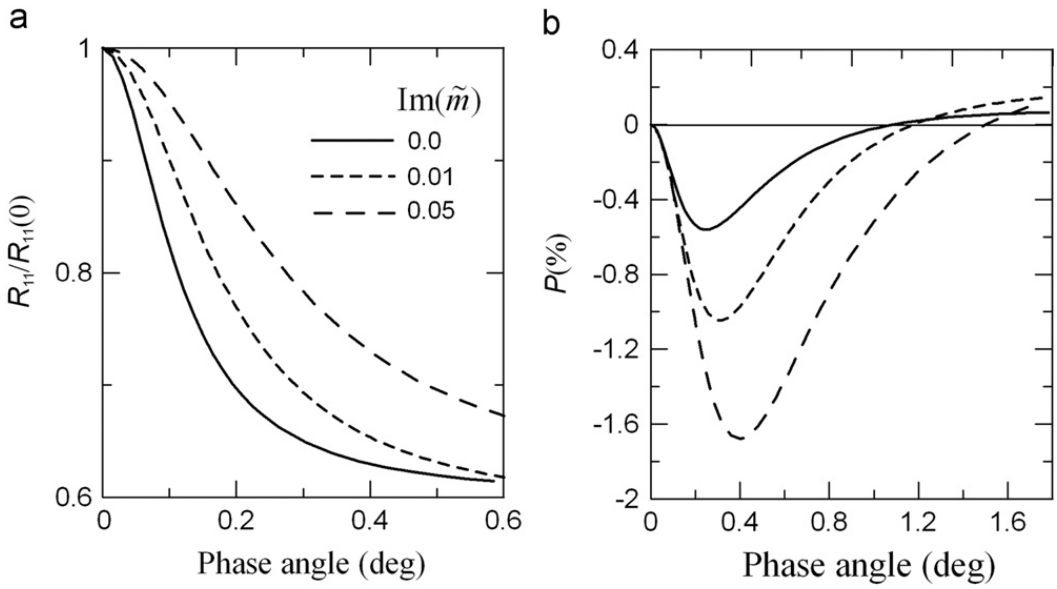

Fig. 11. As in Fig. 10, but for $\mathrm{Re}(\tilde{m}) = 1.5$, $\xi = 0.01$, and three values of the imaginary part of the particle refractive index.

The dependence of WL characteristics on the particle size parameter $\tilde{x}$ is illustrated in Fig. 12a (the particle refractive index is fixed at $\tilde{m} = 1.5$). For all the models considered, the imaginary part of the effective refractive index is assumed to be the same: $\mathrm{Im}(m_{eff}) = 0.00403$. It is seen that the interference intensity peak and the degree of linear polarization vary with particle size in a rather complex way. The behavior of polarization is especially noteworthy: depending on $\tilde{x}$, P can be either negative or positive. Recall that in the laboratory measurements for powder-like samples [83] and observations of atmosphereless celestial bodies [11], only negative polarization has been detected at small phase angles. The "optical mechanism" of its formation has been discussed in many papers (e.g., Refs. [84–86]). The WL explanation is based on the assumption that the degree of linear polarization of singly scattered radiation is positive in the whole range of scattering angles. However, the degree of linear polarization for particles with $\tilde{x} \geq 2$ and $\tilde{m} = 1.5$ depends on the particle sizes and the scattering angle in a complex way and can be both positive and negative. In such cases, the interference may result in a positive degree of linear polarization of radiation scattered by the particulate medium or in a more complex phase-angle dependence of polarization [72–75]. For the model results shown in Figs. 10–12a, the common feature of the polarization curves is their asymmetry. Specifically, the minimum (or maximum) of polarization is closer to exact backscattering than to the inversion angle. This trait is explained by weak extinction in the media considered: for the particles

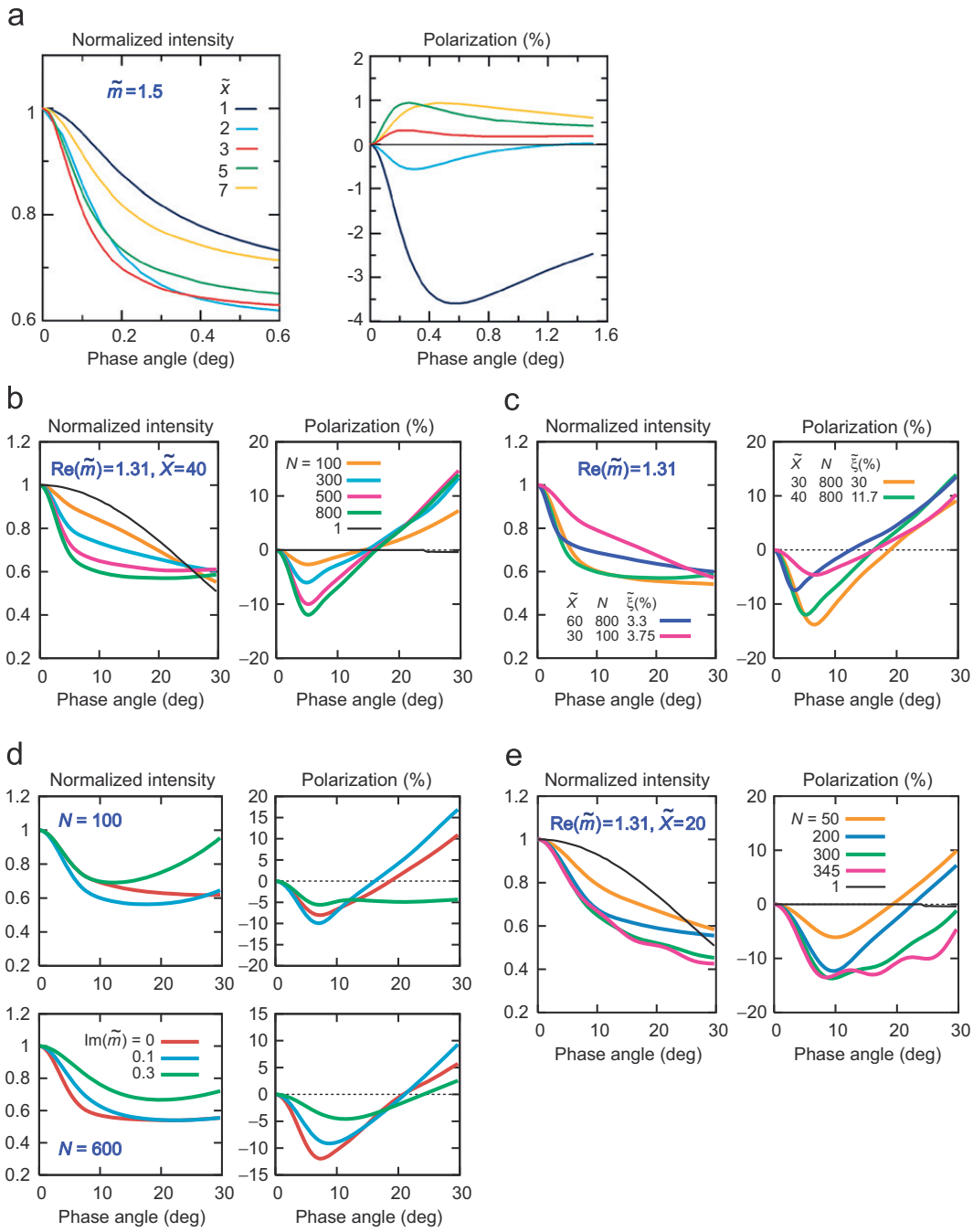

Fig. 12. (a) As in Fig. 10, but for $\mathrm{Im}(m_{eff})=0.00403$ and five values of the particle size parameter $\tilde{x}$. (b) Scattering characteristics of a $\tilde{X}=40$ scattering volume randomly filled with a number N of $\tilde{x}=2$ spherical particles (after Ref. [110]). The packing density $\tilde{\xi}$ varies between 1.5% (N=100) and 11.7% (N=800). The particle refractive index is fixed at $\tilde{m}=1.31$. (c) Scattering characteristics of random particulate volumes with size parameters in the range $30<\tilde{X}<60$ (after Dlugach et al. [110]). The particle refractive index and size parameter are fixed at $\tilde{m}=1.31$ and $\tilde{x}=2$, respectively. The values of the packing density $\tilde{\xi}$ are given in the legend. (d) Scattering characteristics of a $\tilde{X}=30$ random particulate volume composed of N identical spherical particles with $\mathrm{Re}(\tilde{m})=1.5$ and $\tilde{x}=1.76$. N=100 and $\tilde{\xi}=2.4\%$ in the upper row; N=600 and $\tilde{\xi}=14.5\%$ in the lower raw. The imaginary part of the particle refractive index varies in the range $0<\mathrm{Im}(\tilde{m})<0.3$ according to the color legend (after Ref. [110]). (e) Optical characteristics of a $\tilde{X}=20$ random particulate volume composed of N identical spherical particles with $\tilde{m}=1.5$ and $\tilde{x}=2$ (after Ref. [110]). The packing density $\tilde{\xi}$ varies between 7% (N=50) and 47% (N=345).

with $\tilde{x}=2$ and $\tilde{m}=1.5$, $\min(\mathrm{Im}(m_{eff}))=0.00169$ if $\xi=0.005$ and $\max(\mathrm{Im}(m_{eff}))=0.00674$ if $\xi=0.02$. For such values of $\mathrm{Im}(m_{eff})$, the influence of distant particles on a given particle is stronger than that of neighboring particles (see the discussion in Section 4.2), which leads to the asymmetry in the negative polarization branch.

5. Interaction of particles in the near field as revealed by scattering properties of aggregates

As we could see in the preceding sections, the problem of describing the scattering properties of a particulate random medium becomes extremely complicated when

the distances between the particles are not much greater than the particle sizes and the wavelength, i.e., when the particles are not in the far zones of each other, so that a wave propagating from one particle to another cannot be considered spherical. In this case, the equations derived are much more complicated than those for a sparse medium since they do not involve the conventional single-scattering characteristics of individual particles. Moreover, for a densely packed medium, effects caused by the contribution of the interference of waves scattered once and twice, twice and three times, etc. can be observed, unlike the case of a sparse medium wherein only the ladder and cyclical diagrams contribute to the scattered light.

The purpose of this section is to demonstrate how the interaction of particles in the near-zone affects the characteristics of light scattered by a particle ensemble. Since only approximate analytical solutions of the problem are currently available for densely packed random particulate media, we will use particle ensembles with a limited number of components and a limited volume. In order to perform computer simulations of electromagnetic scattering by a finite volume filled with randomly positioned particles, one can use one of the currently available techniques based on the direct numerically exact solutions of the macroscopic Maxwell equations (MMEs). We use one of these solutions, the so-called superposition *T*-matrix method [24,87], to compute the scattered intensity and degree of linear polarization for complex ensembles of particles. Within the range of its numerical convergence, the corresponding public-domain *T*-matrix computer code [88] yields results with a guaranteed accuracy, which makes it numerically exact. Although the computer resources available to us do not allow computations for realistic particulate targets such as particulate planetary surfaces, the results obtained for ensembles containing a limited yet large number of particles do reveal trends in the light-scattering characteristics caused by increasing packing density.

5.1. Effects of near-field interactions on scattering characteristics

5.1.1. Inhomogeneity of near-zone fields

In order to explain the way in which the near-field components affect the characteristics of the reflected light, it is necessary to consider the field structure in the vicinity of the particles. Everywhere in space, only the total field, i.e., the sum of the incident and scattered components, is a real physical field [58]. If the scattered wave contained only components decreasing as $1/r$ then the wave leaving the particle would be spherical at large as well as at small distances from the particle. Then, in the close vicinity of the scatterer, the propagation directions of the scattered and incident waves would not coincide (except for the forward-scattering direction $\mathbf{k}_{sc}=\mathbf{k}_0$), and these waves would not be connected. However, the real scattered field near the particle contains components decreasing faster than $1/r$ (compare Eqs. (4) and (14)). These terms describe the near field [14,35,41,42] which causes a connection of the incident and scattered fields to some distance from the particles. This connection causes inhomogeneity of the total field in the particle's vicinity. This effect is most pronounced if the particle size is comparable to the wavelength. Direct calculations using the Lorentz–Mie theory for spherical particles show that the constant-phase surface of the total field near the particle is funnel shaped (Fig. 13). Consequently, the field inhomogeneity near the particle causes a rotation of the total electric field vector relative to the incident field vector. As a result, $E_z\neq 0$ (see also Refs. [13,15,89,90]).

Under such conditions, neighboring particles experience the influence of the inhomogeneous field and, consequently, scatter light in a different way than that predicted by the theory considering only plane waves. To examine the influence of the field inhomogeneity in the vicinity of particles on the characteristics of light scattered by a particle ensemble in more detail, let us consider Rayleigh test particles placed on the surface $k_0z_0\approx\pi$ in Fig. 13. Fig. 14 shows the scheme illustrating

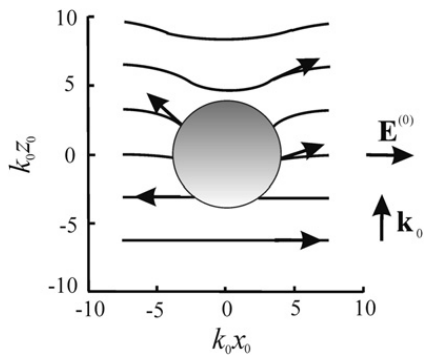

Fig. 13. Constant-phase surfaces and local directions of the total electric field (i.e., the sum of the incident and scattered waves) in the close vicinity of a particle with a size parameter $\tilde{x}=4$ and refractive index $\tilde{m}=1.32+i0.05$. The incident wave propagates along the wave vector $\mathbf{k}_0$ and is polarized in the x_0z_0 plane.

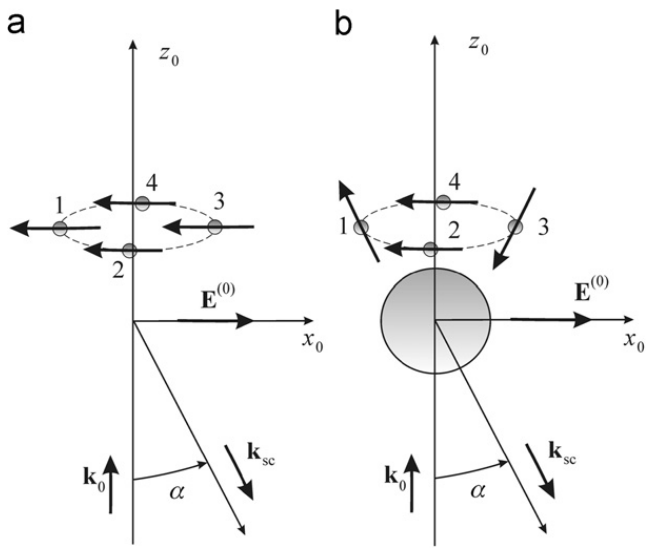

Fig. 14. Scattering of (a) homogeneous and (b) inhomogeneous waves by Rayleigh test particles. Particles 1 and 3 are in the x_0z_0 plane, while particles 2 and 4 are in the y_0z_0 plane. The incident wave $\mathbf{E}^{(0)}$ propagates along the positive z_0-axis (along the vector $\mathbf{k}_0$) and is polarized in the x_0z_0 plane. The scattered wave propagates in the direction of the phase angle α (along the vector $\mathbf{k}_{sc}$). The vectors centered at the Rayleigh particles show the directions of the dipole moments induced.

the conditions of the light scattering by four test particles located in the homogeneous field (a) and in the inhomogeneous zone near the larger particle (b).

Let us first analyze the case when the incident field is polarized in the scattering plane x_0z_0 as shown in Fig. 14. If the test particles are far from each other and from other particles, i.e., they are subjected to a homogeneous field (Fig. 14a), their dipole moments are parallel to the x_0-axis. In this case, the intensity of the scattered light is determined by all four test particles–dipoles in the directions $\alpha=0^\circ$ and 180°, and it is zero in the direction $\alpha=90^\circ$. However, if the test particles are in the inhomogeneous zone near a wavelength-sized particle (Fig. 14b) then the dipole moments induced in particles 1 and 3 have a non-zero component in the direction of wave propagation, i.e., along the z_0-axis. This results in a decrease of the intensity of the scattered light in the directions $\alpha=0^\circ$ and 180°, and the intensity in the direction $\alpha=90^\circ$ becomes non-zero. In both cases, the scattered wave is polarized in the same way as the incident one in the scattering plane.

If the incident wave is polarized perpendicularly to the scattering plane then, in the case of the homogeneous field, the scattered radiation is also polarized perpendicularly to the scattering plane and the intensity does not depend on the phase angle. In the inhomogeneous field, particles 1 and 3 produce radiation that is polarized perpendicularly to the scattering plane and does not depend on the phase angle. While the radiation scattered by particles 2 and 4 has a component parallel to the z_0-axis (i.e., polarized in the scattering plane) which depends on α, the intensity decreases in the directions $\alpha=0^\circ$ and 180° and increases in side directions. So, for any polarization of the incident wave, the field inhomogeneity in the vicinity of the scattering particle induces a rotation of the field vector and leads to the appearance of a component of the total field $E_z\neq 0$, which, in turn, diminishes the intensity of the light and causes negative polarization (see also Refs. [13–15,42,89,90]). This effect should depend on the sizes of the particles and can be expected to be most pronounced for wavelength-sized particles since the spatial scale of field inhomogeneities is comparable to the wavelength (Fig. 13).

5.1.2. Mutual shielding of particles

One more manifestation of near-field effects is the shielding of particles by each other [16]. The scheme with the test dipoles (Fig. 14) can help us to estimate qualitatively the result of the shielding of, for example, dipole 1 by the large particle for the specified direction of observation. For the sake of simplicity, let us assume that for the given polarization of the incident radiation, the dipole moment of particle 1 is oriented exactly opposite to the vector $\mathbf{k}_{sc}$. In this case, particle 1 does not radiate in the direction $\mathbf{k}_{sc}$. It is of no importance whether we take the shielding into account or not. If the incident radiation is polarized in the y_0z_0 plane then particle 1 radiates as particle 3 (or as all the particles in the homogeneous field), provided that the shielding is ignored. However, when the large particle shields particle 1 then the latter does not radiate in this direction (i.e., does not contribute to the positive polarization). In other words, the shielding diminishes the contribution of the positively polarized scattered radiation and reduces the intensity in the α direction. However, in the backscattering direction, dipole 1 contributes to the scattered radiation, which causes an increase in the intensity with respect to that in the α direction. In this regard, we note that the geometric-optics description of the shadowing effect does not lead to negative polarization [83,91,92]. Unlike the field inhomogeneity in the near zone, which is most pronounced for wavelength-sized particles, the mutual shielding effect is independent of the sizes of the particles located in the near field.

It is convenient to illustrate the effects of mutual shielding of wavelength-sized particles by considering light scattering by bispheres with touching components. Fig. 15 depicts the intensity of light scattered by such

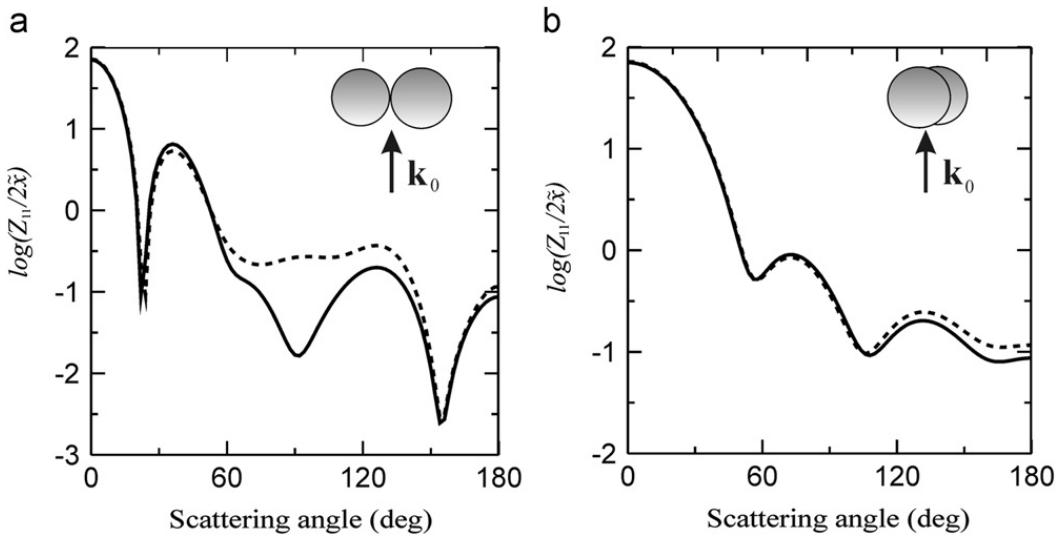

Fig. 15. The angular dependence of the intensity of light scattered by a bisphere having its axis in (a) the scattering plane and (b) in the perpendicular plane. The solid and dashed curves correspond to the calculations accounting for the near-field components and ignoring them, respectively. The calculated values of the relative intensity are normalized in the same way.

bispheres in two orientations relative to the scattering plane given, in this case, by the plane of the page. The size parameters of the bisphere components are $\tilde{x}=4$ and their refractive indices are $\tilde{m}=1.32+0.05\mathrm{i}$. The incident quasi-monochromatic beam is unpolarized, and its propagation direction is indicated by the vector $\mathbf{k}_0$. The results are shown for two models. The first one accounts for all the components of the scattered field including those decreasing faster than $1/r$, i.e., including the near-field components (solid curves). In other words, the coefficients $H^{(q)}_{LMlm}$ in Eq. (20) are given by their most general form, Eq. (19), wherein their radial dependence is determined by the Hankel spherical functions. The second model accounts for only the components decreasing as $1/r$, i.e., ignores the near-field components (dashed curves). In other words, the second model is based on Eq. (46) implying the far-zone assumption.

The comparison of the model results shown in Fig. 15 reveals that when the bisphere axis lies in the scattering plane then the intensity of the scattered light along the axis ($\alpha=90^\circ$) calculated with full account of the near field is substantially smaller (by approximately one order of magnitude) than that calculated by ignoring the near field. However, if the bisphere axis is perpendicular to the scattering plane then there is no difference between the model results for the intensity of light scattered in side directions. Hence, in the case of the bisphere axis lying in the scattering plane, the cause of the intensity decrease is the mutual shielding (shadowing) of the bisphere components. In other words, each sphere acts as an obstacle for the propagation of the radiation scattered along the bisphere axis.

As was noted in Section 2, Eq. (20) provides a complete description of all the details of the field surrounding the particles which, in particular, result in the mutual shielding of particles [16]. In fact, if the field components decreasing faster than $1/r$ are ignored by using Eq. (46) then Eq. (20) describes spherical waves, i.e., the particle sizes are ignored in comparison with the distances between them. In other words, under the far-zone assumption, the shielding concept becomes irrelevant. Therefore, for the scattering direction parallel to the bisphere axis, the intensity calculated in the far-field approximation far exceeds that calculated with full account of near-field interactions. Calculations show that in this case the shielding effect is noticeable for interparticle distances up to several times the particle diameters.

5.1.3. Examples of near-field effects in aggregates

The influence of the near field on the intensity and degree of linear polarization of the scattered light can also be illustrated with a more complex example. Fig. 16 displays the scattering characteristics of a partially oriented cluster consisting of one relatively large particle with a size parameter of $\tilde{x}=4$ and a refractive index of $\tilde{m}=1.32+\mathrm{i}0.05$ and eight small particles, each having a size parameter of $\tilde{x}=1.5$ and a refractive index of $\tilde{m}=1.5+\mathrm{i}0.1$. The coordinates of the cluster components are detailed in the figure caption. The incident light propagates along the positive z-axis. The scattering characteristics of the cluster are averaged over all rotations of the cluster about the z-axis and over variations of the angles ϑ_i of small particles within the $\pm 5^\circ$ interval. The relatively strong absorption and the random positioning of the particles in the cluster were used in order to diminish the contribution of interference effects resulting from a regular arrangement of the particles.

The comparison of the model results calculated with the near-field components accounted for and ignored shows that the interaction of particles in the near field suppresses the intensity in a wide angular range and induces negative polarization in backscattering directions. It is worth noting that the intensity, at least for the given cluster, is mostly affected by shielding, since it is the shielding that suppresses the intensity in the side-scattering directions.

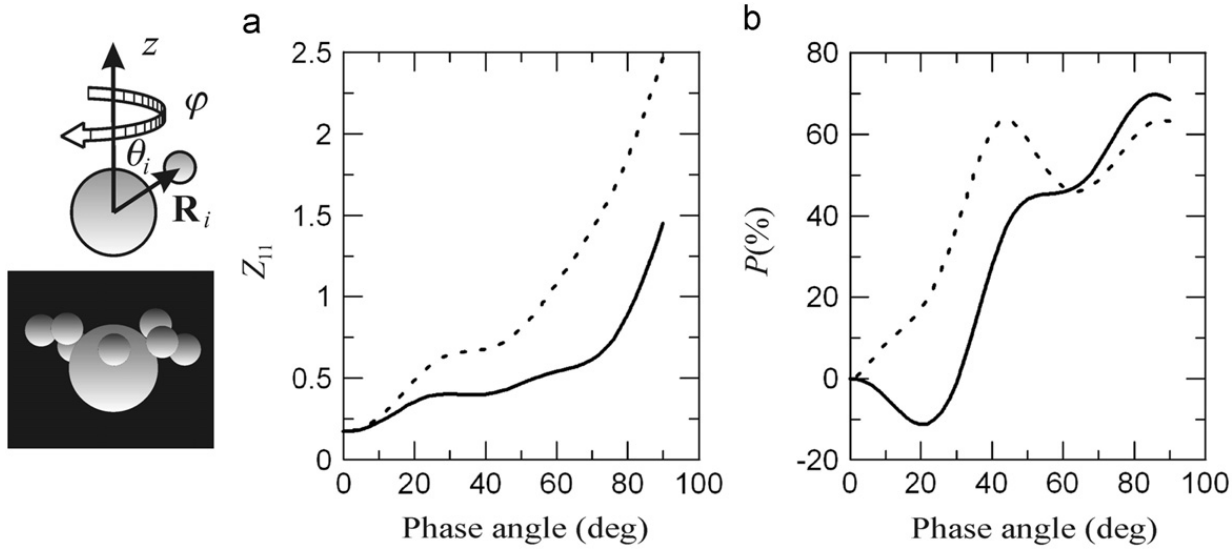

Fig. 16. The phase-angle dependence of (a) intensity and (b) linear polarization of light scattered by the cluster shown in the left-most panel. The coordinates of eight small particles in the spherical coordinate system centered at the large particle (see the scheme on the left) are $R_i=5.5$, 6.5, 5.8, 6.7, 6.2, 5.9, 7.1, and 6.8 (in units of size parameter), $\vartheta_i=75^\circ$, 70°, 65°, 60°, 55°, 65°, 75°, 55°, and $\varphi_i=0^\circ$, 45°, 90°, 135°, 180°, 225°, 270°, and 315°. The results calculated with the near-field components accounted for and ignored are shown by solid and dashed curves, respectively.

The influence of the shielding and the near-field inhomogeneity on the polarization is difficult to distinguish, because in this case both effects have the same sign.

For the interpretation of astronomical observations and laboratory measurements, it is especially important to distinguish the manifestations of different scattering mechanisms in the range of small phase angles, where a nonlinear increase of brightness and a narrow minimum of negative polarization, the so-called brightness and polarization opposition effects (BOE and POE), are often observed (e.g., Refs. [11,83,93–95] and references therein). Both effects have been attributed to CB caused by scattering in particulate media (see, e.g., Refs. [4,11] and references therein). However, one should keep in mind that the CB concept is strictly applicable only in the limit of very small packing density [4,11]. In the case of densely packed media, the interaction of particles in the near field may distort the influence of CB [15].

An example demonstrating the near-field effects on the scattering characteristics of a densely packed cluster is presented in Fig. 17. The results calculated by accounting for the near-field components and by ignoring them are shown. It is clearly seen that the contribution of the near-field interaction smoothes the opposition enhancement of intensity and shifts the polarization minimum and the inversion angle away from the exact backscattering direction. For this particular cluster, the near-field contribution also makes the negative-polarization branch deeper. However, as numerous model calculations show, the latter effect depends strongly on the size parameter and refractive index of the constituent particles.

It should be noted that the artificial removal of the near-field components from the scattering computation can also strengthen the contribution of coherent and diffuse scattering. Therefore, a more correct way to study the consequences of the near-field interactions on the scattering properties of random particulate media is to examine the characteristics of aggregates with varying porosities.

5.2. Coherent backscattering and near-field effects for ensembles of particles with varying packing densities

5.2.1. Model description

Recently, a number of papers devoted to the parametric analysis of the scattering characteristics of particle aggregates and particulate volumes have been published (see, e.g., Refs. [96–103] and references therein). Their main objective has been to explain the results of photometric and polarimetric observations of various comets, atmosphereless celestial bodies, and laboratory samples. However, from the standpoint of the analysis of packing density effects, the most robust method has been that proposed by Mishchenko et al. [96] and later adopted in Refs. [97,104–110]. To examine whether all backscattering effects predicted by the low-density theory of CB also take place in the case of densely packed media, the model of a random particulate medium in the form of a macroscopic spherical volume randomly filled with N identical non-overlapping spherical particles has been used.

This approach is based on using only one multiparticle configuration, with particle positions inside the spherical volume prescribed by a random-number generator. Although the mutual positions of the N particles with respect to each other remain the same, they are sufficiently "random" from the outset. Therefore, averaging over all orientations of this configuration yields, in effect, an infinite continuous set of random realizations of the scattering volume while enabling one to apply the efficient orientation averaging technique afforded by the superposition T-matrix method [87]. Of course, this scattering model cannot be expected to reproduce exactly the great diversity of morphologies of discrete random media encountered in laboratory and natural settings. However, it is sufficiently representative to permit a meaningful analysis of the effects of packing density on EM scattering by discrete random media.

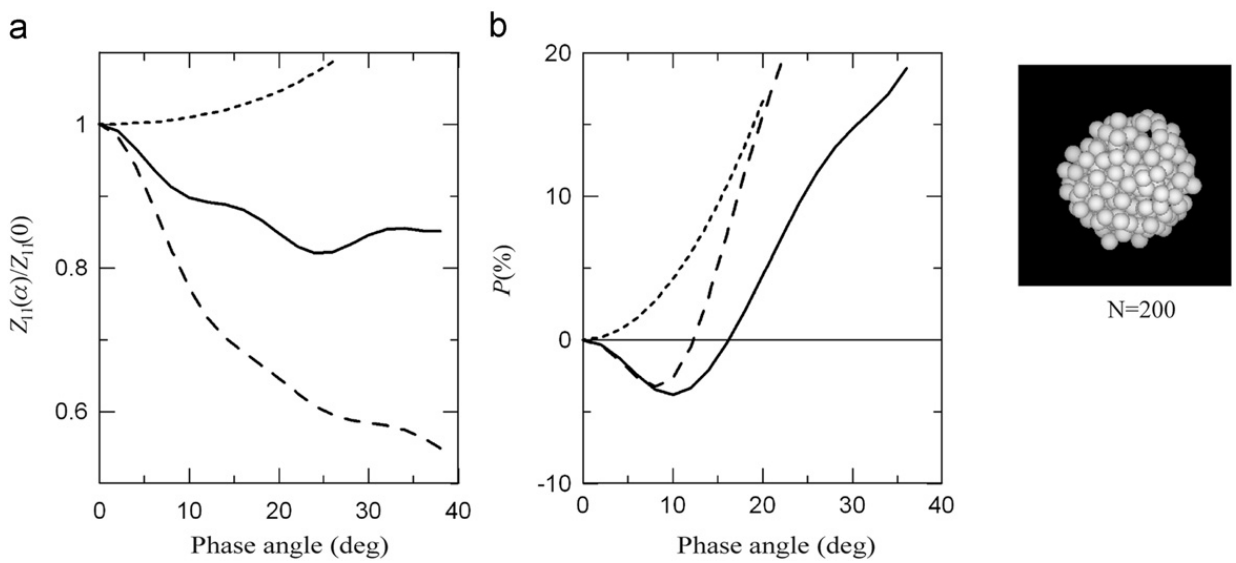

Fig. 17. Intensity normalized to its value at zero phase angle and polarization versus phase angle calculated for the cluster shown in the right-most panel. The parameters of spherical particles constituting the cluster are $\tilde{x} = 1.5$ and $\tilde{m} = 1.55 + i0.1$. The results calculated with the near-field components accounted for and ignored are shown by solid and dashed curves, respectively. The dotted curves show the results for a single particle.

In the framework of this approach, it is assumed that the statistically random particulate volume is illuminated by a parallel quasi-monochromatic beam of light. The observer is located in the far-field zone of the entire spherical volume. Since all scattering and absorption properties of the particulate volume are averaged uniformly over all orientations of the N-particle configuration, they depend only on the phase angle.

Mishchenko et al. [96,97,104], Mishchenko and Mackowski [69], Mackowski and Mishchenko [108,109], and Dlugach et al. [110] performed extensive computations of the scattering characteristics of particulate volumes with size parameters $\tilde{X}=k_0R$ (where R is the radius of the volume) ranging from 20 up to 60, filled with non-absorbing spherical particles with real-valued refractive indices $\tilde{m}$ ranging from 1.194 to 1.6. Depending on $\tilde{x}$ and $\tilde{m}$, the number of monomers N was varied from 1 up to 1875. Some numerical data were obtained for absorbing particles with the imaginary part of the refractive index $\mathrm{Im}(\tilde{m})=0.01$, 0.1, or 0.3. The values of the particle packing density in a finite volume depend on the way the particle volume fraction is defined. In the papers by Mishchenko et al. [97,104] and Dlugach et al. [110], the packing density is defined as $\tilde{\xi}=N\tilde{a}^3/(R-\tilde{a})^3$, where $(R-\tilde{a})$ is the radius of the sphere enclosing all constituent-particle centers.

To control the behavior of the negative polarization branch at small phase angles with increasing number of interacting particles, it is convenient to use constituent particles causing neutral single-scattering polarization in a sufficiently wide range of backscattering angles [97]. To ensure that, proper {refractive index, size parameter} combinations for the constituent spheres were selected. For example, the refractive index of ice, $\tilde{m}=1.31$, dictates the monomer size parameter $\tilde{x}=2$.

5.2.2. Numerical results

Representative examples of the results obtained by Dlugach et al. [110] for the case of unpolarized incident light are shown in Fig. 12b–e. The phase-angle dependences of the intensity and polarization for volumes containing ice particles with packing densities less than 30% (Fig. 12b and c) show perfect qualitative agreement with the predictions of the low-density theory of CB. Indeed, the normalized scattered intensity exhibits backscattering peaks which rapidly grow with N but have virtually the same angular widths. In the phase-angle range from 0° to 30°, linear polarization rapidly develops a pronounced minimum of negative values. The phase angle of minimal polarization is essentially independent of N and decreases with increasing $\tilde{X}$ approximately as $1/\tilde{X}$. The angular position of the polarization minimum is comparable to the angular semi-width of the BOE. Furthermore, the phase-angle profile of the negative branch is asymmetric, so that its minimum is significantly closer to zero phase angle than to the inversion angle. This means that the polarization minima in Fig. 12b and c have the same basic morphology as the POE predicted by the low-density theory of CB [4,82]. Moreover, T-matrix calculations for different real refractive indices show that the angular widths of the backscattering intensity peaks are virtually independent of $\tilde{m}$, while the negative-polarization features are almost identical.

Since non-zero absorption can weaken various manifestations of multiple scattering significantly, it is important to verify whether the WL interpretation of the backscattering features identified previously for non-absorbing particles is consistent with the expected behavior of these features with growing $\mathrm{Im}(\tilde{m})$. The results of extensive computations for absorbing particles [110] (sample results are presented in Fig. 12d) have revealed a rather complex behavior of the opposition features in this case. The changes in the amplitude and width of the backscattering intensity peak as well as in the depth and width of the negative-polarization branch with increasing absorption can be non-monotonic. One has to conclude that increasing absorption can either enhance or suppress various manifestations of CB depending on the particle packing density and the real part of the refractive index [110]. This is not surprising, since increasing $\mathrm{Im}(\tilde{m})$ modifies not only the absorptivity of the constituent particles but also their single-scattering properties.

The optical effect of increasing the number of particles in a volume can be expected to be twofold [97]. At the outset, it facilitates multiple scattering and thus enhances the classical RT and CB features. Eventually, however, it causes scattering patterns not predicted by the low-packing-density theories of RT and CB. This implies that the RT and CB interpretation of the T-matrix results may fail if the packing density becomes exceedingly large.

Fig. 12e shows one example illustrating the effect of increasing packing density in ensembles of non-absorbing particles. Indeed, starting from packing densities $\sim$30%, the phase curves develop high-frequency interference ripples typical of a single spherical particle with a size greater than the wavelength [24]. This behavior is obviously inconsistent with the RT and CB predictions. To better distinguish packing-density effects in closely packed aggregates, the interference features can be smoothed by distorting the regular spherical shape of the particulate volume [107], as shown in Fig. 18. It is seen that for such non-spherical volumes, the BOE becomes wider and the polarization minimum moves away from opposition when the packing density grows. Moreover, depending on the size parameter of the constituent particles and the real part of the refractive index, the negative branch of polarization may become wider and deeper, while the BOE is weakened in more closely packed absorbing aggregates. Evidently, this behavior of the phase-angle curves does not follow from the low-density theory of CB. Similarly to the case with a spherical volume [110], the modeling with absorbing distorted spherical volumes also shows that changes in the backscattering features are not completely monotonic when the absorption and/or packing density increases [107].

5.2.3. Discussion

In an optically thick non-absorbing or weakly absorbing particulate layer, the interference base is controlled by the transport mean free path, while in a finite and relatively small volume randomly filled with particles it is controlled by the volume size parameter. Therefore, numerically exact computations for finite particulate volumes cannot always

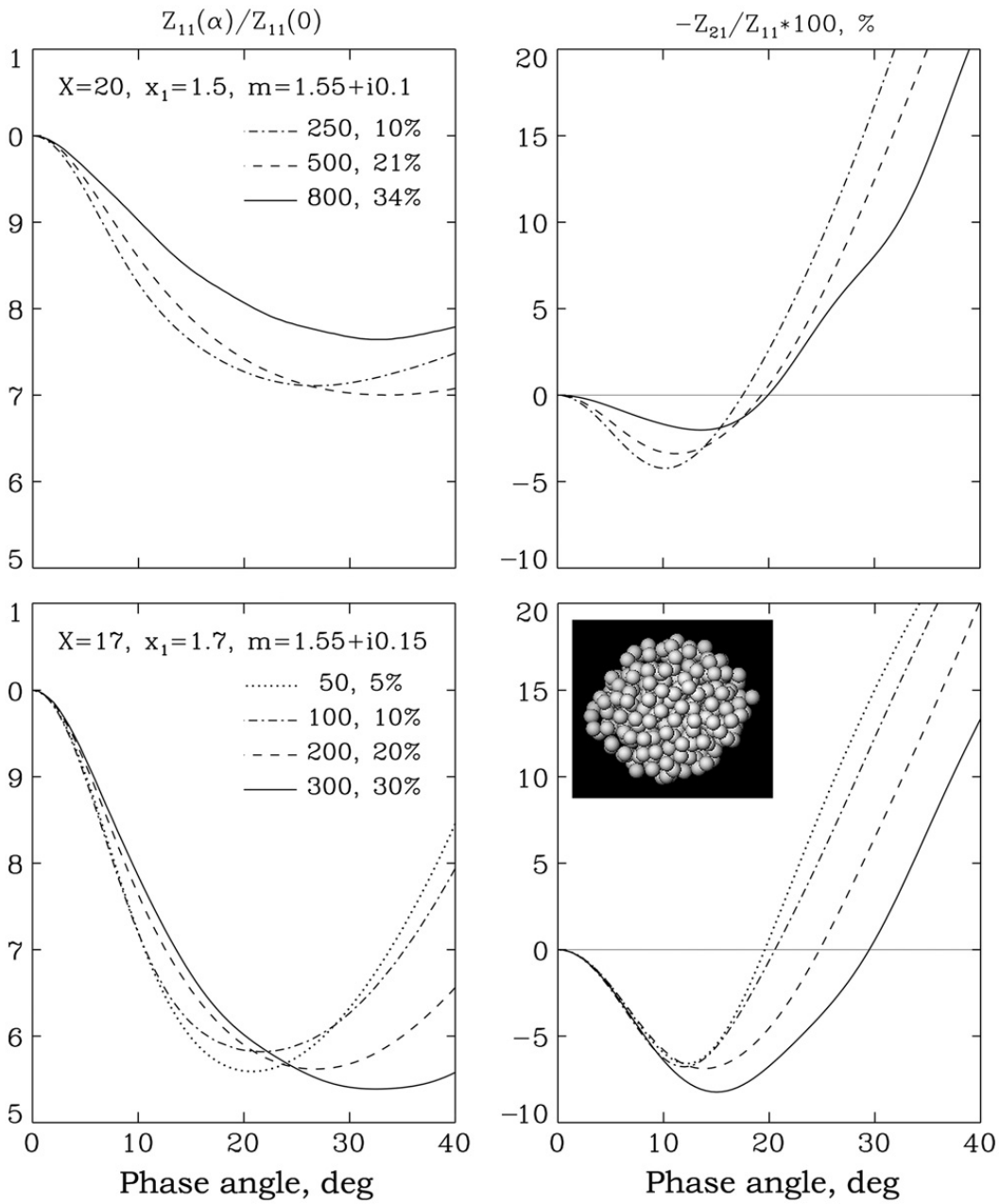

Fig. 18. Optical characteristics of the scattering volumes randomly filled with a number N of spherical particles with parameters indicated in the plots. The numbers of particles in the volume and the corresponding values of the packing density defined as $\xi = N\tilde{a}^3/R^3$ are also shown in the legends. The shape of the volumes is a "distorted" sphere, as illustrated by the inset showing an aggregate of 300 particles with $\tilde{x}=1.7$ filling a $\tilde{X}=17$ volume.

reproduce the behavior of the scattering characteristics typical of natural particulate media. However, the model of a finite scattering volume allows one to obtain direct computer solutions of the MMEs without making the simplifying yet questionable assumption of a small packing density. Consequently, the evolution of multiple-scattering effects, especially for CB and near-filed interactions, in complex ensembles of particles with increasing packing density can be traced unequivocally.

The results of extensive numerically exact computer simulations described above imply that:

(1) For ensembles of non-absorbing or weakly absorbing particles, the backscattering effects such as the BOE and POE predicted by the low-density theory of CB also take place for densely packed media. If the packing density exceeds ~25–30% (depending on the particle refractive index and size parameters), the backscattering characteristics start to exhibit behavior deviating from the classical low-density predictions. Nevertheless, we may conclude that the CB features still survive packing densities typical of particulate surfaces and particle suspensions encountered in natural and artificial environments.

(2) For ensembles of absorbing particles, the changes in the behavior of the backscattering features with increasing packing density are not monotonic and do not always obey the low-density CB theory. In general, the opposition intensity surge becomes wider and the negative-polarization minimum shifts away

from opposition with growing packing density. In addition, depending on the particle size parameter and real part of the refractive index, the negative-polarization minimum can become more pronounced. This behavior of the backscattered intensity and polarization is consistent with the increasing contribution of the near-field effects (see Section 5.1 as well as Refs. [14,15,42]).

The rapidly growing body of evidence appears to corroborate the conclusion that CB is the likely cause of the remarkably narrow BOE and POE observed for high-albedo objects of the Solar System and bright laboratory samples (e.g., Refs. [11,111]). The explanation of the robustness of the typical manifestations of CB can be as follows: the waves that are multiply scattered by widely separated particles in a rather closely packed medium still provide a significant cumulative contribution to the scattered radiation [96]. In an absorbing densely packed medium, the near-field effects play a significant role and weaken the manifestations of CB. Moreover, depending on the properties of the constituent particles, the near-field interactions may strengthen the negative polarization at small phase angles. The latter effect may explain the negative-polarization branch observed for dark objects exhibiting no opposition effect in the scattered intensity (e.g., Ref. [107]).

6. Concluding remarks

This review was focused on certain aspects of the theory of EM scattering by systems of particles and discrete random media. All equations and numerical results were obtained from the MMEs either directly or by using a well-defined and reproducible approximation. Phenomenological and approximate theories and methods with poorly defined accuracies and ranges of applicability were intentionally left out (cf. Refs. [58,112]).

Special attention was paid to EM scattering by densely packed discrete random media. The particular importance of this subject is explained by the need for an adequate, physically based interpretation of remote-sensing data obtained for different objects, including data of ground-based observations of atmosphereless celestial bodies, optical studies of the terrestrial surface and atmosphere from spacecraft, etc. Unfortunately, a complete and practically usable theory of EM scattering by densely packed media is still not available, while the scattering theory for sparse particulate media is rather advanced. The optical characteristics of sparse discrete random media are determined by only two types of scattering: diffuse (or incoherent) scattering and CB described by the RTT and the theory of WL, respectively. Although these theories are based on the far-field assumption (i.e., the constituent particles are assumed to be in the far-field zones of each other), the results of numerically exact computer solutions of the MMEs for macroscopic volumes filled with randomly positioned spherical particles show that the actual range of applicability of the RT and CB concepts can be significantly wider. In particular, observations can be correctly interpreted even if the particle packing density reaches 20–30% provided that the particles are non-absorbing or weakly absorbing.

To calculate the characteristics of radiation reflected from a densely packed medium, it is insufficient to solve the RT and WL equations, even if they are written in the form based on the neglect of the far-field assumption. In these media, the incident and scattered fields are related in the vicinity of a particle. Consequently, effects caused by the interference, such as that of waves scattered once and twice, can be observed that do not exist in sparse media. The results of multiple-scattering calculations for ensembles of randomly positioned particles show that a considerable increase of packing density changes significantly the phase-angle dependences of the scattered intensity and polarization at backscattering geometries. This allows one to estimate the contribution of the near-field effects and, consequently, the packing density of particles and their absorption properties. However, the quantitative interpretation of measurements of radiation reflected by a densely packed medium in terms of particle sizes, refractive indices, and packing densities still remains problematic. That is why direct computer solutions of the MMEs have recently been used with great success for the study of scattering characteristics of large, though still limited, multi-particle systems. It is not claimed that such modeling can reproduce exactly the scattering properties of natural particulate media. However, its critical advantage is that it permits a thorough qualitative and semi-quantitative analysis of the effects of packing density on multiple scattering. This analysis allows one not only to determine the range of applicability of the low-density RT and WL theories, but also to understand the complex scattering mechanisms acting in density packed media. The latter is important for the development of improved theories of EM scattering by realistic particulate surfaces and dense particle suspensions.

Acknowledgments

We gratefully acknowledge extensive discussion with Anatoli Borovoi, Zhanna Dlugach, Klaus Jockers, Nikolai Khlebtsov, Pavel Litvinov, Anatoli Minakov, Gorden Videen, and many other colleagues. This research was sponsored in part by the NASA Radiation Sciences Program managed by Hal Maring.

Appendix A. Spherical and helical basis vectors

Covariant spherical basis vectors are defined as follows [34]:

$$\mathbf{e}_n = -n\frac{1}{\sqrt{2}}(\mathbf{e}_x + in\mathbf{e}_y), \quad \mathbf{e}_0 = \mathbf{e}_z.$$

Here, $n = \pm 1$ and $\mathbf{e}_x, \mathbf{e}_y, \mathbf{e}_z$ are unit vectors along the corresponding axes of a Cartesian coordinate system. Contravariant spherical basis vectors $\mathbf{e}^n$ can be expressed in the covariant ones as follows: $\mathbf{e}^n = \mathbf{e}_n^*$. Spherical basis vectors form a complex orthonormal basis:

$$\mathbf{e}_q\mathbf{e}^p = \mathbf{e}_q\mathbf{e}_p^* = \delta_{qp} \quad (p,q = \pm 1,0).$$

Any vector can be decomposed as follows:

$$\mathbf{A}=\sum_p A^p\mathbf{e}_p=\sum_p A_p\mathbf{e}^p,$$

where A_p and A^p are the covariant and contravariant components, respectively:

$$A_n=-A^{-n}=-n\frac{1}{\sqrt{2}}(A_x+\mathrm{i}nA_y),$$

$$A_0=A^0=A_z.$$

Covariant helical basis vectors are determined as follows:

$$\mathbf{e}_n^{(h)}=-n\frac{1}{\sqrt{2}}(\mathbf{e}_\vartheta+\mathrm{i}n\mathbf{e}_\phi),\quad \mathbf{e}_0^{(h)}=\mathbf{e}_r,$$

where $n=\pm 1$, and $\mathbf{e}_r,\mathbf{e}_\vartheta,\mathbf{e}_\phi$ are the corresponding unit vectors of the spherical coordinate system. Contravariant helical basis vectors are defined as complex-conjugate covariant helical vectors.

Appendix B. Spherical vectors

Spherical vectors (or irreducible spherical tensors of rank 1) can be represented in the form [34]:

$$\mathbf{Y}_{JM}^L(\vartheta,\varphi)=\sum_p C_{Lm1p}^{JM}Y_{Lm}(\vartheta,\varphi)\mathbf{e}_p.$$

Here, C_{Lm1p}^{JM} are CGCs [34] (see also Appendix D), $m=M-p$, $Y_{Lm}(\vartheta,\varphi)$ are scalar spherical harmonics [34], and $\mathbf{e}_p$ are covariant spherical basis vectors ($p=0,\pm 1$). The indices J and L are non-negative integers, $-J\le M\le J,-L\le m\le L$. For a fixed J, L takes the values $L=J,L=J\pm 1$. Three such vectors with identical J and M form an orthogonal basis:

$$\mathbf{Y}_{JM}^L(\vartheta,\varphi)\cdot\mathbf{Y}_{JM}^{*L_1}(\vartheta,\varphi)=0,\quad (L\ne L_1).$$

The representation of the spherical vectors in terms of helical basis vectors has the form

$$\mathbf{Y}_{JM}^L(\vartheta,\varphi)=\sum_p[\mathbf{Y}_{JM}^L(\vartheta,\varphi)]^p\mathbf{e}_p^{(h)},$$

where the contravariant components $[\mathbf{Y}_{JM}^L(\vartheta,\varphi)]^p$ of the vector $\mathbf{Y}_{JM}^L(\vartheta,\varphi)$ are given by

$$[\mathbf{Y}_{JM}^L(\vartheta,\varphi)]^p=\sqrt{\frac{2L+1}{4\pi}}C_{L01p}^{Jp}D_{-p-M}^J(0,\vartheta,\varphi)$$
$$=\sqrt{\frac{2L+1}{4\pi}}C_{L01p}^{Jp}D_{Mp}^{*J}(\varphi,\vartheta,0).$$

Here $D_{Mp}^{*J}(\varphi,\vartheta,0)=D_{-p-M}^J(0,\vartheta,\varphi)$ is the Wigner D function [34] (see also Appendix C). The covariant and contravariant components of the spherical vector $\mathbf{Y}_{JM}^L(\vartheta,\varphi)$ are related:

$$[\mathbf{Y}_{JM}^L(\vartheta,\varphi)]_p=(-1)^p[\mathbf{Y}_{JM}^L(\vartheta,\varphi)]^{-p}.$$

The expansion of a plane wave in spherical vectors $\mathbf{Y}_{JM}^L(\vartheta,\varphi)$ has the form [34]

$$\boldsymbol{\varepsilon}(\hat{\mathbf{k}})\exp(\mathrm{i}\mathbf{kr})=4\pi\sum_{JLM}\mathrm{i}^L j_L(kr)[\boldsymbol{\varepsilon}(\hat{\mathbf{k}})\cdot\mathbf{Y}_{JM}^{*L}(\vartheta_0,\varphi_0)]\mathbf{Y}_{JM}^L(\vartheta,\varphi).$$

Here, ϑ_0,φ_0 and ϑ,φ are spherical angles of the vectors $\mathbf{k}$ and $\mathbf{r}$, respectively. A vector $\boldsymbol{\varepsilon}(\hat{\mathbf{k}})$ determines the state of wave polarization. If $\boldsymbol{\varepsilon}(\hat{\mathbf{k}})$ is a helical vector then the above expansion can be rewritten as follows:

$$\mathbf{e}_n^{(h)}(\hat{\mathbf{k}})\exp(\mathrm{i}\mathbf{kr})=\sum_{LM}w_{LM}\left[nj_L(kr)\mathbf{X}_{LM}(\vartheta,\varphi)+\frac{1}{k}\nabla\times j_L(kr)\mathbf{X}_{LM}(\vartheta,\varphi)\right],$$

where $w_{LM}=-4\pi\mathrm{i}^L\sqrt{(2L+1)/8\pi}D_{Mn}^L(\vartheta_0,\varphi_0,0)$ and $\mathbf{X}_{JM}(\vartheta,\varphi)\equiv\mathbf{Y}_{JM}^J(\vartheta,\varphi)$.

The vectors $\mathbf{F}_{JM}^L(\mathbf{r})=z_L(kr)\mathbf{Y}_{JM}^L(\vartheta,\varphi)$ are solutions of the vector Helmholtz equation

$$\Delta\mathbf{F}+k^2\mathbf{F}=0$$

and are known as the vector Helmholtz harmonics [26]. Here $z_L(x)=\sqrt{\pi/(2x)}Z_{L+1/2}(x)$ and $Z_{L+1/2}(x)$ is any cylindrical function of order $L+1/2$. If $\nabla\cdot\mathbf{F}=0$ then the solution of the vector Helmholtz equation can be expressed in the vectors $z_L(kr)\mathbf{X}_{LM}(\vartheta,\varphi)$ and $(1/k)\nabla\times z_L(kr)\mathbf{X}_{LM}(\vartheta,\varphi)$ only. These vectors are closely related to the transverse vector spherical wave functions $\mathbf{M}_{mn}(kr,\vartheta,\varphi)$ and $\mathbf{N}_{mn}(kr,\vartheta,\varphi)$ [24]:

$$h_n(kr)\mathbf{X}_{nm}(\vartheta,\varphi)=\mathrm{i}\mathbf{M}_{mn}(kr,\vartheta,\varphi),$$
$$\frac{1}{k}\nabla\times h_n(kr)\mathbf{X}_{nm}(\vartheta,\varphi)=\mathrm{i}\mathbf{N}_{mn}(kr,\vartheta,\varphi),$$

$$j_n(kr)\mathbf{X}_{nm}(\vartheta,\varphi)=\mathrm{iRg}\mathbf{M}_{mn}(kr,\vartheta,\varphi),$$
$$\frac{1}{k}\nabla\times j_n(kr)\mathbf{X}_{nm}(\vartheta,\varphi)=\mathrm{iRg}\mathbf{N}_{mn}(kr,\vartheta,\varphi),$$

where $h_n(kr)$ and $j_n(kr)$ are Hankel and Bessel spherical functions, respectively. Let us denote $\boldsymbol{M}_{LM}(z_L(kr),\mathbf{r})=z_L(kr)\mathbf{X}_{LM}(\vartheta,\varphi)$ and $\boldsymbol{N}_{LM}(z_L(kr),\mathbf{r})=(1/k)\nabla\times z_L(kr)\mathbf{X}_{LM}(\vartheta,\varphi)$, where $z_L(kr)$ is the Bessel or Hankel spherical function. Let a vector $\mathbf{r}$ be represented as $\mathbf{r}=\mathbf{r}_1-\mathbf{r}_2$. Then the translation addition theorem for vectors $\boldsymbol{M}_{LM}(z,\mathbf{r})$ and $\boldsymbol{N}_{LM}(z,\mathbf{r})$ in a compact notation of functions $z_L(kr)$ reads as follows [22,38]:

$$\boldsymbol{M}_{LM}(z,\mathbf{r})=\sum_{lm}[H_{lmLM}(\mathbf{r}_2)\boldsymbol{M}_{lm}(y,\mathbf{r}_1)+K_{lmLM}(\mathbf{r}_2)\boldsymbol{N}_{lm}(y,\mathbf{r}_1)],$$

$$\boldsymbol{N}_{LM}(z,\mathbf{r})=\sum_{lm}[K_{lmLM}(\mathbf{r}_2)\boldsymbol{M}_{lm}(y,\mathbf{r}_1)+H_{lmLM}(\mathbf{r}_2)\boldsymbol{N}_{lm}(y,\mathbf{r}_1)],$$

where

$$\left.\begin{matrix}H_{JNLM}(\mathbf{r}_2)\\K_{JNLM}(\mathbf{r}_2)\end{matrix}\right\}=(-1)^{M+1}\sqrt{(2J+1)(2L+1)}\sum_l\mathrm{i}^{J-l-L}g_l(kr_2)$$
$$\times D_{m_1 0}^l(\varphi_2,\vartheta_2,0)C_{JNL-M}^{lm_1}C_{J1L-1}^{l0}\left\{\begin{matrix}I_{JLl}^+\\I_{JLl}^-\end{matrix}\right.,$$

$$y=j_l(kr_1),\quad g_l(kr_2)=z_l(kr_2)\quad\text{if}\ \ r_1<r_2,$$
$$y=z_l(kr_1),\quad g_l(kr_2)=j_l(kr_2)\quad\text{if}\ \ r_1>r_2,$$

$m_1=N-M$, $I_{LL_1}^{\pm}=[1\pm(-1)^{l+L+L_1}]/2$, and φ_2,ϑ_2 are spherical coordinates of the vector $\mathbf{r}_2$.

Appendix C. Wigner *D* functions

Wigner D functions represent the matrix elements of the rotation operator and are defined as follows [34]:

$$D_{MN}^L(\hat{\mathbf{n}}_0,\hat{\mathbf{n}}_1)\equiv D_{MN}^L(\alpha,\beta,\gamma)=\exp(-\mathrm{i}M\alpha)d_{MN}^L(\beta)\exp(-\mathrm{i}N\gamma).$$

Here $L=0,1,\ldots,-L\le M\le L,-L\le N\le L$, and the Euler angles α,β, and γ determine the rotation from a coordinate system $\hat{\mathbf{n}}_0$ to a coordinate system $\hat{\mathbf{n}}_1$. The Wigner d functions $d_{MN}^L(x)$

are closely related to the generalized spherical functions $P^l_{mn}(x)$

$$P^l_{mn}(x) = \mathrm{i}^{m-n} d^l_{mn}(x).$$

Spherical functions $Y_{LM}(\vartheta,\varphi)$ are a particular case of the Wigner D functions

$$Y_{LM}(\vartheta,\varphi) = \sqrt{\frac{2L+1}{4\pi}} D^L_{0-M}(0,\vartheta,\varphi) = \sqrt{\frac{2L+1}{4\pi}} D^{*L}_{M0}(\varphi,\vartheta,0).$$

The addition theorem for the Wigner D functions reads

$$D^L_{Mm}(\hat{\mathbf{n}}_1,\hat{\mathbf{n}}_2) = \sum_{m_1} D^L_{Mm_1}(\hat{\mathbf{n}}_1,\hat{\mathbf{n}}_0) D^L_{m_1 m}(\hat{\mathbf{n}}_0,\hat{\mathbf{n}}_2) = \sum_{m_1} D^{*L}_{m_1 M}(\hat{\mathbf{n}}_0,\hat{\mathbf{n}}_1) D^L_{m_1 m}(\hat{\mathbf{n}}_0,\hat{\mathbf{n}}_2).$$

A direct consequence of the addition theorem is the unitarity condition

$$\sum_{m_1} D^L_{Mm_1}(\hat{\mathbf{n}}_1,\hat{\mathbf{n}}_2) D^{*L}_{mm_1}(\hat{\mathbf{n}}_1,\hat{\mathbf{n}}_2) = \delta_{Mm}.$$

The D functions have many symmetry properties; several are listed below:

$$D^L_{Mm}(\hat{\mathbf{n}}_1,\hat{\mathbf{n}}_2) = (-1)^{M-m} D^{*L}_{-M-m}(\hat{\mathbf{n}}_1,\hat{\mathbf{n}}_2),$$
$$D^L_{Mm}(\hat{\mathbf{n}}_1,\hat{\mathbf{n}}_2) = D^{*L}_{mM}(\hat{\mathbf{n}}_2,\hat{\mathbf{n}}_1),$$
$$D^L_{Mm}(\hat{\mathbf{n}}_1,\hat{\mathbf{n}}_2) = (-1)^{M-m} D^{*L}_{Mm}(-\hat{\mathbf{n}}_1,-\hat{\mathbf{n}}_2),$$
$$D^L_{Mm}(\hat{\mathbf{n}}_1,\hat{\mathbf{n}}_2) = (-1)^{L} D^{L}_{M-m}(\hat{\mathbf{n}}_1,-\hat{\mathbf{n}}_2).$$

A product of two Wigner D function can be decomposed into a CGS:

$$D^L_{Mm}(\hat{\mathbf{n}}_1,\hat{\mathbf{n}}_2) D^{L_1}_{M_1 m_1}(\hat{\mathbf{n}}_1,\hat{\mathbf{n}}_2) = \sum_{L_2 M_2 N_2} C^{L_2 M_2}_{LML_1 M_1} C^{L_2 N_2}_{LmL_1 m_1} D^{L_2}_{M_2 N_2}(\hat{\mathbf{n}}_1,\hat{\mathbf{n}}_2),$$

where the symbols C with indices are CGCs (Appendix D). The orthogonality property of the D functions reads as follows:

$$\int_0^{2\pi} d\alpha \int_0^{2\pi} d\gamma \int_0^{\pi} D^L_{MN}(\alpha,\beta,\gamma) D^{*l}_{mn}(\alpha,\beta,\gamma) \sin\beta\, d\beta = \frac{8\pi^2}{2L+1} \delta_{Ll} \delta_{Mm} \delta_{Nn}.$$

In the particular case of one D function this formula takes the form

$$\int_0^{2\pi} d\alpha \int_0^{2\pi} d\gamma \int_0^{\pi} D^L_{MN}(\alpha,\beta,\gamma) \sin\beta\, d\beta = 8\pi^2 \delta_{L0} \delta_{M0} \delta_{N0}.$$

Appendix D. Clebsch–Gordan coefficients

Explicit forms of the CGCs can be found in many publications (see, e.g., Ref. [34]). The CGCs $C^{L_1 M_1}_{LMlm}$ are real-valued coefficients which are non-zero only when $|l-L| \le L_1 \le l+L$, $M_1 = m+M$, $L \ge |M|$, $l \ge |m|$, and $L_1 \ge |M_1|$. The indices L, L_1, l are non-negative integers or half-integers, while M, M_1, m are integers or half-integers.

The unitarity relation for the CGCs reads

$$\sum_{Mm} C^{L_1 M_1}_{LMlm} C^{L_2 M_2}_{LMlm} = \delta_{L_1 L_2} \delta_{M_1 M_2}.$$

The CGCs have many symmetry properties, in particular,

$$C^{L_1 M_1}_{LMlm} = (-1)^{L_1+L+l} C^{L_1 -M_1}_{L-Ml-m} = (-1)^{L_1+L+l} C^{L_1 M_1}_{lmLM}$$
$$= (-1)^{l+m} \sqrt{\frac{2L_1+1}{2L+1}} C^{L-M}_{L_1 -M_1 lm}$$
$$= (-1)^{L-M} \sqrt{\frac{2L_1+1}{2l+1}} C^{l-m}_{LML_1 -M_1}.$$

Explicit forms of the CGCs for some frequently encountered combinations of indices are given below:

$$\sqrt{\tfrac{2L+1}{4\pi}} C^{J\pm 1}_{L01\pm 1} = \sqrt{\tfrac{J}{8\pi}}, \quad \sqrt{\tfrac{2L+1}{4\pi}} C^{J0}_{L010} = -\sqrt{\tfrac{J+1}{4\pi}}, \quad (L=J+1),$$

$$\sqrt{\tfrac{2L+1}{4\pi}} C^{J\pm 1}_{L01\pm 1} = \mp\sqrt{\tfrac{2J+1}{8\pi}}, \quad \sqrt{\tfrac{2L+1}{4\pi}} C^{J0}_{L010} = 0, \quad (L=J),$$

$$\sqrt{\tfrac{2L+1}{4\pi}} C^{J\pm 1}_{L01\pm 1} = \sqrt{\tfrac{J+1}{8\pi}}, \quad \sqrt{\tfrac{2L+1}{4\pi}} C^{J0}_{L010} = \sqrt{\tfrac{J}{4\pi}}, \quad (L=J-1).$$

References

[1] Tatarskii VI. Wave propagation in a turbulent medium. New York: McGraw-Hill; 1961;
Mudaliar S. Remarks on the radiative transfer approach to scattering of electromagnetic waves in layered random media. J Quant Spectrosc Radiat Transfer 2010;111:1015–124.
[2] Rytov SM, Kravtsov YuA, Tatarsky VI. Principles of statistical radiophysics, vols. 1–4. Berlin: Springer; 1987.
[3] Tsang L, Kong JA. Scattering of electromagnetic waves: advanced topics. New York: Wiley; 2001.
[4] Mishchenko MI, Travis LD, Lacis AA. Multiple scattering of light by particles: radiative transfer and coherent backscattering. Cambridge: Cambridge University Press; 2006.
[5] Gnedin YuN, Dolginov AZ. Theory of multiple scattering. Sov Phys JETP 1964;18:784–91.
[6] Watson KM. Multiple scattering of electromagnetic waves in an underdense plasma. J Math Phys 1969;10:688–702.
[7] Barabanenkov YN. Wave correction to the transfer equation for "back" scattering. Radiophys Quantum Electron 1973;16:65–71.
[8] Wolf P, Maret G. Weak localization and coherent backscattering of photons in disordered media. Phys Rev Lett 1985;55:2696–9.
[9] Akkermans E, Wolf PE, Maynard R, Maret G. Theoretical study of the coherent backscattering of light by disordered media. J Phys France 1988;49:77–98.
[10] Barabanenkov YuN, Kravtsov YuA, Ozrin VD, Saichev AI. Enhanced backscattering in optics. Prog Opt 1991;29:65–197.
[11] Mishchenko MI, Rosenbush VK, Kiselev NN, Lupishko DF, Tishkovets VP, Kaydash VG, et al. Polarimetric remote sensing of Solar System objects. Kyiv: Akademperiodyka; 2010 〈arXiv:1010.1171〉.
[12] Tishkovets VP. Negative polarization of light scattered by closely packed media. In: 28th annual lunar and planetary science conference, Houston, TX; 1997. p. 1437–8.
[13] Tishkovets VP. Backscattering of light by close-packed system of particles. Opt Spectrosc 1998;85:212–7.
[14] Tishkovets V, Petrova E, Jockers K. Optical properties of aggregate particles comparable in size to the wavelength. J Quant Spectrosc Radiat Transfer 2004;86:241–65.
[15] Petrova EV, Tishkovets VP, Jockers K. Modeling of opposition effects with ensembles of clusters: interplay of various scattering mechanisms. Icarus 2007;188:233–45.
[16] Tishkovets VP. Light scattering by closely packed clusters: shielding of particles by each other in the near field. J Quant Spectrosc Radiat Transfer 2008;109:2665–72.
[17] Foldy LL. The multiple scattering of waves. Phys Rev 1945;67:107–19.
[18] Lax M. Multiple scattering of waves. Rev Mod Phys 1951;23:287–310.
[19] Lax M. Multiple scattering of waves. II. Effective field in dense systems. Phys Rev 1952;85:621–9.
[20] Twersky V. On propagation in random media of discrete scatterers. Proc Symp Appl Math 1964;16:84–116.
[21] Mishchenko MI, Travis LD, Mackowski DW. *T*-matrix computations of light scattering by nonspherical particles: a review. J Quant Spectrosc Radiat Transfer 1996;55:535–75.
[22] Fuller KA, Mackowski DW. Electromagnetic scattering by compounded spherical particles. In: Mishchenko MI, Hovenier JW,

Travis LD, editors. Light scattering by nonspherical particles: theory, measurements, and applications. San Diego: Academic Press; 2000. p. 225–72.
[23] Tsang L, Kong JA, Ding K-H. Scattering of electromagnetic waves: theories and applications. New York: Wiley; 2000.
[24] Mishchenko MI, Travis LD, Lacis AA. Scattering, absorption, and emission of light by small particles. Cambridge, UK: Cambridge University Press; 2002.
[25] Mishchenko MI, Videen G, Babenko VA, et al. *T*-matrix theory of electromagnetic scattering by particles and its applications: a comprehensive reference database. J Quant Spectrosc Radiat Transfer 2004;88:357–406.
[26] Borghese F, Denti P, Saija R. Scattering from model nonspherical particles. Theory and applications to environmental physics. Berlin: Springer; 2007.
[27] Mishchenko MI, Videen G, Babenko VA, et al. Comprehensive *T*-matrix reference database: a 2004–06 update. J Quant Spectrosc Radiat Transfer 2007;106:304–24.
[28] Mishchenko MI, Videen G, Khlebtsov NG, et al. Comprehensive *T*-matrix reference database: a 2006–07 update. J Quant Spectrosc Radiat Transfer 2008;109:1447–60.
[29] Peterson B, Ström S. *T* matrix for electromagnetic scattering from an arbitrary number of scattering and representation of $E(3)^*$. Phys Rev D 1973;8:3661–78.
[30] Peterson B. Multiple scattering of waves by an arbitrary lattice. Phys Rev A 1977;16:1363–70.
[31] Peterson B, Ström S. *T*-matrix formulation of electromagnetic scattering from multilayered scatterers. Phys Rev D 1974;10:2670–84.
[32] Waterman PC. Symmetry, unitarity, and geometry in electromagnetic scattering. Phys Rev D 1971;3:825–39.
[33] Born M, Wolf E. Principles of optics. Cambridge, UK: Cambridge University Press; 1999.
[34] Varshalovich DA, Moskalev AN, Khersonskii VK. Quantum theory of angular momentum. Singapore: World Scientific; 1988.
[35] Tishkovets VP. Incoherent and coherent backscattering of light by a layer of densely packed random medium. J Quant Spectrosc Radiat Transfer 2007;108:454–63.
[36] Cruzan OR. Translational addition theorems for spherical vector wave function. Q Appl Math 1962;20:33–40.
[37] Felderhof BU, Jones RB. Addition theorems for spherical wave solutions of the vector Helmholtz equation. J Math Phys 1987;28: 836–9.
[38] Tishkovets VP, Litvinov PV. Coefficients of light extinction by randomly oriented clusters of spherical particles in the double scattering approximation. Opt Spectrosc 1996;81:288–91.
[39] Mishchenko MI, Travis LD, Mackowski DW. 〈http://www.giss.nasa.gov/~crmim〉.
[40] Gradshtein IS, Ryzhik IM. Tables of integrals, series, and products. New York: Academic Press; 1980.
[41] Greffet J-J, Carminati R. Image formation in near-field optics. Prog Surf Sci 1998;56:133–237.
[42] Tishkovets VP, Litvinov PV, Petrova EV, et al. Backscattering effects for discrete random media: theoretical results. In: Videen G, Yatskiv Ya, Mishchenko M, editors. Photopolarimetry in remote sensing. Dordrecht: Kluwer; 2004. p. 221–42.
[43] Van de Hulst HC. Light scattering by small particles. New York: Wiley; 1957.
[44] Newton RG. Scattering theory of waves and particles. New York: Springer; 1982.
[45] Bohren CF, Huffman DR. Absorption and scattering of light by small particles. New York: Wiley; 1983.
[46] Dolginov AZ, Gnedin YuN, Silant'ev NA. Propagation and polarization of radiation in cosmic media. Basel: Gordon and Breach; 1995.
[47] Tishkovets VP, Mishchenko MI. Coherent backscattering of light by a layer of discrete random medium. J Quant Spectrosc Radiat Transfer 2004;86:161–80.
[48] Borovoi AG. Multiple scattering of short waves by uncorrelated and correlated scatterers. Light Scattering Rev 2006;1:181–248.
[49] Mishchenko MI. The electromagnetic optical theorem revisited. J Quant Spectrosc Radiat Transfer 2006;101:404–10.
[50] Varadan VV, Varadan VK. Multiple scattering of electromagnetic waves by randomly distributed and oriented dielectric scatters. Phys Rev D 1980;21:388–94.
[51] Varadan VK, Bringi VN, Varadan VV. Coherent electromagnetic wave propagation through randomly distributed dielectric scatterers. Phys Rev D 1979;19:2480–9.
[52] Varadan VK, Bringi VN, Varadan VV, Ishimaru A. Multiple scattering theory for waves in discrete random media and comparison with experiments. Radio Sci 1983;18:321–7.
[53] Bringi VN, Seliga TA, Varadan VK, Varadan VV. Bulk propagation characteristics of discrete random media. In: Chow PL, Kohler WE, Papanicolaou GC, editors. Multiple scattering and waves in random media. Amsterdam: North-Holland; 1981. p. 43–75.
[54] Bringi VN, Varadan VV, Varadan VK. Coherent wave attenuation by a random distribution of particles. Radio Sci 1982;17:946–52.
[55] Bringi VN, Varadan VV, Varadan VK. The effect on pair correlation function of coherent wave attenuation in discrete random media. IEEE Trans Antennas Propag 1982;30:805–8.
[56] Percus JK, Yevick GJ. Analysis of classical statistical mechanics by means of collective coordinates. Phys Rev 1958;110:1–13.
[57] Waterman PC, Truell R. Multiple scattering of waves. J Math Phys 1961;2:512–37.
[58] Mishchenko MI, Tishkovets VP, Travis LD, et al. Electromagnetic scattering by a morphologically complex object: fundamental concepts and common misconceptions. J Quant Spectrosc Radiat Transfer 2011;112:671–92.
[59] Mishchenko MI. Multiple scattering, radiative transfer, and weak localization in discrete random media: unified microphysical approach. Rev Geophys 2008;46:RG2003.
[60] Mackowski DW. An effective medium method for calculation of the *T* matrix of aggregated spheres. J Quant Spectrosc Radiat Transfer 2001;70:441–64.
[61] Tishkovets VP, Jockers K. Multiple scattering of light by densely packed random media of spherical particles: dense media vector radiative transfer equation. J Quant Spectrosc Radiat Transfer 2006;101:54–72.
[62] van Albada MP, Lagendijk A. Observation of weak localization of light in a random medium. Phys Rev Lett 1985;55:2692–5.
[63] van Albada MP, van der Mark MB, Lagendijk A. Polarization effects in weak localization of light. J Phys D 1988;21:S28–31.
[64] van der Mark MB, van Albada MP, Lagendijk A. Light scattering in strongly scattering media: multiple scattering and weak localization. Phys Rev B 1988;37:3575–92.
[65] Wolf PE, Maret G, Akkermans E, Maynard R. Optical coherent backscattering by random media: an experimental study. J Phys France 1988;49:63–75.
[66] Tsang L, Chen CT, Chang ATC, Guo J, Ding KH. Dense media radiative transfer theory based on quasicrystalline approximation with applications to passive microwave remote sensing of snow. Radio Sci 2000;35:731–49.
[67] Yanovitskij EG. Light scattering in inhomogeneous atmospheres. New York: Springer; 1997.
[68] Mishchenko MI. Vector radiative transfer equation for arbitrarily shaped and arbitrarily oriented particles: a microphysical derivation from statistical electromagnetics. Appl Opt 2002;41: 7114–34;
Mishchenko MI. Microphysical approach to polarized radiative transfer: extension to the case of an external observation point. Appl Opt 2003;42:4963–7.
[69] Mishchenko MI, Mackowski DW. Coherent backscattering in the cross-polarized channel. Phys Rev A 2011;83:013829.
[70] Mishchenko MI. Enhanced backscattering of polarized light from discrete random media: calculations in exactly the backscattering direction. J Opt Soc Am A 1992;9:978–82.
[71] Saxon DS. Tensor scattering matrix for the electromagnetic field. Phys Rev 1955;100:1771–5.
[72] Mishchenko MI, Tishkovets VP, Litvinov PV. Exact results of the vector theory of coherent backscattering from discrete random media: an overview. In: Videen G, Kocifaj M, editors. Optics of cosmic dust. Dordrecht: Kluwer; 2002. p. 239–60.
[73] Tishkovets VP, Litvinov PV, Lyubchenko MV. Coherent opposition effect for semi-infinite discrete random medium in the double-scattering approximation. J Quant Spectrosc Radiat Transfer 2002;72:803–11.
[74] Tishkovets VP, Litvinov PV, Tishkovets SV. Interference effects in backscattering of light by a layer of a discrete random medium. Opt Spectrosc 2002;93:899–907.
[75] Litvinov P, Tishkovets V, Ziegler K. Coherent backscattering effects for discrete random media. J Quant Spectrosc Radiat Transfer 2007;103:131–45.
[76] Ozrin VD. Exact solution for coherent backscattering of polarized light from a random medium of Rayleigh scatterers. Waves Random Media 1992;2:141–64.
[77] Amic E, Luck JM, Nieuwenhuizen ThM. Multiple Rayleigh scattering of electromagnetic waves. J Phys I (France) 1997;7:445–83.
[78] Muinonen K. Coherent backscattering of light by complex random media of spherical scatters: numerical solution. Waves Random Media 2004;14:365–88.

[79] Tishkovets VP. Multiple scattering of light by a layer of discrete random medium: backscattering. J Quant Spectrosc Radiat Transfer 2002;72:123–37.
[80] Tishkovets VP, Mishchenko MI. Approximate calculation of coherent backscattering for semi-infinite discrete random media. J Quant Spectrosc Radiat Transfer 2009;110:139–45.
[81] Sobolev VV. Light scattering in planetary atmospheres. New York: Pergamon Press; 1975.
[82] Mishchenko MI, Luck J-M, Nieuwenhuizen T. Full angular profile of the coherent polarization opposition effect. J Opt Soc Am A 2000;17:888–91.
[83] Shkuratov Yu, Ovcharenko A, Zubko E, et al. The opposition effect and negative polarization of structural analogs for planetary regoliths. Icarus 2002;159:396–416.
[84] Shkuratov YuG. A new mechanism for the negative polarization of light scattered by the solid surfaces of cosmic bodies. Astron Vestnik 1989;23:176–80 [in Russian].
[85] Muinonen K. Light scattering by inhomogeneous media: backward enhancement and reversal of linear polarization. PhD dissertation. University of Helsinki; 1990.
[86] Mishchenko MI. On the nature of the polarization opposition effect exhibited by Saturn's rings. Astrophys J 1993;411:351–61.
[87] Mackowski DW, Mishchenko MI. Calculation of the *T* matrix and the scattering matrix for ensembles of spheres. J Opt Soc Am A 1996;13:2266–78.
[88] Mackowski DW. ftp://ftp.eng.auburn.edu/pub/dmckwski/scatcodes/index.html.
[89] Tishkovets VP, Litvinov PV. Opposition effects in light scattering by regolith-type media. Solar Syst Res 1999;33:162–8.
[90] Tishkovets V, Shkuratov Yu, Litvinov P. Comparison of collective effects at scattering by randomly oriented clusters of spherical particles. J Quant Spectrosc Radiat Transfer 1999;61:767–73.
[91] Shkuratov YuG, Muinonen K, Bowell E, et al. A critical review of theoretical models of negatively polarized light scattered by atmosphereless solar system bodies. Earth Moon Planets 1994;65:201–46.
[92] Shkuratov YuG, Grynko YeS. Light scattering by media composed of semitransparent particles of different shapes in ray optics approximation: consequences for spectroscopy, photometry, and polarimetry of planetary regoliths. Icarus 2005;173:16–28.
[93] Lyot B. Recherches sur la polarisation de la lumière des planets et de quelques substances terrestres. Ann Obs Paris Sect Meudon 1929;8:1–161.
[94] Muinonen K, Piironen J, Shkuratov YuG, et al. Asteroid photometric and polarimetric phase effects. In: Bottke Jr. WF, Cellino A, Paolicchi P, Binzel RP, editors. Asteroids III. Tucson, AZ: University of Arizona Press; 2002. p. 123–38.
[95] Rosenbush V, Kiselev N, Avramchuk V, Mishchenko M. Photometric and polarimetric phenomena exhibited by solar system bodies. In: Videen G, Kocifaj M, editors. Optics of cosmic dust. Dordrecht: Kluwer; 2002. p. 191–224;
Rosenbush VK, Mishchenko MI. Opposition optical phenomena in planetary astrophysics: observational results. In: Mishchenko MI, Yatskiv YaS, Rosenbush VK, Videen G, editors. Polarimetric detection, characterization, and remote sensing. Berlin: Springer; 2011. p. 409–36.
[96] Mishchenko MI, Liu L, Mackowski DW, et al. Multiple scattering by random particulate media: exact 3D results. Opt Express 2007;15:2822–36.
[97] Mishchenko MI, Dlugach JM, Liu L, et al. Direct solutions of the Maxwell equations explain opposition phenomena observed for high albedo solar system objects. Astrophys J 2009;705:L118–22.
[98] Kolokolova L, Kimura H. Effects of electromagnetic interaction in the polarization of light scattered by cometary and other types of cosmic dust. Astron Astrophys 2010;513:A40.
[99] Lasue J, Levasseur-Regourd AC, Hadamcik E, Alcouffe G. Cometary dust properties retrieved from polarization observations: application to C/1995 O1 Hale–Bopp and 1P/Halley. Icarus 2009;199:129–44.
[100] Lumme K, Penttilä A. Light scattering by dust particles in the solar system: applications to cometary comae and planetary regoliths. J Quant Spectrosc Radiat Transfer, in press. doi:10.1016/jqsrt.2011.01.016.
[101] Vilaplana R, Luna R, Guirado D. The shape influence on the overall single scattering properties of a sample in random orientation. J Quant Spectrosc Radiat Transfer, in press. doi:10.1016/jqsrt.2011.01.006.
[102] Zubko E, Kimura H, Shkuratov Yu, et al. Effect of absorption on light scattering by agglomerated debris particles. J Quant Spectrosc Radiat Transfer 2009;110:1741–9.
[103] Zubko E, Furusho R, Kawabata K, et al. Interpretation of photopolarimetric observations of comet 17P/Holmes. J Quant Spectrosc Radiat Transfer, in press. doi:10.1016/jqsrt.2011.01.020.
[104] Mishchenko MI, Dlugach JM, Liu L. Azimuthal asymmetry of the coherent backscattering cone: theoretical results. Phys Rev A 2009;80:053824.
[105] Okada Y, Kokhanovsky AA. Light scattering and absorption by densely packed groups of spherical particles. J Quant Spectrosc Radiat Transfer 2009;110:902–17.
[106] Mishchenko MI, Liu L. Electromagnetic scattering by densely packed particulate ice at radar wavelengths: exact theoretical results and remote-sensing implications. Appl Opt 2009;48:2421–6.
[107] Petrova EV, Tishkovets VP. Light scattering by aggregates of varying porosity and the opposition phenomena observed in the low-albedo particulate media, J Quant Spectrosc Radiat Transfer, in press. doi:10.1016/jqsrt.2011.01.011.
[108] Mackowski DW, Mishchenko MI. Direct simulation of multiple scattering by discrete random media illuminated by Gaussian beams. Phys Rev A 2011;83:013804.
[109] Mackowski DW, Mishchenko MI. A multiple sphere *T*-matrix Fortran code for use on parallel computer clusters. J Quant Spectrosc Radiat Transfer 2011, doi:10.1016/j.jqsrt.2011.02.019.
[110] Dlugach JM, Mishchenko MI, Liu L, Mackowski DW. Numerically exact computer simulations of light scattering by densely packed random particulate media. J Quant Spectrosc Radiat Transfer, in press. doi:10.1016/j.jqsrt.2011.02.009.
[111] Mishchenko MI, Rosenbush VK, Kiselev NN. Weak localization of electromagnetic waves and opposition phenomena exhibited by high-albedo atmosphereless solar system objects. Appl Opt 2006;45:4459–63.
[112] Tishkovets VP, Mishchenko MI. Coherent backscattering: conceptions and misconceptions. J Quant Spectrosc Radiat Transfer 2010;111:645–9.